IV

An Auger Electron Spectroscopic Study of Surface Segregation on Fe-Cr, Fe-C and Fe-Cr-C Alloys

Keith Roger Jones CChem MRSC

Submitted to the Department of Physics,
University of Warwick for the degree
of Doctor of Philosophy
January 1982

ABSTRACT

This thesis reports an Auger Electron Spectroscopic study of the surface behaviour of a high-carbon-chrome (HCC) steel, and of its pure binary and ternary analogues, with particular reference to the kinetics of surface segregation. In all, four pure alloys were studied: iron - 0.65wt% carbon, iron - 0.87wt% carbon, iron - 1.50wt% chromium and iron - 1.46wt% chromium - 0.91wt% carbon. The temperature range of the experiments was limited at its lower end to 550°C by the slow rate of segregation, and at its upper end to 850°C by evaporation of the segregants from the surface.

Two types of surface behaviour were observed on the pure alloys: segregation and precipitation. The discussion considers each in turn, followed by a consideration of the results from the commercial HCC alloy. Surface segregation occurred on all the alloys studied; surface precipitation was restricted to the plain-carbon alloys. Sulphur was the dominant segregant on the pure alloys, but segregations of phosphorus, nitrogen, chromium and possibly carbon were also observed. On the plain-carbon alloys, segregation occurred in competition with graphite precipitation.

An analysis of the sulphur segregation kinetics permitted the calculation of reasonable values of the lattice diffusion coefficient. Some previously unreported features of its segregation kinetics were explained in terms of interference by labile sulphide particles at or near the surface. The average sizes and spacings of these particles were estimated from the kinetic experiments. When sulphur was depleted at the surface, segregation of the other elements became important. A limited analysis of the phosphorus segregation kinetics permitted the calculation of reasonable values of the lattice diffusion coefficient. On the commercial HCC alloy, the presence of manganese was found to largely suppress sulphur segregation. Where segregation of sulphur did occur it was thought to be due to surface effects such as manganese evaporation. Phosphorus segregation was the most important feature on HCC.

An Auger calibration for monolayer graphite upon iron was deduced from the precipitation results. With the aid of this calibration, the graphite growth processes were elucidated. The mechanism of graphite precipitation at a sulphur-covered surface was found to be different to the reported precipitation mechanism at a clean surface. It was found possible to measure the attenuation of Auger electrons in graphite, and the values obtained were in good agreement with a theoretical analysis.

CONTENTS

CHAPTER ONE	INTRODUCTION	1
CHAPTER TWO	BACKGROUND INFORMATION	3
2.1.	Metallurgy	3
2.1.1.	Background to the HCC problem	3
2.1.2.	Equilibrium phase diagrams	4
2.1.3.	Phase transformations	6
2.2.	Auger electron spectroscopy	8
2.2.1.	Auger electrons	8
2.2.2.	Development of AES	8
2.2.3.	Application to this work	9
2.3.	Surface segregation and precipitation	11
2.3.1.	Surface segregation	11
2.3.2.	Grain boundary segregation related to surface segregation	16
2.3.3.	Surface precipitation	17
2.4.	Segregation kinetics	21
2.4.1.	Grain boundary segregation	21
2.4.2.	Surface segregation	21
References		27
CHAPTER THREE	EXPERIMENTAL DETAILS	29
3.1.	The ultra-high vacuum (UHV) system	29
3.1.1.	General	29
3.1.2.	Ion bombardment	31
3.1.3.	The sample-heating stage	33
3.1.4.	The electron gun	35
3.1.5.	The cylindrical mirror analyser (CMA)	36

3.2. Control of the analysis system 37

3.2.1. Electronics 37

3.2.2. Computer control 37

3.2.3. Data processing 38

3.3. The samples 40

3.3.1. Alloy production 40

3.3.2. Sample preparation 40

References 41

CHAPTER FOUR RESULTS 42

4.1. The Fe.87C alloy 44

4.1.1. General 44

4.1.2. The α+Fe_3C phase region 45

4.1.3. The γ+Fe_3C phase region 47

4.1.4. The γ phase region 48

4.2. The Fe.65C alloy 50

4.2.1. General 50

4.2.2. The α+Fe_3C phase region 50

4.2.3. The α+γ phase region 51

4.2.4. The γ phase region 52

4.3. The FeCr alloy 53

4.3.1. General 53

4.3.2. The α+$(Fe,Cr)_3C$ phase region 54

4.3.3. The α+γ phase region 55

4.4. The FeCrC alloy 56

4.4.1. General 56

4.4.2. The α+$(Fe,Cr)_3C$ phase region 56

4.4.3. The α+γ+$(Fe,Cr)_3C$ phase region 57

4.4.4. The γ+$(Fe,Cr)_3C$ phase region 57

4.5. The commercial HCC alloy 58

4.5.1. General 58

4.5.2. The α+$(Fe,Cr)_3C$ phase region 58

4.5.3. The α+γ+$(Fe,Cr)_3C$ phase region 58

4.5.4. The γ+$(Fe,Cr)_3C$ phase region 59

References 59

CHAPTER FIVE DISCUSSION 60

5.1. Surface segregation 60

5.1.1. Sulphur 60

5.1.2. Phosphorus 72

5.1.3. Nitrogen 75

5.1.4. Chromium 75

5.1.5. Site competition 77

5.2. Surface precipitation 80

5.2.1. General aspects of graphite precipitation 80

5.2.2. Auger calibrations for monolayer graphite on iron 84

5.2.3. Graphite layer growth 88

5.3. Surface behaviour of the HCC alloy 100

5.3.1. Sulphur 100

5.3.2. Phosphorus 102

5.3.3. Carbon 103

5.3.4. Nitrogen 104

5.3.5. Chromium 104

References 105

CHAPTER SIX	CONCLUSIONS AND FUTURE WORK	108
6.1.	The Fe.65C and Fe.87C alloys	108
6.2.	The FeCr and FeCrC alloys	109
6.3.	The HCC commercial alloy	110
6.4.	Suggestions for future work	111
APPENDIX A	Glossary of Metallurgical Terms	
APPENDIX B	Auger Calibrations	

CHAPTER SIX	CONCLUSIONS AND FUTURE WORK	108
6.1.	The Fe.65C and Fe.87C alloys	108
6.2.	The FeCr and FeCrC alloys	109
6.3.	The HCC commercial alloy	110
6.4.	Suggestions for future work	111
APPENDIX A	Glossary of Metallurgical Terms	
APPENDIX B	Auger Calibrations	

ACKNOWLEDGEMENTS

I am most grateful to Dr. D.P. Woodruff for his supervision of my work and for his patience during the extended preparation of this thesis. I would also like to thank Prof. A.J. Forty for the provision of facilities within the Department of Physics. This work was carried out under a C.A.S.E. award with Tube Investments Ltd. and my thanks are extended to Dr. M.J. Stowell for his assistance.

I would like to thank the members of the Surface Physics Group for their aid; especially Dr. P.D.Johnson, and Mr. O.S. Simpson for his excellent technical support.

Finally, my thanks are due to Ros and Martine who gave me such support and helped to bring this work to a conclusion.

MEMORANDUM

The work reported in this thesis is my own unless specifically acknowledged as being otherwise. It was performed at the University of Warwick, in the Department of Physics.

The references cited in each chapter have been listed at the end of the chapter, rather than at the end of the thesis.

CHAPTER ONE INTRODUCTION

This thesis describes the application of Auger electron spectroscopy to a study of interfacial impurity segregation in iron alloys. The project arose as a result of commercial interest in establishing whether grain boundary segregation of sulphur was responsible for the irregular hot-workability of EN31 high-carbon-chrome (HCC) steel. This is used for the production of bearing rings, and good hot-workability at the hot-piercing stage is essential if tubes of sufficiently good bore quality are to result. HCC steel has a nominal composition of 1wt% carbon, 1.5wt% chromium, the balance being iron.

Commercial alloys are very complex systems with high levels of impurities. It was therefore decided to carry out the major part of the work on pure binary and ternary alloys whose carbon and chromium contents corresponded to the HCC nominal composition. Past segregation studies on iron-carbon alloys have concentrated on hypo-eutectoid compositions. A pure alloy containing 0.65wt% carbon was therefore used for comparative purposes. Well-homogenised samples of HCC steel were produced to test the behaviour of the commercial product. The relevant metallurgical details of these alloys are described in Chapter Two, and a glossary of metallurgical terms is presented as Appendix A.

Auger electron spectroscopy has played an important part in the development of a theoretical understanding of the process of segregation. It permits direct, surface-specific qualitative and quantitative analyses to be made at an interface. An electron beam is directed at the sample surface and the re-emitted electrons are energy analysed. For grain boundary segregation to be studied, this implies fracturing along embrittled boundaries to make them accessible. It is necessary to avoid surface contamination by atmospheric gases

because they can destroy the original segregation pattern. For this reason, Auger electron spectroscopy is normally conducted under ultra-high vacuum (UHV) conditions. A description of the Auger process is given in Chapter Two, and the experimental details and a description of the UHV system are included in Chapter Three.

As originally framed, the majority of the work was to have involved the measurement of grain boundary segregation, with recourse to the free surface if grain boundary fracture could not be obtained. In the event, there were experimental difficulties with the original UHV system and the ultimate vacua obtained were not adequate to prevent surface contamination. Eventually, a new UHV system was constructed. This was not as sophisticated as the original system but gave much better ultimate vacua. The reduction in experimental facilities favoured a change in emphasis to surface segregation studies. As will be described in Chapter Two, surface segregation is related to grain boundary segregation.

The surface behaviour of each alloy was studied as a function of temperature, and hence of phase region. Consequently, the results in Chapter Four are split first by alloy and then by phase region. This division simplifies the location of a particular result, but it was was not considered to be suitable for the discussion chapter. Two types of surface process were observed on the nominally pure alloys: segregation and precipitation. Chapter Five considers each in turn, followed by a discussion of the results from the commercial HCC alloy. The main conclusions are summarised in Chapter Six, together with an outline of the course that future work might usefully take.

CHAPTER TWO BACKGROUND INFORMATION

2.1. Metallurgy

2.1.1. Background to the HCC problem

HCC steel is used for the production of bearing rings. The molten steel is cast into five-ton ingots. Solidification introduces gross compositional inhomogeneities into the steel. These take the form of local concentrations of certain elements, low-melting inclusions and large carbide particles. The ingots are "soaked" for seven hours at 1200°C. This partially removes the compositional inhomogeneities and dissolves most of the large carbide particles. Commercial considerations limit the time allowed for this homogenisation, which is a slow process because of the low diffusivity of chromium. The soaked ingots are "cogged" and rolled into round "blooms". A rotary-piercing operation at 1130°C converts the blooms into tubes which are then cut into bearing rings.

Good hot-workability is essential during the rotary-piercing operation because of the high stresses involved. Rollers are positioned and shaped so as to produce a tensile stress at the centre of the bar, just ahead of the piercing tool. If the ductility is deficient, areas of folded metal called "bore-laps" are produced on the interior surface of the tube, rendering it useless for bearing-ring production. The most common causes of poor hot-workability are hard precipitates, low-melting inclusions and a loss of cohesion at grain boundaries in which sulphur segregation might play a part. Manganese has traditionally been added to steels because of its known effectiveness in removing hot-shortness. This ability appears to be the result of manganese sulphide precipitation which ties-down the free sulphur usually present as an impurity in commercial steels.

Sawle (1974) has studied the hot-workability of chromium steels with various manganese:sulphur ratios. He found that provided the sulphur content was low, alloys with high Mn:S ratios performed better than alloys with low Mn:S ratios. At low temperatures, manganese induces precipitation of virtually all the free sulphur. As the temperature rises, however, more and more sulphur goes into solution and may segregate to the grain boundaries. Sawle suggested sulphur segregation as a possible cause of poor hot-workability in HCC steel but was unable to confirm this because he did not use a suitable surface analysis technique. Auger electron spectroscopy may be used to measure grain boundary segregation provided that the grain boundaries are sufficiently embrittled to be exposed by fracture. The mechanical properties of metals can be impared by levels of impurity segregation too low to permit grain boundary fracture.

In the present study, pure alloys were used in an attempt to clarify the effects of carbon and chromium upon interfacial segregation. HCC steel, with its many deliberate and accidental elemental additions, was considered too complex a system to use when determining the underlying causes of segregation in the iron-carbon-chromium system. Some measurements on HCC samples were still made, however, so that its behaviour could be compared with the pure analogues.

2.1.2. Equilibrium phase diagrams

The compositions of the pure alloys used were chosen so that their carbon and chromium contents matched the HCC nominal composition: 1wt% carbon, 1.5wt% chromium, the balance being iron. Two binary alloys with iron were produced; one containing 0.87wt% carbon, the other containing 1.50wt% chromium. These will be referred to as the Fe.87C and FeCr alloys. A ternary alloy containing 0.91wt% carbon and 1.46wt%

chromium was also produced, and will be called the FeCrC alloy. A pure sample of iron containing 0.65wt% carbon was obtained from the National Physical Laboratory. This Fe.65C alloy was included in the study to investigate the effect of carbon concentration and permit a comparison between the behaviour of hypo- and hyper-eutectoid constitutions. The detailed chemical analyses of the stock alloys are shown in Table 2.1.

An equilibrium phase diagram of the iron-carbon system, due to Hansen & Anderko (1958), is shown in Fig. 2.1. The compositions of the two plain-carbon alloys are marked. Phase regions of both the stable iron-graphite and metastable iron-cementite systems are shown. Cementite, although a metastable transformation product, nucleates much more readily than graphite in the bulk, and once formed is so stable kinetically that it may for most purposes be treated as an equilibrium phase. If plain-carbon steels are given a suitable heat-treatment, the cementite will in time transform to graphite. The growth of graphite in iron involves a volume expansion. Graphite forms readily at the surface of plain-carbon steels (Olney & Smith (1959)) where its growth does not result in lattice strain

A vertical section of the iron-carbon-chromium equilibrium phase diagram due to Tofaute et al (1934) is presented in Fig. 2.2. This section was taken at a constant chromium content of 1.6wt% and is thought to be sufficiently accurate to be applied to all the chromium-containing alloys. It shows the effect of carbon content on the phase relationships, and the compositions of the FeCr, FeCrC and HCC alloys are marked. Although FeCr was intended to be a binary alloy, there was sufficient carbon present as an impurity to cause significant changes from the iron-chromium phase diagram.

ALLOY	Carbon	Chromium	Sulphur	Phosphorus	Manganese	Nitrogen
Fe.87C	0.87	<.002	0.002	<.002	<.002	.0023
Fe.65C	0.65	-	C.003	0.0017	-	.0006
FeCr	0.025	1.50	<.002	<.002	<.002	.0019
FeCrC	0.91	1.46	0.002	<.002	<.002	.0022
HCC	1.03	1.42	0.018	0.023	0.38	-

ALLOY	Silicon	Aluminium	Nickel	Cobalt	Copper	Tin
Fe.87C	0.009	0.001	0.005	<.002	<.003	<.002
Fe.65C	0.003	0.003	-	-	-	-
FeCr	0.009	0.001	0.007	0.002	<.003	<.002
FeCrC	0.008	<.002	0.007	<.002	<.003	<.002
HCC	0.30	-	0.08	-	0.11	-

Table 2.1 Detailed analyses of the alloys (wt%)

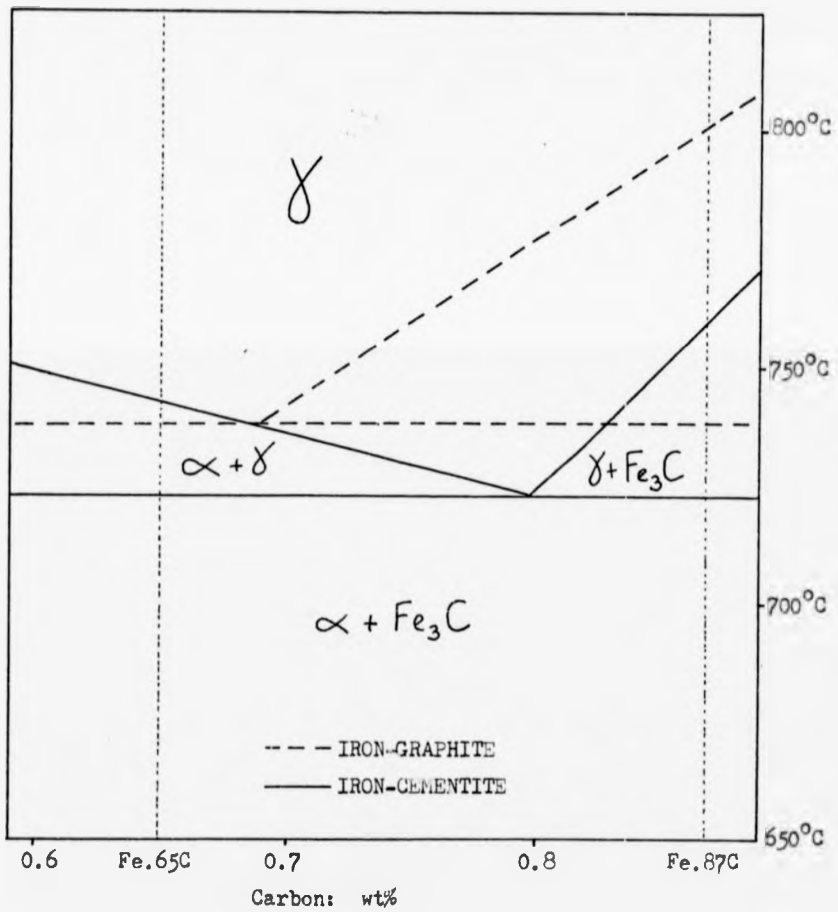

Fig. 2.1 Iron-carbon equilibrium phase diagram

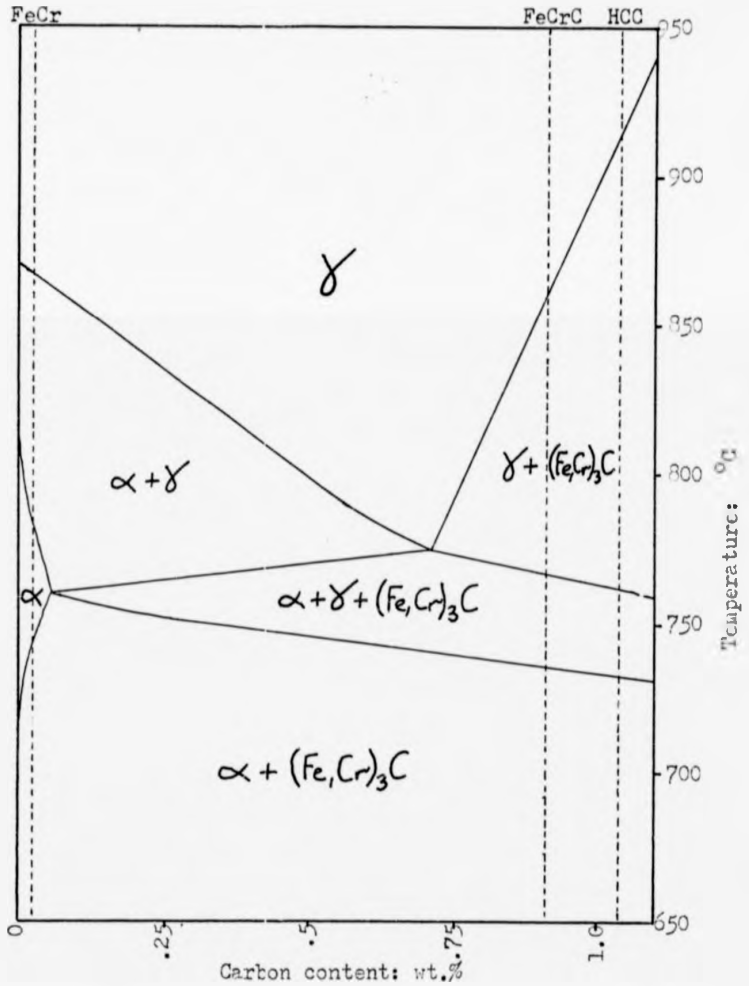

Fig. 2.2 Equilibrium phase diagram of iron - 1.6wt% chromium with carbon additions

Chromium is a strongly carbide-forming element and stabilises cementite. As a result, bulk graphitisation is not expected to occur in alloys containing more than about 1wt% chromium (Smith (1948)). For this reason, only the iron-cementite system is shown in Fig. 2.2. It should be borne in mind, however, that the diagrams presented in this section refer to the bulk, and that surface behaviour could be different.

2.1.3. Phase transformations

In plain-carbon steels, phase transformations upon heating go to completion very quickly. Austenite nucleates preferentially at grain-boundary carbides, and its rate of growth is usually limited by the rate of carbon diffusion to the transformation front (Hillert et al (1971)). In a hypo-eutectoid steel, some ferrite remains when all the cementite has dissolved in the gamma phase. Similarly, in a hyper-eutectoid steel some cementite remains when all the ferrite has transformed. When chromium is added to the steel, however, the rate of transformation is much reduced. This is the result of the partial substitution of iron atoms in cementite by chromium atoms. The dissolution of a carbide particle now requires chromium diffusion to take place, and as this is much slower than carbon diffusion the rate of transformation is reduced. Another factor which can limit the rate of transformation is carbide morphology. The rate of supply of carbon is dependent upon the area of the carbide-matrix interface through which it must diffuse. Spheroidising the carbide particles can reduce the rate of transformation to austenite by reducing their surface area.

The rate of transformation upon cooling from the gamma phase is strongly dependent upon the rate of pearlite nucleation as well as

the rate of carbon diffusion. The nucleation rate is proportional to the degree of undercooling below the eutectoid temperature and so increases with decreasing temperature. The diffusion rate decreases with decreasing temperature. The result of these conflicting temperature dependences is that the transformation rate passes through a maximum some 100 - 200°C below the eutectoid temperature. It is convenient to depict the transformation characteristics of individual alloys by means of time-temperature-transformation (TTT) diagrams such as the one presented for the Fe.65C alloy in Fig. 2.3. The approximate times for onset and completion of transformation, and the nature of the transformation products, are shown as a function of equilibration temperature. TTT diagrams are presented for Fe.87C in Fig. 2.4 and for both FeCrC and HCC in Fig. 2.5. All these diagrams were taken from the Atlas of Isothermal Transformation Diagrams, U.S. Steel (1953). It was not possible to quench samples in the UHV sample-holder. The effect of the slow rate of cooling (Fig. 3.6) will have been to shift that portion of the TTT curves above the transformation "nose" to longer times. Cooling within the UHV system will have invariably produced pearlitic structures.

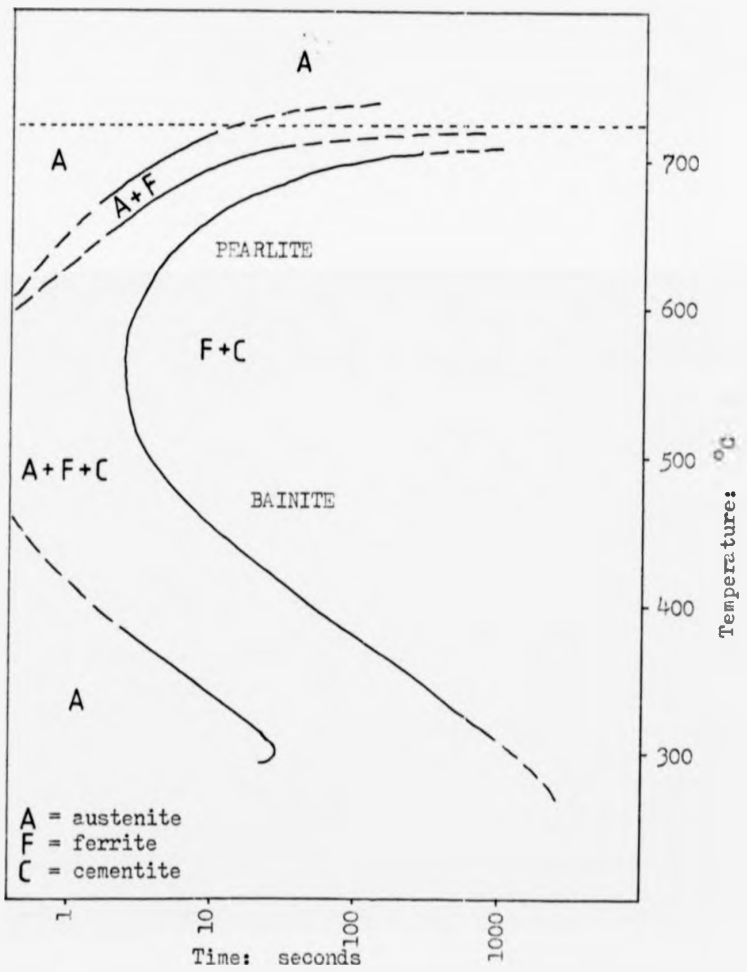

Fig. 2.3 Time-temperature-transformation diagram for a 0.65wt% carbon steel

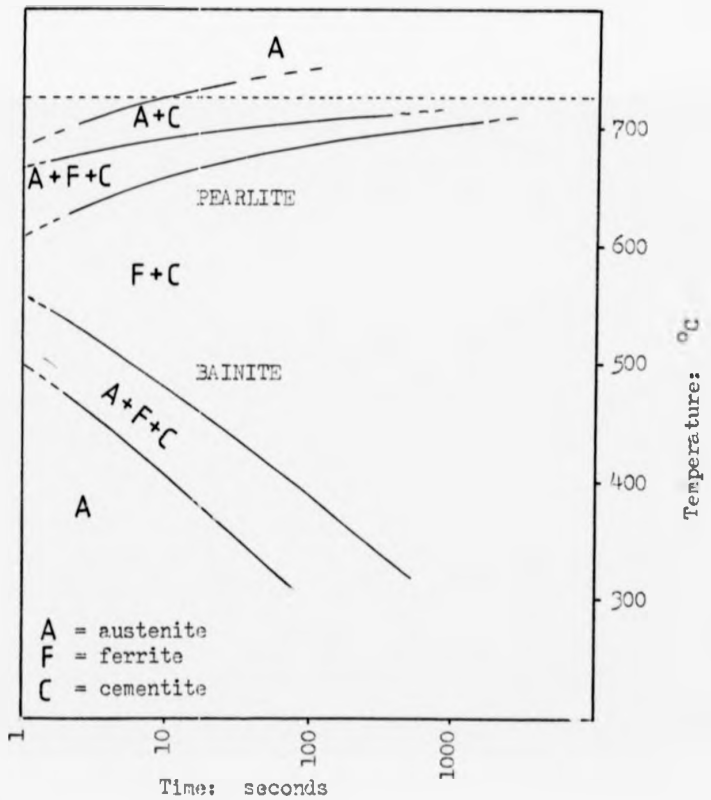

Fig. 2.4 Time-temperature-transformation diagram for a 0.87wt% carbon steel

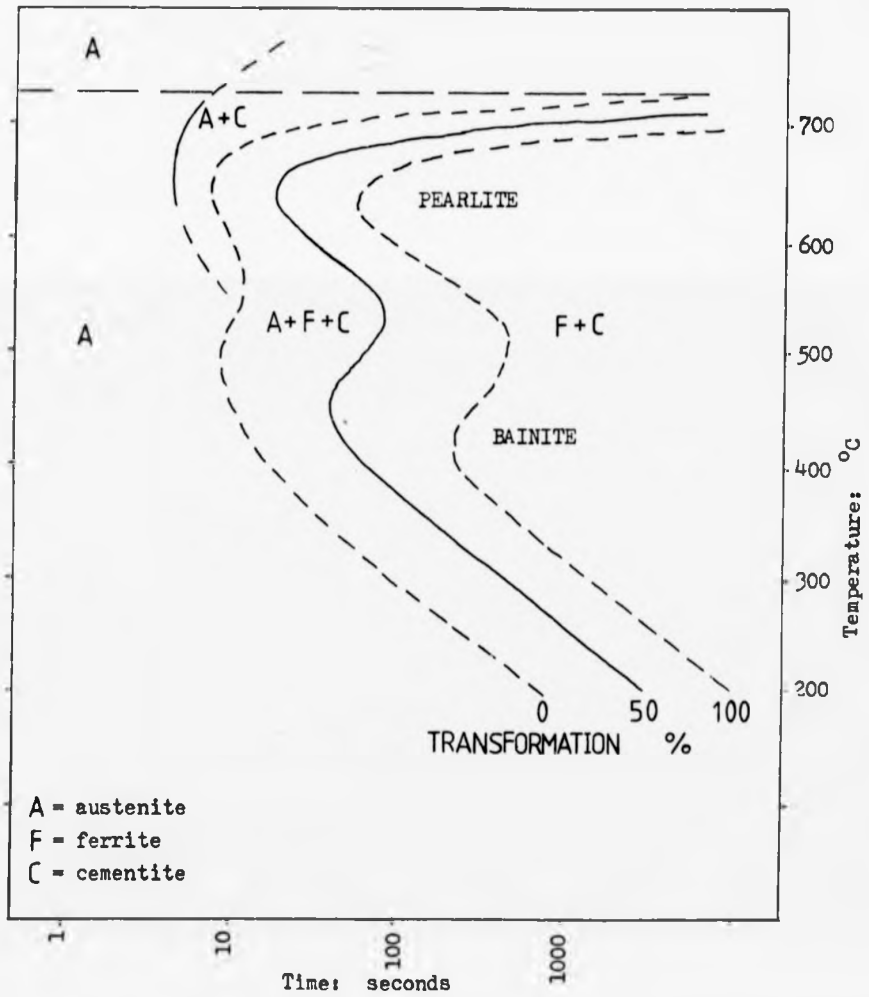

Fig. 2.5 Time-temperature-transformation diagram for a 1wt% carbon, 1¼wt% chromium steel

2.2. Auger electron spectroscopy

Auger electron spectroscopy (AES) is the surface analysis technique upon which the present work was based. The electronic process is described, followed by a brief history of the technique and a description of its application in the present case.

2.2.1. Auger electrons

When an atom is ionised by the removal of an inner-shell electron, the vacancy may be filled by a less well bound electron dropping down from an outer shell. The excess energy from this transition may either be emitted as X-radiation or transferred to a second outer-shell electron. In the latter case, the second electron is emitted from the ion with a kinetic energy equal to the difference in energy of the levels involved. This process is illustrated in Fig. 2.6 for an isolated atom (after Rivière (1973)). This electron-loss process was discovered by Auger (1925) during an experiment on the X-ray bombardment of gas atoms, and the emitted electrons have come to be known as Auger electrons.

2.2.2. Development of AES

The production of Auger electrons by electron bombardment of a solid surface was first demonstrated by Lander (1953). Although it was recognised at that time that the peaks in the ejected-electron spectra were characteristic of the bombarded atoms, two further developments were necessary before the potential of the technique could be realised. Weber & Peria (1967) demonstrated that the already numerous low energy electron diffraction (LEED) systems could be readily modified for electron energy analysis, and Harris (1968) electronically differentiated the electron energy spectrum from an electrostatic deflection analyser to remove the large and varying

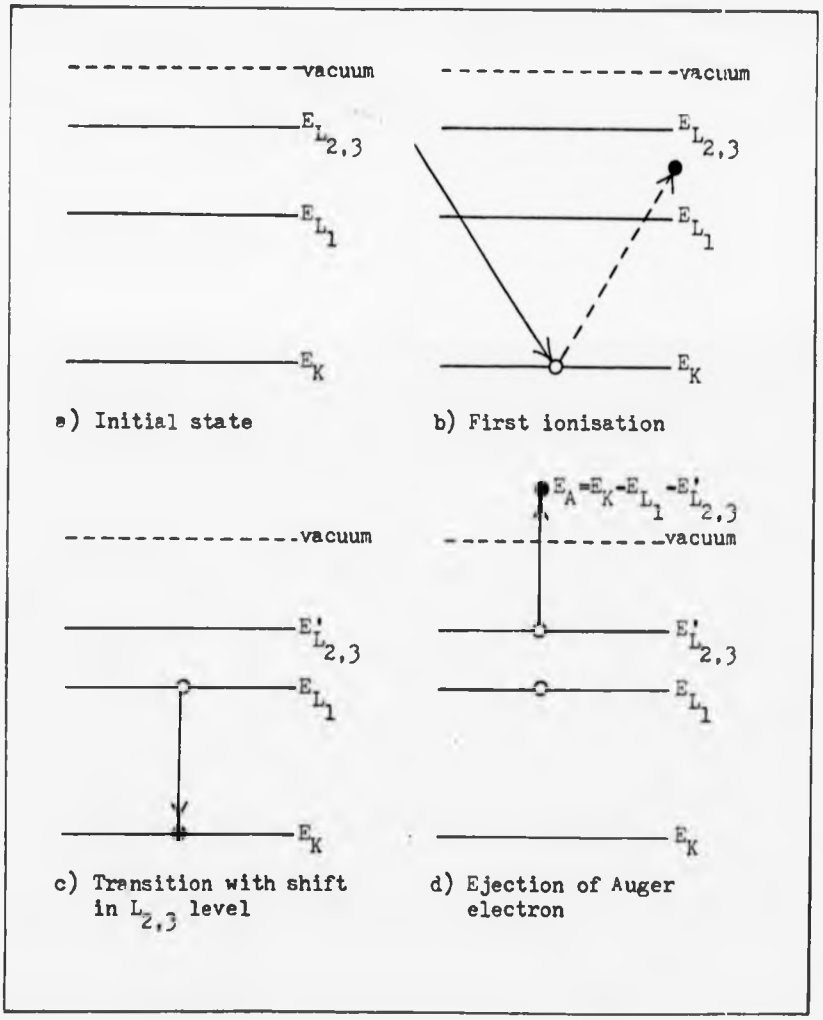

Fig. 2.6 The Auger process in an isolated atom

background. This permitted the Auger signal to be sufficiently amplified for AES to become a sensitive surface analysis technique. The great advantage of AES over conventional surface analysis methods, such as electron microprobe analysis, lay in its high degree of surface specificity. An Auger electron will only contribute to the peak characteristic of its emitting atom if it is able to leave the surface layers without losing energy by inelastic collision. The most commonly analysed characteristic Auger peaks lie in the energy range 40 - 1000eV. The inelastic mean free paths of electrons in this energy range when passing through solid materials have been reviewed by Seah & Dench (1979), and are less than 50Å. In favourable cases they can be as low as 5Å. This indicates how highly surface specific AES can be.

2.2.3. Application to this work

The sample surfaces were bombarded by a 2.5keV electron beam, and the electrons emitted from the surface were collected by a cylindrical mirror energy analyser (CMA). This type of analyser was first suggested as being suitable for Auger analysis by Palmberg et al (1969). It consists of two co-axial cylinders, to the outer of which is applied a repulsive voltage while the inner is earthed. Electrons enter the co-axial space through an aperture, follow a curved path in the electrostatic field and leave again via a second aperture if their energy is such that their path has been bent by the correct amount. They are then collected and the current measured while sweeping the applied voltage over an appropriate range to produce an energy spectrum. The experimental details of the use of this type of analyser are given in Chapter Three, together with details of the electron gun used for the bombardment.

Qualitative analysis relies upon the position of the Auger peaks in the energy spectrum; these are known for all the analysable elements. For quantitative analysis the Auger peak-to-peak height of an element in the differentiated spectrum is related to that element's peak-to-peak height from a standard. Alternatively, for a thin layer of an element at the surface of another element, the peak-to-peak heights of the two elements may be compared. This ratio can be compared with those established by other workers as corresponding to particular degrees of surface coverage. Care must be taken that this method is not used for those systems where the overlayer causes attenuation of the Auger signal from the matrix. Differences in experimental conditions must also be taken into account. The Auger calibrations that were used in the present work are described in Appendix B.

2.3. Surface segregation and precipitation

Segregation has been defined by Hondros & Seah (1977) as "the highly localised changes in concentrations achieved during the solid-state thermal redistribution of species between the matrix and interfaces". Used in this way, the term segregation does not describe the chemical state of the species at the interface, but only the diffusion process which results in its concentration there. In the present work, a distinction will be made such that surface segregation describes a single-phase process and surface precipitation describes a two-phase process. A review of surface segregation studies on ferrous alloys made using AES is presented below. Although the present work is limited to surface studies, the original commercial problem concerned grain boundary segregation. For this reason, the relationship between surface and grain boundary segregations is also described. The final part of this section is devoted to a description of surface precipitation studies relevant to the present work.

2.3.1. Surface segregation

The first analysis of surface segregation using AES was made by Harris (1968A,B), who showed that sulphur was concentrated at the surface of iron samples which had been heat-treated in vacuo. He also found sulphur, together with chromium and antimony, at the surface of a nickel-chromium steel. Subsequently, much use was made of AES to study grain boundary segregation, and this work has been reviewed by Hondros & Seah (1977). AES has also been found to be a useful tool for establishing the degree of surface cleanliness.

The first attempt to study surface segregation on iron under controlled conditions was made by Bishop & Rivière (1970). They found that ion bombardment, when used to clean the surface, produced

a small Auger peak due to implanted argon but also a large carbon Auger peak which they attempted to explain in terms of a buried carbon layer. On heating at 500°C for five minutes, the carbon Auger peak was reduced while that due to argon was much increased as the argon outgassed. Heat treatments at successively higher temperatures removed both carbon and argon but produced increased levels of sulphur, boron and nitrogen. Their sample was doped with boron; the other two elements were impurities in the iron. Surface treatments designed to remove sulphur increased the segregation of both boron and nitrogen. These were the first observations of competition between surface segregants.

Shell & Rivière (1973) investigated phosphorus segregation to a clean iron surface as a function of both temperature and bulk phosphorus concentration. They produced an Auger calibration for phosphorus on iron by comparing measured phosphorus:iron peak height ratios with values predicted by a calculation. This was based upon Crank's diffusion equation, and plausible assumptions were made about the distribution of phosphorus at the surface. Their results indicated that the surface saturation level was independent of both temperature and bulk phosphorus content, and was in good agreement with Hondros' value (1965) from a study of surface energy lowering. Shell & Rivière observed site-competition between sulphur and phosphorus. It was necessary to produce a near-surface sulphur depletion layer before true phosphorus segregation occurred. Throughout their experiments the levels of carbon, nitrogen and oxygen were either zero or very low.

Also in 1973, workers at the National Physical Laboratory began to report a systematic study of interfacial segregation in iron alloys (see for example Seah & Lea (1975)). Their aim was to be able

to produce a coherent set of theories of interfacial segregation. The two systems that they chose to study were iron-sulphur and iron-tin-sulphur. Iron was chosen as solvent because of its economic importance. Both tin and sulphur were known to embrittle iron as a result of grain boundary segregation. Sulphur is commonly present in steels as a result of poor steelmaking cleanliness; tin is introduced into steel by the recycling of ferrous scrap. The main findings of the surface segregation studies were that:

1) tin segregation saturated at two monolayers coverage,
2) sulphur segregation never exceeded one monolayer,
3) there was strong site-competition between tin and sulphur when total surface coverages exceeded one monolayer,
4) evaporation from the free surface was significant at temperatures above 500°C for sulphur and 700°C for tin,
5) sulphur still segregated after manganese had been added to tie it down, but only after an induction period. Manganese evaporation from the free surface was thought to be responsible for the occurrence of sulphur segregation in the manganese-treated alloys.

The relationship between surface segregation and grain boundary segregation was also determined for these systems. This is discussed below.

The first results on single-crystals of iron were reported by Grabke et al (1975). Their samples were doped with 10 - 90ppm of carbon and also contained low levels of sulphur as an impurity. The sulphur segregated freely, suppressing carbon segregation. No effects of evaporation were observed below 700°C. In a later paper (1977) they demonstrated that, given sufficient time, sulphur would displace both carbon and nitrogen from an iron surface. A bulk sulphur content of

only 10ppm produced a saturated surface layer (c(2x2) on Fe(100)) between 600°C and 850°C. Below 600°C the rate of sulphur segregation was very slow. Nitrogen gave saturation coverage up to 500°C, above which temperature desorption became important.

Swartz & Holloway (1977) examined surface segregation on samples of iron produced by compression of iron powder. These contained lower levels of carbon than of sulphur (0.01% carbon, 0.02% sulphur). They found that carbon segregated to the surface in the range 100°C to 600°C. At higher temperatures, sulphur gradually began to replace carbon at the surface until by 700°C it had become the dominant segregant. The level of carbon segregation did not saturate and varied from sample to sample. Their conclusion was that carbon desorbed rapidly above 500°C and they presented some mass-spectroscopic evidence in support of this theory.

Yen et al (1978) investigated phosphorus segregation to the free surface of a ferritic-iron alloy. The phosphorus saturation level was independent of temperature in the alpha range and was in good agreement with that reported by Hondros (1965). The time-history of the approach to saturation was, however, far from reproducible until they used an 'at-temperature' ion-bombardment to deplete any fast sub-surface diffusion paths. They were then able to deduce sensible values of the phosphorus lattice diffusion coefficient from their kinetic studies of surface segregation.

Clayton & Burstein (1979) used AES to study the pattern of surface segregation in the iron-nickel-antimony system. Sulphur was present as an impurity and they observed surface site-competition between sulphur and antimony. When the sulphur segregation had been removed by at-temperature ion-bombardments, the equilibrium segregation

level of antimony was found to be 1.3 monolayers and was independent of temperature. Equilibrium segregation levels of nickel decreased with increase in temperature, from 0.5 monolayers at 770K to 0.2 monolayers at 1150K.

As more and more data from AES studies of segregation have become available, so the theoretical understanding of the segregation process has developed. Hondros & Seah (1977) have produced a comprehensive review of this development, and so only a brief outline will be given here.

The first adsorption isotherm developed which has subsequently been applied to interfacial segregation is that of Langmuir (1916). It assumes a single layer of a single adsorbate, occupying a fixed number of identical sites with no site-site interactions. Seah & Hondros (1973) have used this isotherm to describe their results for sulphur segregation at iron grain boundaries. It predicts that the segregation level should be proportional to solute content, and inversely proportional to temperature. Brunauer et al (1940) have produced another version of this isotherm using a different approach and this has also been applied to interfacial segregation.

If the single-layer requirement is relaxed, the adsorption may be described by the more general BET isotherm (so-called after the initials of its authors; Brunauer, Emmett & Teller (1938)). This is the most commonly applied isotherm in gas adsorption studies. Seah & Hondros (1973) found an excellent correlation between its predictions and their grain-boundary results from the iron-tin system. They found that there was no site-competition between sulphur and tin at the grain boundaries and extended the isotherm to account for this case.

The most important remaining development in the use of isotherms that will be described here is the taking into account of site-site interactions (Fowler & Guggenheim (1939)). These interactions may be intra- or inter-species, and may be attractive or repulsive in nature. Shelton et al (1974) used an 'intra-species attractive interaction' version of this isotherm to describe the behaviour of carbon at the surface of nickel. For strong attractive forces, the temperature dependence of segregation can become discontinuous. Shelton et al had found that there was a very sharp onset of graphite precipitation as the temperature of the nickel surface was reduced. Attractive, inter-species interactions have been used by Guttmann (1975) to explain the apparently co-operative segregation of certain impurities and alloying elements in steels. If one element segregates to an interface it may attract a second element, increasing the second element's segregation level at the same interface. Lea & Seah (1975) were able to explain the observed site-competition between tin and sulphur at the surface of iron in terms of a repulsive, inter-species interaction.

2.3.2. Grain boundary segregation related to surface segregation

The present work is a study of surface segregation while the commercial problem was one of possible grain boundary segregation. It is therefore worthwhile to consider the relationship between segregations at the two types of interface. Seah & Lea (1975) have made the only complete study of this relationship. They measured the equilibrium segregation levels of tin at the surface of iron and correlated their results with some grain boundary results from the same system which had been reported previously (Seah & Hondros (1973)). For dilute systems at 550°C the surface segregation level was 130 times the grain boundary

level. The ratio of the segregation levels at the two interfaces fell with increasing temperature. The ratio at 1420°C has been found from interfacial energy measurements to be 6. There was a qualitatively similar variation of the ratio with increasing solute concentration as with increasing temperature.

Seah & Lea were able to show that the above results were all compatible with a BET-based theory of segregation, provided that all the relevant entropy terms were included (site-multiplicity, vibrational and anharmonic). The implication is that if the surface segregation behaviour is studied in a particular system it may be possible to predict the corresponding grain boundary levels. The conversion relies on the measurement of the high-temperature surface to grain-boundary ratio using interfacial energy techniques. This high-temperature ratio is then extrapolated down to the required temperature by means of the version of the modified BET equation relevant to the particular system. Seah & Lea suggested that an alternative might be to set up a data-bank containing experimental results for each major system, so that the surface segregation level could be correlated with the equivalent grain boundary level simply by looking up the relevant diagram.

2.3.3. Surface precipitation

When a species has segregated to the surface it may take part in the formation of a new phase. The precipitation of graphite at the surface of iron is a good example of this type of behaviour. Olney & Smith (1959) made a detailed study of this phenomenon using optical techniques. They concluded that:

1) graphite would only precipitate on hyper-eutectoid samples,

2) graphite precipitation only occurred upon cooling from the gamma

phase, not when holding in the alpha range,

3) surface precipitation was inhibited by the presence in the steel of carbide-forming elements such as chromium and manganese,

4) the extent of the precipitation was strongly dependent upon the surface orientation, and graphite layer growth could be accompanied surface facetting,

5) graphite precipitation produced a sub-surface region depleted of carbon, inhibiting cementite precipitation upon subsequent thermal cycling.

This work was followed up by Speich (1961) who demonstrated that the graphite layer was always formed with its basal plane parallel to the substrate surface. He also investigated the effect of surface orientation in some detail, finding that graphite precipitation on gamma iron occurred most readily on close-packed (111) surfaces. Speich suggested that the high rate of graphite nucleation on surface orientations close to (111) was a result of the good matching between the austenite surface and the graphite basal plane, and hence the low energy of the interface. Fig. 2.7 illustrates this close matching for an iron sample containing 0.88wt% carbon at 700°C. L'nyanoi (1975) has measured interfacial energies as low as 25 - 50 erg cm^{-2} for this system.

When modern surface analysis techniques such as AES and LEED were applied to the study of graphite precipitation upon iron, it was found that the first two of Olney & Smiths' conclusions were not in fact correct. Grabke et al (1975) found that graphite would precipitate at the surface of a sample of iron doped with only 90ppm of carbon when it was held in the alpha range. The graphite was, however, only a few monolayers thick at most and could not have been

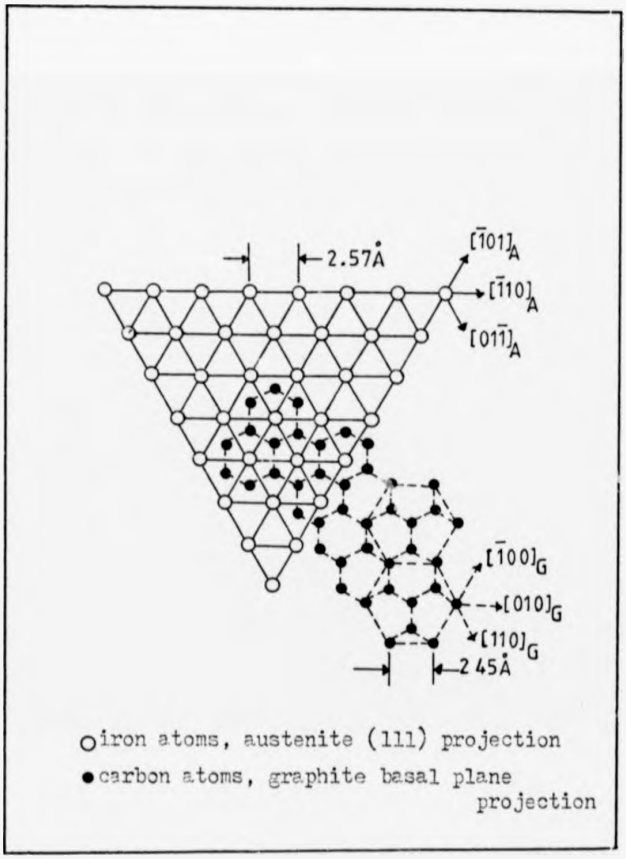

Fig. 2.7 lattice matching between the austenite (111) surface and the graphite basal plane

observed by Olney & Smiths' optical techniques. Grabke et al observed that on an iron (100) surface the graphite layer dissolved at the temperature predicted from the iron-graphite equilibrium phase diagram, leaving a layer of segregated carbon with a c(2x2) structure. The fine-structure of the carbon Auger peak was found to depend on its chemical state, so that graphite and segregated carbon could be distinguished.

Grabke et als' results represent the only substantial study of graphite precipitation on iron that has been published. There has, however, been much work undertaken on the nickel-graphite system, and these results are reviewed here because they contain relevant information. Coad & Riviere (1971) studied the fine structure of the carbon Auger peak from a nickel surface. They also identified two distinct types of structure, but attributed them to nickel carbide and graphite. The carbide structure was produced by quenching the sample, and it was irreversibly transformed to the graphite structure upon heating in the temperature range 400 - 600°C.

Shelton et al (1974) studied equilibrium segregation of carbon to th (111) surface of nickel single crystals doped with carbon. They found three distinct equilibrium states of the surface:

1) a high-temperature dilute carbon phase (segregation),
2) a condensed graphitic monolayer,
3) a multilayer epitaxial graphite precipitate.

The multilayer precipitate was present at temperatures below the equilibrium temperature for dissolution into the nickel crystal. Above this temperature, a graphitic monolayer persisted for a further 100°C. Carbon was only present as a segregant at high temperatures. Shelton et al were able to produce a coverage calibration for graphite

upon nickel based on the observed attenuation of the nickel substrate Auger signal in the graphite overlayer.

Mojica & Levenson (1976) attempted to derive the kinetics of graphite precipitation at a polycrystalline nickel surface by monitoring the carbon Auger signal. Their carbon time-histories had two distinct regions. At the start of the experiments, a background level of carbon was formed. They interpreted this as being a layer of segregated carbon. With time, the carbon level increased and the carbon Auger peak began to show the fine structure associated with graphite. The precipitation process thus appeared to proceed in two stages. Upon heating the sample to the equilibration temperature carbon diffused out of the bulk to form a segregated base-level carbon concentration. When graphite had nucleated at favourable sites, its island growth was fed by cross-surface diffusion of the segregated carbon. They assumed that the base-level concentration was constantly being replenished by further carbon diffusion from the bulk.

Gijzeman et al (1973) commented that while they agreed with Mojica & Levenson's interpretation of the graphite growth mechanism, they thought that the way the data had been treated was incorrect. Mojica & Levenson had normalised their carbon Auger peak to the nickel substrate Auger peak, and the latter was obviously suffering some variable attenuation due to the growing graphite layer. Gijzeman et al went on to derive an analysis of the data, based on a treatment of two-dimensional nucleation and growth by Avrami (1939). Their resulting equation gave an excellent fit to Mojica & Levensons' results.

2.4. Segregation kinetics

2.4.1. Grain boundary segregation

During the process of interfacial segregation, atoms of the segregant must diffuse out of the bulk to the interface. The kinetics are therefore controlled both by diffusion in the bulk and by the boundary conditions at the interface. McLean (1957) evaluated the time-dependence of grain boundary segregation by applying Fick's law for bulk diffusion, with the rate of solute diffusion out of the grains set equal to the rate of accumulation at the interface. As a boundary condition he assumed that there was a constant ratio between the solute concentration in the interface, C_s^t, and the solute concentration at the faces of the adjacent grains, C_o^t, such that:

$$C_s^t = \alpha C_o^t$$

where α is called the enrichment ratio. This lead to a fairly simple solution describing the time dependence of solute concentration at any distance, x, from the grain boundary:

$$C_x^t = C_\infty - C_\infty (1 - 1/\alpha) \exp\left\{ \frac{2x}{\alpha d} + \frac{4Dt}{\alpha^2 d^2} \right\} \operatorname{erfc}\left(\frac{x}{2\sqrt{Dt}} + \frac{2\sqrt{Dt}}{\alpha d} \right)$$

where C_∞ is the bulk solute concentration, D is the bulk diffusion coefficient and d is the thickness of the interface. This solution has not been applied to many systems but Seah (1977) found that it could be used to explain some metallurgical results where embrittlement due to phosphorus segregation was suspected.

2.4.2. Surface segregation

Surface segregation is conceptually the same as grain boundary segregation except that segregant atoms can only arrive from one side of the interface. Lea & Seah (1977) have applied McLean's analysis

to surface segregation using the same boundary condition. They produced the following equation:

$$C_x^t = C_\infty - C_\infty(1 - 1/\alpha)\exp\left(\frac{x}{\alpha d} + \frac{Dt}{\alpha^2 d^2}\right)\operatorname{erfc}\left(\frac{x}{2\sqrt{Dt}} + \frac{\sqrt{Dt}}{\alpha d}\right)$$

where d is now interpreted as the solute monolayer thickness or atomic size. Lea & Seah had accumulated a great deal of data on the iron-tin system. When they attempted to apply the above equation, they found that it could not adequately describe their results.

Lea & Seah next modified their equation to take into account evaporation from the free surface into the vacuum. Evaporation was represented as being proportional to surface concentration. The prediction of the modified equation was that if evaporation was a significant factor, the surface concentration would not reach saturation but would pass through a maximum before falling to a low level. The incorporation of a correction for evaporation was, however, still insufficient to make the equation more than an approximation to their results. They then altered the boundary condition from a constant to a time-variant enrichment ratio. The time variance was chosen to give the best fit between the prediction of the equation and the observed segregation time-histories. While this allowed Lea & Seah to deduce solute diffusivity data for the iron-tin system, it did not make the equation universally applicable because the exact nature of the time varience would be expected to depend on the system observed.

A second example of the use of surface segregation studies in the calculation of solute diffusivity data was reported by Yen et al (1978). They made observations of phosphorus segregation to the surface of a ferritic iron alloy and found that by using a solution of diffusion to a plane with Langmuirian adsorption they were able to

deduce sensible values of the phosphorus lattice diffusion coefficient. The solution that they used was due to Reinmuth (1961). He had begun (as had McLean) with Fick's law of bulk diffusion and the assumption that the material flux at the boundary was equal to the rate of adsorption. He also assumed that Langmuir's adsorption isotherm was obeyed, ie.

$$\Gamma_t / \Gamma_e = C/(C + a)$$

where Γ_t is the instantaneous surface coverage, Γ_e is the saturation coverage and 'a' is the isotherm constant. His boundary condition, however, was that the surface and bulk solute concentrations were related by:

$$C_s^t = C_\infty - (D/\pi)^{\frac{1}{2}} \int_0^t (\partial C/\partial x)\,(t - \tau)^{-\frac{1}{2}}\, d\tau$$

where τ is an integration variable. Reinmuth obtained this relationship by adapting an equation from Carslaw & Jaeger's (1947) treatment of heat conduction in a solid. It is the solution, using Duhamel's Theorem, of the surface temperature's time-dependence when a body at zero temperature with a surface at a finite temperatur. is llowed to equilibrate. The surface temperature falls with time until the body is at a uniform temperature. This can be seen to be the reverse of the process of segregation.

Reinmuth defined three dimensionless parameters:

$$\mu = \Gamma_t/\Gamma_e \qquad \psi = C_\infty/a \qquad \theta = 4\pi a^2 D t/\Gamma_e^2$$

He found a general solution which was of the form:

$$\mu = \sum_0^\infty a_j \theta^{j/2}$$

where the coefficients, a_j, are given by a rather cumbersome recurrence formula. However, if there is no adsorption at time zero then the first of these, a_o, is zero and the second, a_1, is equal to Ψ/π. The remaining coefficients may be neglected, so that the final solution is:

$$\Gamma_t/\Gamma_e = \frac{2C_\infty}{\Gamma_e}(Dt/\pi)^{\frac{1}{2}}$$

Hence, plotting log(coverage) against log(time) should give straight lines of slope 0.5 and intercepts from which D may be calculated. There is no correction for evaporation in this equation but Yen et al were probably working at low enough temperatures for evaporation to be neglected.

Rowlands & Woodruff (1979) approached the problem in a different way. They started from the basic physical mechanism of surface segregation: jumping probabilities in-to and out-of the surface layer. The bulk was treated as a series of planes, with the change in concentration with time of the n^{th} plane being given by:

$$\frac{\partial C_n}{\partial t} = P_B \left\{ (C_{n+1} - C_n) - (C_n - C_{n-1}) \right\}$$

where P_B is the probability per unit time that a solute particle jumps from one layer to the next, ie.

$$P_B = D/d^2$$

where 'd' has now become the interplane spacing. This probability will be uniform in the bulk but will have a different value at the surface because of the different binding energy. Diffusion in the bulk was treated using a diffusion approximation, and probability terms were included to take into account evaporation from the free surface.

In order to arrive at a suitable boundary condition, the vacuum outside the surface was represented by an array of layers with a structure identical to the real medium, but with a different hopping probability. The time dependence of the concentration ratio between the surface layer and the boundary layer was found by Laplace Transform techniques to be:

$$C_b^t = \frac{\sigma}{D^{\frac{1}{2}}} C_s^t + C_b^t C_s^t / C_m$$

where C_b^t and C_s^t are the instantaneous concentrations in the boundary and surface layers, C_m is the maximum concentration that the surface layer can support and σ is given by:

$$P_s = \sigma(D^{\frac{1}{2}}/d)$$

where P_s is the probability per unit time that a particle hops from the boundary layer to the surface layer. It can be seen that this boundary condition is basically McLean's original condition ($C_b \propto C_s$) plus a non-linear saturation term.

Using the above methodology, a general equation describing surface segregation was deduced. Two special cases of this solution will be considered here. The first of these is 'no saturation, no evaporation' when the general equation reduces to:

$$C_s^t = \frac{C_\infty D^{\frac{1}{2}}}{\sigma} \left\{ 1 - \exp(\sigma^2 t)\ \mathrm{erfc}(\sigma t^{\frac{1}{2}}) \right\}$$

This is identical to the form produced by Lea & Seah for their 'no evaporation' case. The second special case is that of 'saturation, no evaporation'. Under these conditions the general equation reduces to a form which may be approximated by a straight line whose equation is:

$$\Gamma_t/\Gamma_e = (2C_a/C_m)\,(Dt/\pi)^{\frac{1}{2}} \qquad \text{where } C_a = C_\infty/d$$

This is identical to the solution by Heinmuth which was described above.

This simple equation will only fail to give an adequate description of surface segregation as saturation is approached or when evaporation becomes significant. Rowlands & Woodruff showed that the effect of saturation at the surface was analagous to Lea & Seahs' time-varient enrichment ratio, and that some of Lea & Seahs' results from the iron-tin system could be described by theoretical curves corresponding to the 'saturation, no evaporation' special case. One advantage of the Rowlands & Woodruff approach is that it is of general use and can easily be extended to account for inter-species interactions. This should be particularly important when considering grain boundary segregation in alloy steels. Interactions between impurities and alloying elements can lead to an increase in segregation levels over the 'unalloyed' case.

REFERENCES for Chapter Two

Auger P., Comptes Rendus 130(1925)65

Avrami M., J. Chem. Phys. 7(1939)1103

Bishop H.E. & Rivière J.C., Acta Met. 18(1970)813

Brunauer S., Deming L.S., Deming W.S. & Teller E., J. Am. Chem. Soc. 62(1940)1723

Brunauer S., Emmett P.H. & Teller E., J. Am. Chem. Soc. 60(1938)309

Carslaw H.S. & Jaeger J.C., Conduction of Heat in Solids 1947, p57

Clayton J.Q. & Burstein G.T., Metal Science, Sept(1979)530

Coad J.P. & Rivière J.C., Surface Science 25(1971)609

Fowler R.H. & Guggenheim E.A., Statistical Thermodynamics 1939, C.U.P.

Gijzeman O.L.J., Schouten F.C. & Bootsma G.A., Surf. Sci. 71(1973)174

Grabke H.J., Tauber G. & Viefhaus H., Scripta Met. 9(1975)1181

Grabke H.J., Paulitschke W., Tauber G. & Viefhaus H., Surface Science 63(1977)377

Guttmann M., Surface Science 53(1975)213

Hansen M. & Anderko K., Constitution of Binary Alloys 1958, McGraw-Hill

Harris L.A., J. App. Phys. 39(1968)1419

Harris L.A., J. App. Phys. 39(1968)1428

Hillert M., Nilsson K. & Torndahl L.E., J.I.S.I. 209(1971)49

Hondros E.D., Proc. Roy. Soc. A286(1965)479

Hondros E.D. & Seah M.P., Int. Met. Reviews N° 222, 1977

Lander J.J., Phys. Rev. 91(1953)1382

Langmuir I., J. Am. Chem. Soc. 38(1916)2219

Lea C. & Seah M.P., Phil. Mag. 35(1977)213

L'nyanoi V.N., Izv. V. U. Z. Fiz. 12(1975)63

McLean D., Grain Boundaries in Metals 1957, O.U.P.

Mojica J.F. & Levenson L.L., Surface Science 59(1976)447

Olney M.J. & Smith G.C., J.I.S.I. 193(1959)107

Palmberg P.W., Bohn G.K. & Tracy J.C., App. Phys. Lett. 15(1969)254

Reinmuth W.H., J. Phys. Chem. 65(1961)473

Rivière J.C., Contemp. Phys. 14(1973)513

Rowlands G. & Woodruff D.P., Phil. Mag. 40(1979)459

Sawle A., Thesis 1974, University of Sheffield

Seah M.P., Acta Met. 25(1977)345

Seah M.P. & Dench W.A., Surf. & Interface Anal. 1(1979)2

Seah M.P. & Hondros E.D., Proc. Roy. Soc. A335(1973)191

Seah M.P. & Lea C., Phil. Mag. 31(1975)627

Shell C.A. & Rivière J.C., Surface Science 40(1973)149

Shelton J.C., Patil H.R. & Blakely J.M., Surf. Sci. 43(1974)493

Smith G.V., Weld. Res. Suppl. 13(1948)277

Speich G.R., Trans. Met. Soc. A.I.M.E. 221(1961)417

Swartz W.E. & Holloway D.M., Appl. Spect. 31(1977)210

Tofaute W., Sponheuer A. & Bennek H., Arch. Eisenhütt. 8(1934)499

Weber R.E. & Peria W.T., J. Appl. Phys. 33(1967)4355

Yen A.C., Graham W.R. & Belton G.R., Met. Trans. 9A(1978)31

CHAPTER THREE EXPERIMENTAL DETAILS

3.1. The ultra-high vacuum (UHV) system

The stainless steel UHV system was constructed at Warwick University. A photograph of the complete system and associated electronics is shown as Fig. 3.1. The major features of the system are detailed in the sections which follow.

3.1.1. General

A schematic of the vacuum system is shown in Fig. 3.2. The main vacuum chamber consisted of two regions: an experimental area and a service well. All pumping facilities were connected to the well; the titanium sublimation pump was placed below the baffle in order to keep evaporated metal out of the experimental chamber. The system was maintained under UHV by a Mullard 150 litre sec^{-1} magnetron ion pump. Supplementary capacity was provided by an Edwards E04 polyphenyl-ether diffusion pump. This was essential during experiments, when outgassing of the sample-heating stage and electron gun were at a maximum, and also during ion bombardment as described in the next section. The diffusion pump was backed by an Edwards ES200 rotary pump via a molecular-sieve oil trap. A liquid nitrogen cooled trap and baffle were placed between the diffusion pump and the service well to keep the pumping oil out of the main system.

System pressures were monitored by Pirani gauges (1 barr to 10^{-3} torr) and ion gauges (10^{-3} torr to 5×10^{-11} torr). A quadrupole mass spectrometer was used to check the composition of residual gasses; a useful diagnostic tool when checking for leaks. The final leak-test involved directing a jet of helium at the outside of the chamber while checking for helium incursions with the mass spectrometer. When the system was in a leak-tight state, its ultimate vacuum was

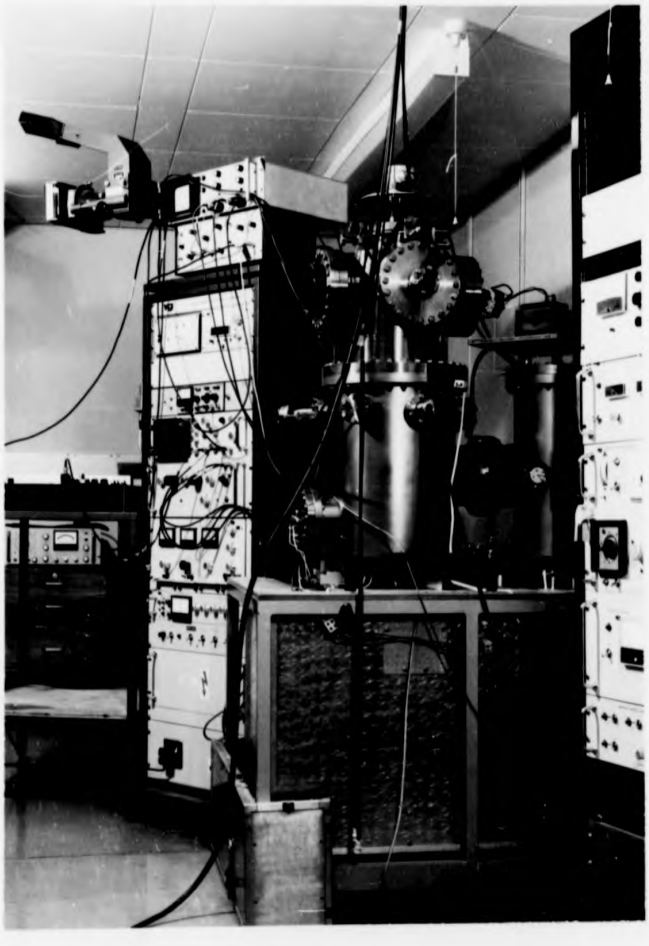

Fig. 3.1 General view of the ultra-high-vacuum system

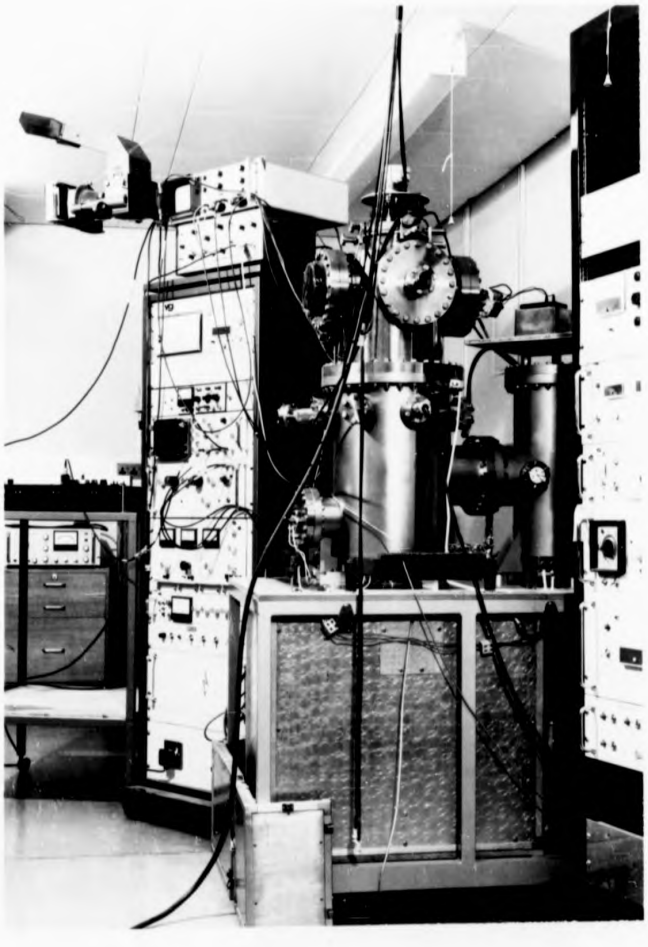

Fig. 3.1 General view of the ultra-high-vacuum system

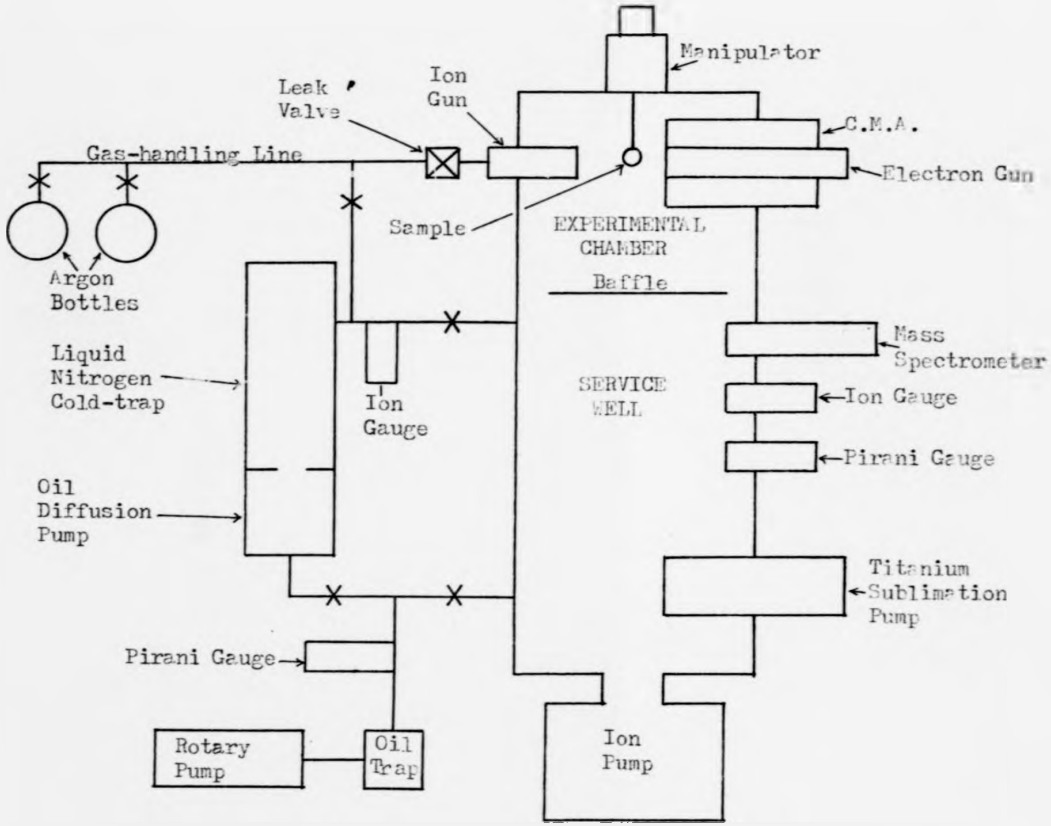

Fig. 2.2 General layout of the UHV system

limited by outgassing of the internal surfaces. As a result, it was necessary to remove as much gas as possible from these surfaces by enclosing the system in an oven and baking it at 250°C for twelve hours. During cooling, but while the system temperature was still above 100°C, all filaments in the chamber were outgassed by running them at, or higher than their normal operating temperatures.

Pressures of 5×10^{-10} torr were routinely achieved during experiments. This permitted several hours of experimental work before sample contamination by the residual gasses became a problem, as may be seen from a simple 'worst-case' calculation. The arrival rate of a gas of molecular weight 'm' at a surface is given by:

$$A = P/(2\pi mkT)^{\frac{1}{2}} \text{ molecules cm}^{-2} \text{ s}^{-1}$$

where P is the partial pressure of the gas above the surface. If we assume that every molecule arriving at the surface sticks to it, the time required for monolayer coverage of, for example, carbon dioxide may be estimated as a function of pressure. This gives times of about 3 minutes at 10^{-8} torr, 30 minutes at 10^{-9} torr and 5 hours at 10^{-10} torr. When the sample was heated, the sticking coefficients of contaminant gas molecules should have been reduced, but this may have been counteracted by local increases in the pressure because of outgassing of the sample-heating stage itself.

The problem of contamination was particularly serious for the present work. If carbon-containing molecules had been deposited on the sample surface, this could have been mistaken for carbon segregation. Oxygen-containing species would also have been a problem because the 500eV oxygen Auger peak can obscure the Auger peaks from chromium which occur at 489 and 529eV.

3.1.2. Ion bombardment

Before each experiment the sample was bombarded by argon ions to remove surface contamination. Two types of ion gun were used during the course of this study. Initially, a conventional 'hot-filament' ion gun was fitted into the system. In this type of gun, argon atoms are ionised by electrons emitted from a heated filament and are accelerated onto the sample by a 500eV potential. Argon was supplied to the gun by maintaining a virtually static argon pressure of 10^{-4} torr in the vacuum chamber. To achieve this, the rate of argon emission through a leak-valve was balanced with a small amount of pumping which was obtained by slightly opening the valve to the diffusion pump. Such high partial pressures of argon made the ion pump unstable and it had to be switched off during bombardments. The 1μA beam current obtained from this ion gun was adequate for sample cleaning. Each segregation experiment, however, produced a sub-surface zone depleted in the segregant. This was removed by bombarding away several microns of the surface, and required a prohibitively long bombardment time when using the conventional gun.

Eventually, the simple ion gun was replaced by a V.G. AG2 ion source. This offered several advantages. The cold-cathode ion source gave rise to very little outgassing and was very reliable. The ion beam could be focussed onto the sample, and the ion energy was continuously variable up to 10keV. The high source-efficiency was complemented by direct delivery of argon to the gun. This allowed normal pumping of the experimental chamber to be maintained during the bombardments. These features, together with the AG2's ten times greater beam current, resulted in very fast sputtering rates and hence fast removal of depletion zones.

The factors which determine the rate of erosion of the sample surface are the ion-beam current, its angle of incidence, the ion kinetic energy and the masses and surface binding energies of the target atoms. If all of these are known then the rate of erosion can be calculated. In theory, the distribution of a segregant with depth into the sample may be obtained by sequential bombardments and Auger analyses. Unfortunately the surface binding energies are poorly defined and have been shown by Schmerling et al (1980) to be of critical importance. So depth profiles can in fact only approximate the actual near-surface distributions. Depth profiling is still, however, a useful technique and it was used on occasion during this work.

Ion bombardment is very effective in removing surface contamination but care must be taken to minimise surface damage. 7keV ion bombardments were used to remove sub-surface depletion zones. High-energy bombardments maintain a relatively flat surface topography when removing large amounts of material but cause deeper surface damage than low-energy sputtering. After removing a depletion zone, a 500eV bombardment was used to remove the damaged layer. Short heat-treatments were also used to anneal the damaged layer. Ion bombardment may also result in ion implantation. Most of the implanted argon atoms would have been outgassed by the annealing heat-treatments. Precautions were taken to avoid the implantation of other ionisable species. Research-grade argon was used and the gas-handling line was twice evacuated and flushed with argon before its first use.

3.1.3. The sample-heating stage

The sample-heating stage was mounted on a manipulator which permitted X, Y and Z translation, 360° rotation about the Z axis and a limited amount of tilt. The heating was radiative and was achieved by passing a current through a thin molybdenum strip set in a slot in the bottom of each sample. A cross-section of this arrangement is shown in Fig. 3.3. A molybdenum heat-shield protected the CMA from evaporated metal. Two photographs of the heating stage are shown in Fig. 3.4.

Temperature measurement was by means of a thermocouple attached to the sample. To avoid measurement errors, the thermocouple was spot-welded to a point on the back of the sample opposite the area of the surface that was analysed. The two faces of the sample were maintained in similar radiative environments but some discrepancy would have arisen because of heat conduction along the thermocouple wires. It proved possible to observe phase transformations of the samples as hesitations in the heating or cooling curves. These could be used as rough internal calibrations.

It was recognised that the current in the heating strip would produce deviations in the paths of electrons approaching and leaving the sample surface. In addition, there was a small shift in Auger peak positions due to sample potentials but this was not a serious problem. Deflection of the incoming electrons would move the area that was being analysed. The likely extent of this problem was estimated by means of a simple model. Consider an electron of mass 'm' and charge 'e' moving with velocity 'V' towards the centre of a wire of length '2x' as shown in Fig. 3.5. If 'I' is the current in the wire and 'a_I' the initial distance of the electron from the

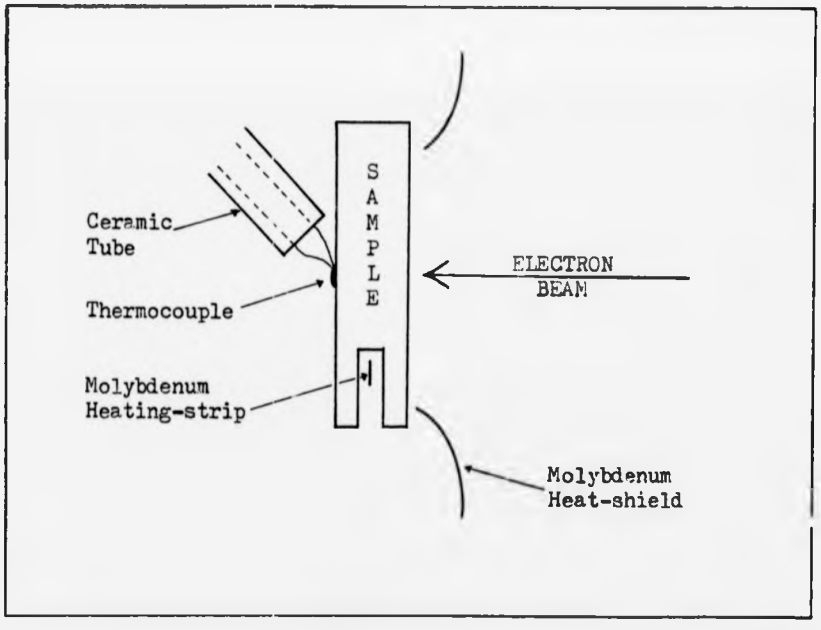

Fig. 3.3 Cross-section of part of the Heating-stage

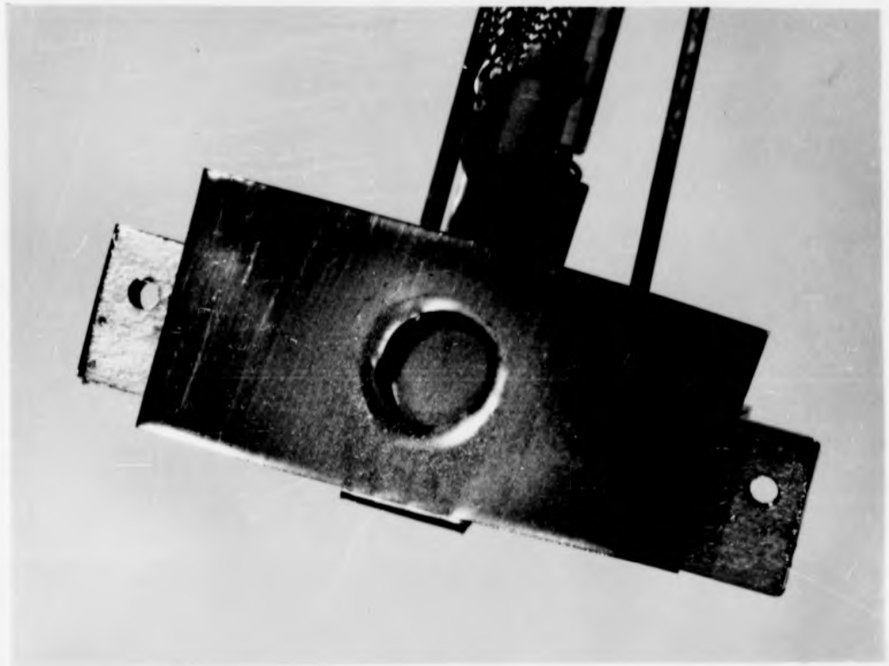

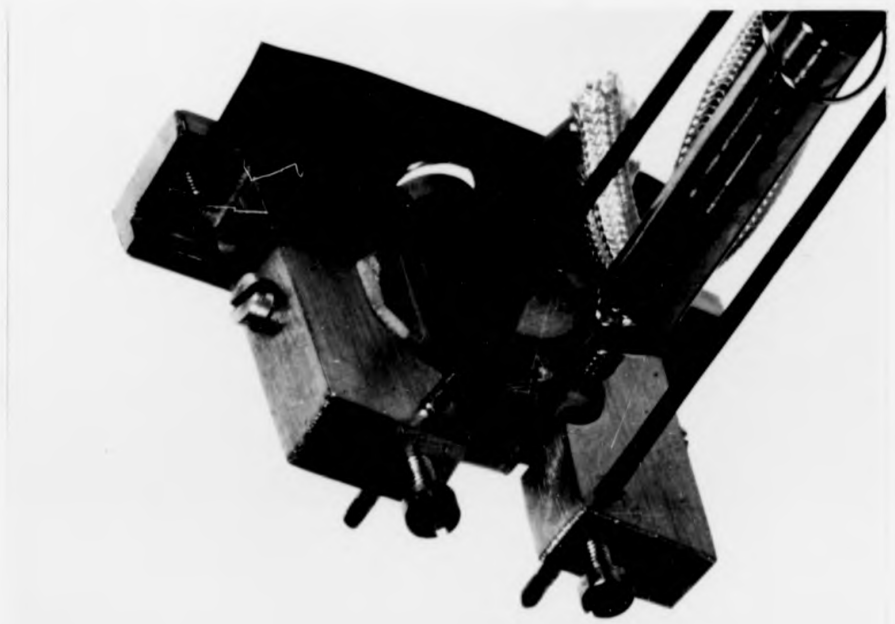

Fig 3.4 Two views of the specimen-heating stage

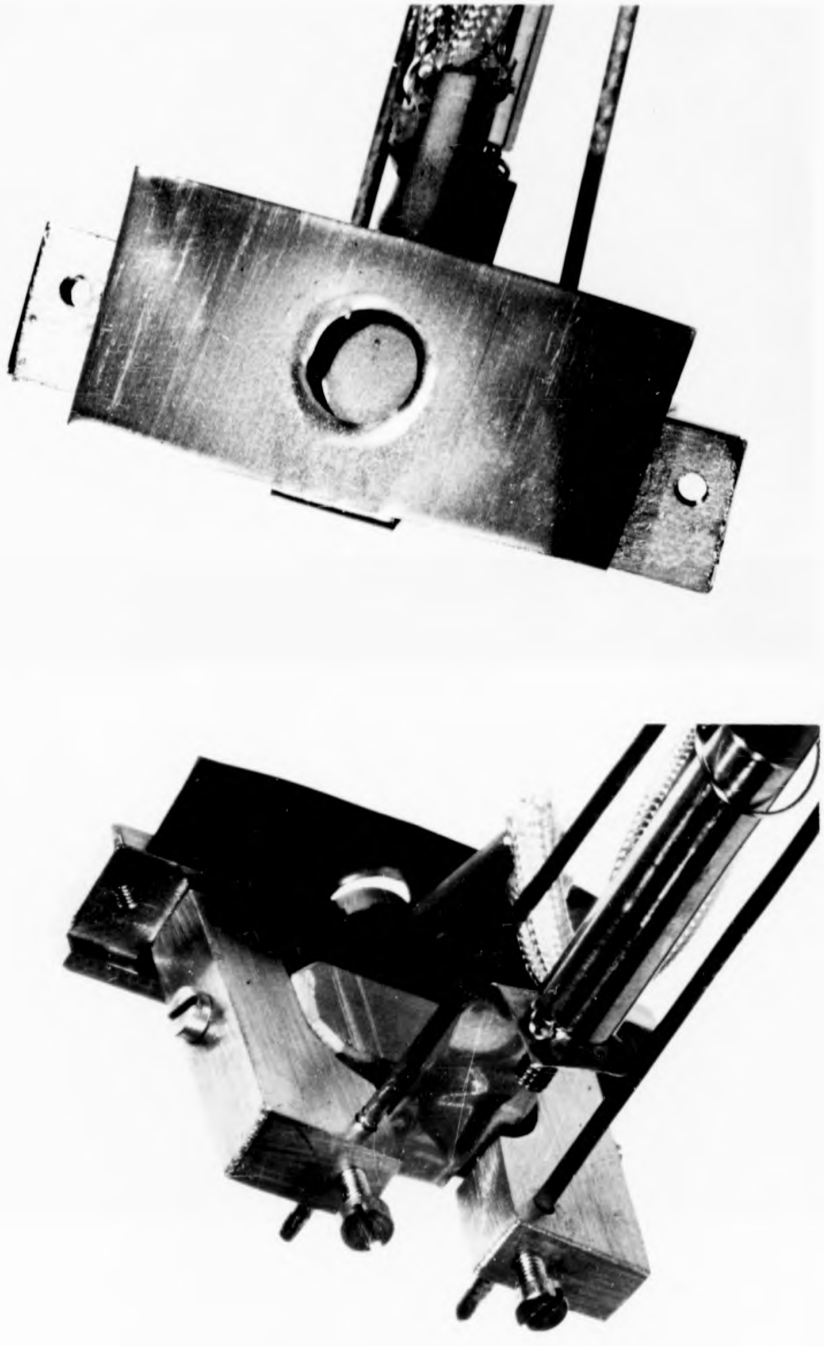

Fig 3.4 Two views of the specimen-heating stage

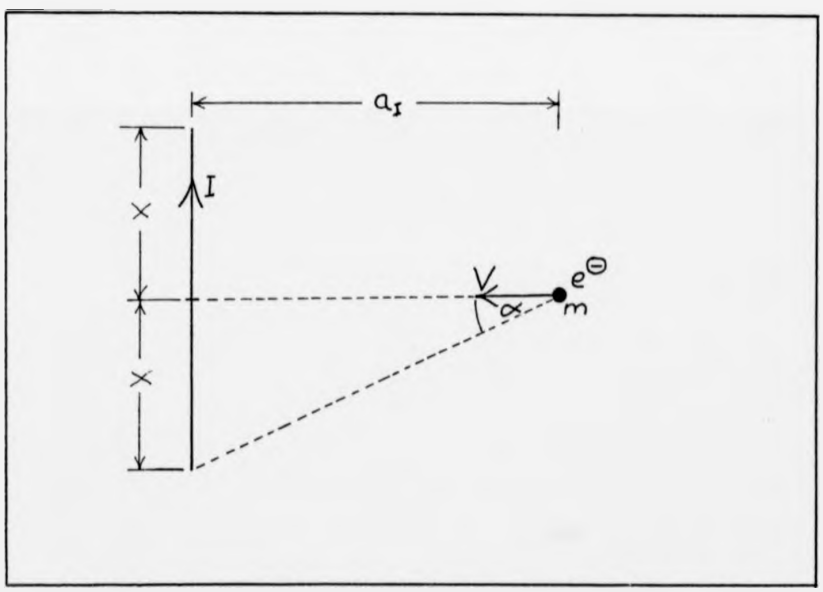

Fig. 3.5 Model of electron deflection by heating-stage field

wire centre then the field experienced by the electron will be:

$$B = \frac{\mu_0 I}{2\pi a_I} \int_{\alpha_1}^{\alpha_2} \cos\alpha \, d\alpha$$

where μ_0 is the permeability of free space. In this configuration $\sin\alpha_1 = 0$ and $\sin\alpha_2 = x/(x^2 + a_I^2)$. Hence the acceleration of the electron out of the plane of the diagram due to the field is:

$$A = BeV = \frac{IeV}{2\pi a_I m} \cdot x/(x^2 + a_I^2)$$

This equation was integrated numerically between the end of the electron gun and the surface of the sample (taking into account the more complicated geometry of the true situation). The total shift in the electron beam was found to be less than 5% of the beam diameter and so could be neglected.

The most serious problem was deflection of the slow, secondary electrons leaving the sample surface and being collected by the electron energy analyser. This very complex problem could not be analysed mathematically, but it was studied experimentally in two different ways. The first method was to measure the N(E) spectrum with the CMA as a function of heating-stage current. This gave an indication of the percentage of electrons deflected away from the analyser at the energy of each relevant Auger peak. The other method was to measure 'at-temperature' Auger peak-to-peak heights, then cool the sample as quickly as possible to room temperature and re-measure. It was assumed that there was no significant change in surface composition during cooling. Heating and cooling curves for a nickel sample are shown in Fig. 3.6. The results of both techniques indicated that Auger peaks with energies higher than about 250eV were not significantly affected by the heating currents used to obtain sample

wire centre then the field experienced by the electron will be:

$$B = \frac{\mu_0 I}{2\pi a_I} \int_{\alpha_1}^{\alpha_2} \cos\alpha \, d\alpha$$

where μ_0 is the permeability of free space. In this configuration $\sin\alpha_1 = 0$ and $\sin\alpha_2 = x/(x^2 + a_I^2)$. Hence the acceleration of the electron out of the plane of the diagram due to the field is:

$$A = BeV = \frac{1eV}{2\pi a_I m} \cdot x/(x^2 + a_I^2)$$

This equation was integrated numerically between the end of the electron gun and the surface of the sample (taking into account the more complicated geometry of the true situation). The total shift in the electron beam was found to be less than 5% of the beam diameter and so could be neglected.

The most serious problem was deflection of the slow, secondary electrons leaving the sample surface and being collected by the electron energy analyser. This very complex problem could not be analysed mathematically, but it was studied experimentally in two different ways. The first method was to measure the N(E) spectrum with the CMA as a function of heating-stage current. This gave an indication of the percentage of electrons deflected away from the analyser at the energy of each relevant Auger peak. The other method was to measure 'at-temperature' Auger peak-to-peak heights, then cool the sample as quickly as possible to room temperature and re-measure. It was assumed that there was no significant change in surface composition during cooling. Heating and cooling curves for a nickel sample are shown in Fig. 3.6. The results of both techniques indicated that Auger peaks with energies higher than about 250eV were not significantly affected by the heating currents used to obtain sample

temperatures of up to 800°C. For Auger peaks at lower energies the percentage loss was not a simple function of either electron energy or heating current. The second method gave the most consistent results and so was the one used wherever possible. It was found necessary to calibrate each sample and heating-filament combination individually.

3.1.4. The electron gun

The fine-spot electron gun that was used was originally developed by B.D. Powell as being capable of delivering 1μA into a 10μm spot diameter. An image of the hairpin filament, produced by a Wehnelt cylinder, was demagnified and projected onto the sample by a single-stage electrostatic lens whose potential could be varied to focus the electron beam. There was one intermediate aperture and, behind the end cap of the gun, a four-quadrant beam deflection system. Precise allignment of all components was achieved by making them a nice fit into a stainless steel tube. The entire assembly was originally bolted into the CMA but this was later modified to allow removal of the gun for maintenance without disturbing the analyser.

Several modifications were made to the electron gun to make it more suitable for the present work and in addition more reliable and easier to maintain. Its excessive outgassing was traced to the massive construction of the Wehnelt cylinder and its associated components. In the modified version, a molybdenum Wehnelt can from a conventional electron gun was combined with components made from machinable glass ceramic. A photograph of the electron gun, with its Wehnelt assembly withdrawn, is shown in Fig. 3.7. During the course of the present work, the intermediate aperture was enlarged to give a larger beam current at the expense of a larger, 20μm spot size.

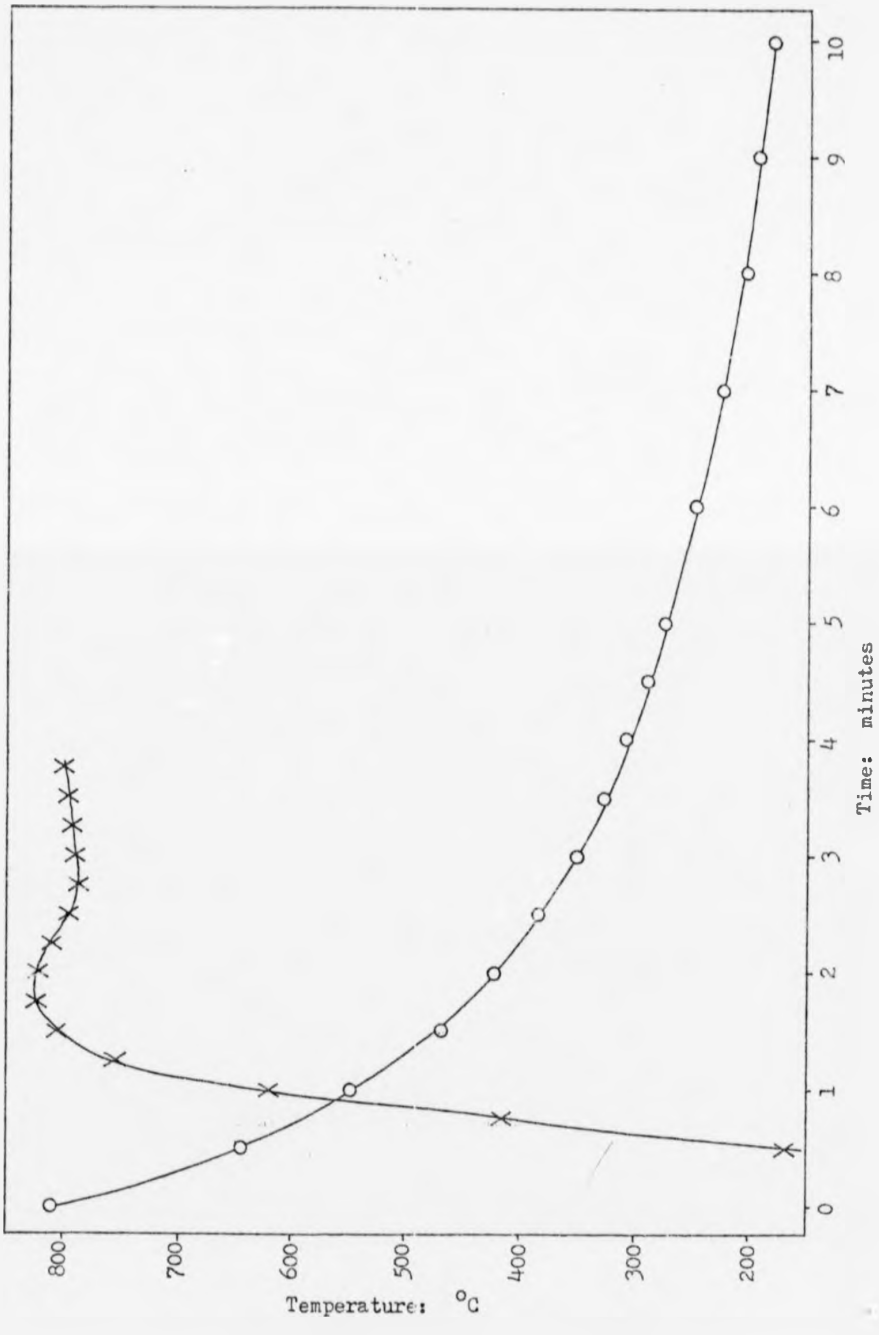

Fig. 3.6 Heating and cooling curves for the heating-stage

Fig. 3.7 The fine-spot electron gun with Wehnelt assembly withdrawn

Fig. 3.7 The fine-spot electron gun with Wehnelt assembly withdrawn

3.1.5. The cylindrical mirror analyser (CMA)

A CMA is an electrostatic deflection analyser which acts as a band-pass filter. The energy dispersive part of the analyser consists of two co-axial cylinders. The band-centre electron energy is determined by a DC voltage applied to the outer cylinder, while the inner is grounded. An electron energy spectrum is obtained by ramping the applied voltage. If a low voltage AC modulation is superimposed on the sweep, it can be shown mathematically (Rivière (1973)) that the output signal of the analyser at the first harmonic of the modulation frequency is proportional to the derivative of the energy spectrum. The proof relies upon the expansion of $I'(V + k\sin\omega t)$ using the alternative form of Taylor's Theorem, where I is the collected current, V the deflection voltage and $k\sin\omega t$ the modulation. The analyser was used in this mode, with a 5 volt peak-to-peak modulation at 10kHz.

A full CMA is a bulky instrument which has a short focussing distance. A $\frac{1}{4}$ segment design was used in the present work, allowing easier access to the sample by ancilliary facilities such as ion bombardment. The analyser was enclosed in a μ-metal shield to reduce the disturbing effects of stray fields. Those electrons which traversed the energy dispersive region of the analyser were accelerated onto a phosphor screen by a 7keV potential. The light emitted by the phosphor under electron impact was monitored by a photomultiplier tube which was situated outside the vacuum system. Before each experiment, the sample was positioned at the optimum focussing point of the analyser. Auger spectra were only taken from that part of the surface which was within the optimum region.

3.2. Control of the analysis system

3.2.1. Electronics

The general electronic layout of the system for AES is shown in Fig. 3.8. The beam from the electron gun could be scanned over the sample in a 'television' raster, and the absorbed electron current amplified and used to modulate the brightness of an oscilloscope display screen. When a suitable area for analysis had been identified from the display, the scan generators were replaced by DC shift voltages which positioned the electron beam on the chosen spot.

The signal from the photomultiplier was fed into a lock-in amplifier which selectively amplified that component of the signal at the first harmonic of the modulation frequency. The DC output from the amplifier was plotted against a voltage proportional to the CMA deflection voltage on an X-Y recorder. In this way, derivative Auger spectra were produced.

3.2.2. Computer control

During the course of this work, advantage was taken of the availability of an on-line computer facility which was capable of controlling the analysis system during experiments. The GEC 4080 was a multiple access computer and one of its remote terminals was located near to the UHV system. Control was achieved via analogue lines from 8 and 12 bit DACs.

The electron gun was controlled via the scan generators. The computer acted as a waveform generator whose output was fed into the scan amplifiers. It could produce a fast-scan picture raster from two 8 bit DACs for setting up, or a slower scan with greater resolution from two 12 bit DACs. Once an analysis point had been selected on this slow-scan picture, it was identified to the computer

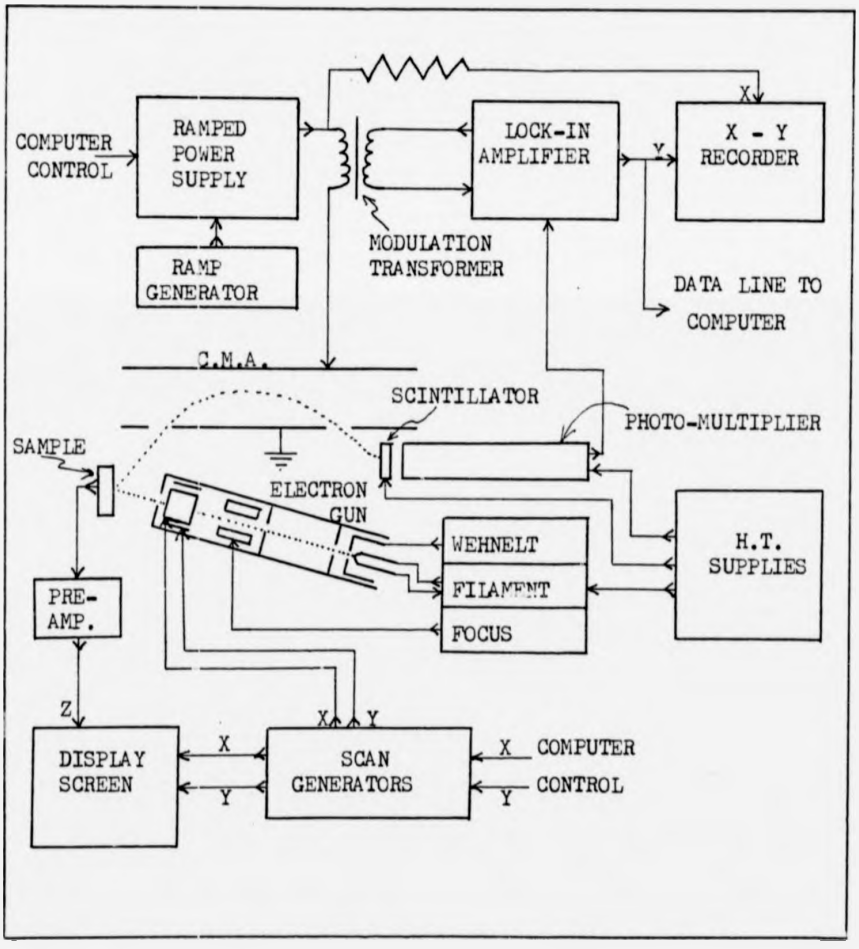

Fig. 3.8 Electronic layout of the system

by means of cursors. During experiments, the computer positioned the electron beam on the selected area while Auger spectra were being taken, and away from the sample at other times. If more than one point was selected, the computer was programmed to cycle between them.

The CMA was controlled by replacing the ramp generator by the output from a 12 bit DAC. This provided 4096 voltage steps to cover a range of 0 - 10 volts. The output was scaled with a ten-turn potentiometer so that the output of the ramped power supply covered the correct range of the energy spectrum. The computer was programmed to run complete 0 - 1000eV Auger spectra whilst setting up. In this way, all the elements that segregated to the surface could be identified. During the more detailed experiments it was necessary to improve the time resolution of the analysis system. This was achieved by restricting the analysis to the areas of the energy spectrum where relevant Auger peaks were located. The computer was programmed to scan through the position of an Auger peak and then jump to the position of the Auger peak that was next higher in energy. The energy range that was scanned for each Auger peak was larger than the actual peak width to allow for movement of the peaks in the energy domain as a result of the small potentials produced on the sample holder by the heating-stage current.

3.2.3. Data processing

The output of the lock-in amplifier was monitored by a 12 bit ADC. The time-constant of the amplifier had to be taken into account when deciding how its output should be sampled. After each increment of the CMA deflection voltage, the computer waited for one time-constant to elapse before taking the first sample. A further

nine samples were taken during the next time-constant's length. The ten samples were averaged to give a value characteristic of that voltage-point in the spectrum.

All data was stored on a magnetic-disc memory as it was collected. Associated with each Auger peak was a time in seconds from the start of the experiment, as noted by the computer's internal clock. From the averaged data, the difference between the maximum and minimum values at each Auger peak's position was taken as a measure of the Auger peak-to-peak height. This information was output at the terminal during the experiment so that its progress could be monitored. After each experiment, the Auger peaks were plotted out on an X-Y recorder via the analogue lines from the 12 bit DACs. Auger peak-to-peak heights were then measured from these records.

3.3. The samples

Samples were produced from each of the five stock alloys: Fe - 0.65wt% C (Fe.65C), Fe - 0.87wt% C (Fe.87C), Fe - 1.50wt% Cr (FeCr), Fe - 1.46wt% Cr - 0.91wt% C (FeCrC) and commercial high-carbon chrome steel containing 1.42wt% Cr - 1.03wt% C (HCC). The details of alloy and sample preparation are given below.

3.3.1. Alloy production

The commercial HCC stock alloy was obtained from Tube Investments as a block of as-cast material which had been cut from the equiaxed region of an ingot. It was sealed into an evacuated silica tube and homogenised for a week at 1200°C before use. The Fe.65C alloy was provided by E.D. Hondros of the National Physical Laboratory. It was given a similar homogenisation to the HCC. The three remaining pure alloys were produced at the Hinxton Hall Laboratories of Tube Investments. They were based upon NPL 99.99% iron, with suitable additions of Koch Light 99.999% chromium and Koch Light 99.99% carbon. Small ingots were cast under argon and extruded into 9mm diameter bars to break up the cast structure. The bars were homogenised as above before use.

3.3.2. Sample preparation

Samples were spark-machined from the stock alloys in order to minimise surface damage. All the samples were 1.5mm thick and were about 10mm across, being either square or circular in shape. A narrow groove about 2mm deep was spark-machined into the edge to accommodate the heating strip. The samples were electrolytically etched to remove surface contamination. False segregation of tin from the cutting wire of the spark machine was observed on samples which had not been etched in this way. Both faces of the samples

were polished; the face that was to be analysed was taken to a $\frac{1}{4}\mu m$ finish with diamond paste. Surface damage was removed by a light electro-polish, after which the samples were washed and mounted in the heating stage. The entire assembly was degreased before insertion into the UHV system.

REFERENCES for Chapter Three

Rivière J.C., Contemp. Phys. 14(1973)513

Schmerling M., Finello D. & Marcus H.L., Scripta Met. 14(1980)1135

CHAPTER FOUR RESULTS

This chapter is divided into five sections, each of which contains the results from one of the five alloys. The alloys are dealt with in the order Fe.87C, Fe.65C, FeCr, FeCrC and HCC. Within each section the results are further divided according to the region of the equilibrium phase diagram to which they apply. These phase regions are listed in order of increasing temperature. For reasons of brevity, the methodologies of the main types of experiment will be outlined below and given short descriptors, enclosed in single quotes, by means of which they will be identified in the main body of the chapter.

When a "clean" surface was heated directly from room temperature to an equilibration temperature, the process will be referred to as 'heating'. The rate of heating employed may be referred to as 'fast' or 'slow'. 'Fast heating' approximated to the heating curve that was shown in Fig. 3.6, while 'slow heating' will be used to imply that the sample was heated at some indeterminate, slower rate. Where one sample equilibration temperature was changed to another within the same phase region, this will be called 'incrementing' and the rate of heating or cooling would have been the maximum possible. A specimen cooling curve was also shown in Fig. 3.6. If the change in the equilibration temperature took the sample across a phase boundary, the term 'transformation' will be used instead of 'increment'.

The type of ion bombardment which was used to clean the sample surface could have been either 'superficial' to remove only the segregated layer at the surface, or 'deep' to remove the sub-surface depletion zone as well. When it was desired to deplete segregants in the fast sub-surface diffusion paths such as grain boundaries, a 'hot' ion

bombardment was used. During this type of bombardment the sample was held at a temperature sufficient to cause surface segregation whilst the surface was bombarded to remove any elements that did segregate. The term 'depth-profiles' will be used to refer to the sub-surface concentration profiles produced by alternate Auger analyses and ion bombardments.

Wherever possible the Auger analyses were corrected for any drift in the sensitivity of the instrumentation by the normalisation of the segregant's Auger peak to the iron substrate's Auger peaks. This procedure is only feasible if there is no large change in the segregation level occurring at the time. For example, if the iron Auger peaks were reducing in amplitude during the surface segregation of an element, this could have been due either to instrumental drift or to an attenuation of the iron Auger signal resulting from the inelastic scattering of the iron Auger electrons in the overlayer of segregant. For this reason, the Auger peaks were only normalised once the segregant had reached saturation or the changes in surface composition that were taking place were slight.

4.1. The Fe.87C alloy

4.1.1. General

An Auger spectrum of a clean surface of this alloy is shown in Fig. 4.1. The most prominent features are the high and low energy iron Auger peaks. There are three smaller features of interest. At 85eV there is a feature which appears to be an Auger peak, but is in fact attributed to electron diffraction in the surface atomic layers (McDonnell et al (1973)). This type of feature may be distinguished from an Auger peak by its strongly temperature-dependent intensity. There is an Auger peak at 210eV from argon atoms implanted into the surface during the ion bombardment that was used to clean the surface. Finally, there is a small carbon Auger peak at 272eV. This is probably present as a result of the bulk carbon content rather than surface contamination by carbon-containing species.

From the results of some general investigatory heating experiments it was clear that carbon and sulphur were competing for surface sites. Carbon dominated surface segregation in the $\alpha+Fe_3C$ phase region, while sulphur was dominant in the γ phase region. In the intermediate $\gamma+Fe_3C$ phase region it was possible to obtain stable mixtures of both elements at the surface but their relative proportions depended upon the rate of 'heating', the equilibration time before an 'increment' and the postion on the sample surface that was examined. There was strong attenuation of the iron Auger peaks whenever carbon was present at the surface to any great extent. This attenuation was also position-dependent. The carbon might have been present either as a dispersed segregant or as precipitated graphite. The evidence for the existence of either form during the present work is discussed in Chapter Five.

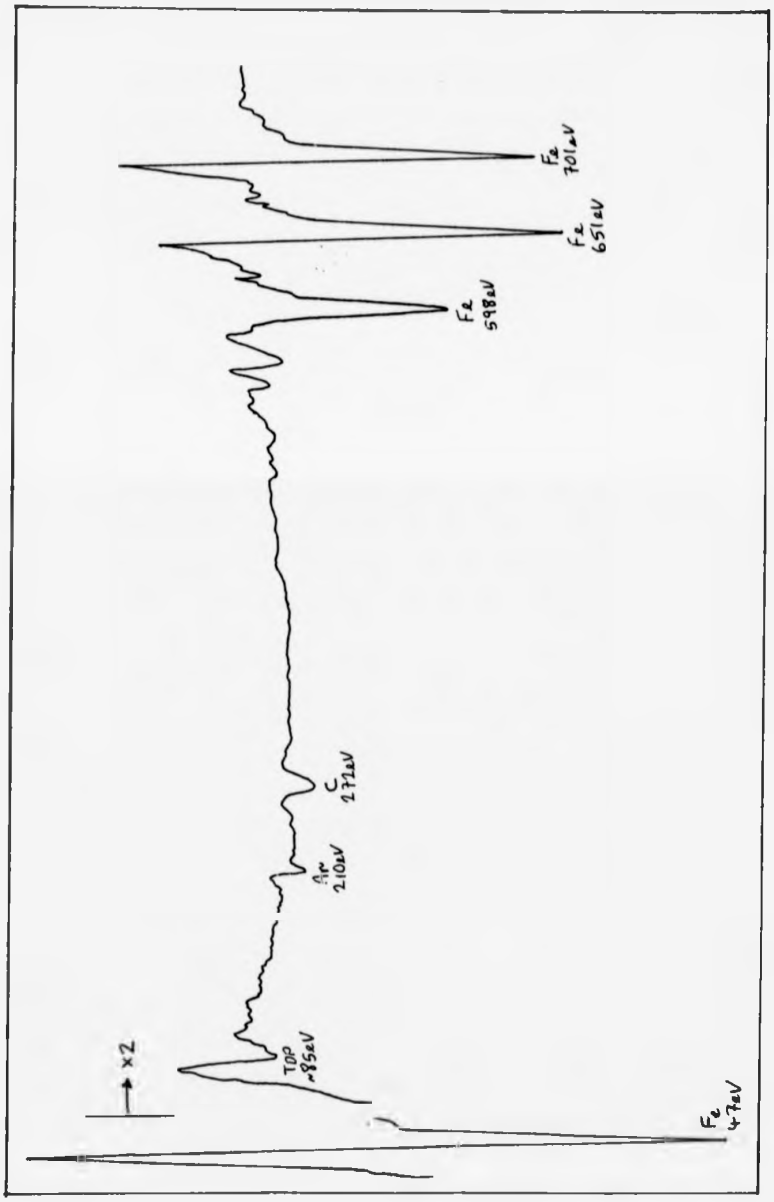

Fig. 4.1 Fe.37C: Auger spectrum of clean surface

Fig. 4.2 shows the result of an experiment where a sample was 'heated' to 700°C and then in 10°C steps up to 800°C. There was particularly strong attenuation of the iron Auger peaks in this area of the surface. It can be seen that this attenuation was in some way proportional to the carbon level at the surface. The question of whether the sulphur was displaced, or its Auger signal attenuated by a carbon overlayer is considered in Chapter Five. The iron-graphite equilibrium phase diagram (Fig. 2.1) predicted that some carbon should be in solution above 738°C. While there was a decline in the carbon Auger signal above 740°C, there was still a significant carbon Auger peak from this area of the surface after prolonged holding at 800°C.

Cooling the sample by stages produced surface changes which were dependent upon the bulk phase-transformation rather than being the reverse of the surface changes upon heating. Fig. 4.3 shows that the surface transformation was in line with the bulk TTT diagram (Fig. 2.4). There was no change in the surface composition until the temperature had been reduced to 700°C. The rate of transformation was increased by a further cooling to 680°C.

4.1.2. The α+Fe_3C phase region

The initial relative sizes of the carbon and sulphur Auger peaks depended upon the rate of 'heating'. This is illustrated by examples of 'fast heating', Fig. 4.4 and 'slow heating', Fig. 4.5. 'Fast heating' produced a small, transient sulphur level while 'slow heating' resulted in a larger sulphur level which was more slowly replaced by carbon. Cooling to 500°C during the latter experiment halted the replacement of sulphur, while subsequent 'incrementing' to 560°C was sufficient to cause its complete replacement by carbon.

Fig. 4.2 Fe.37C: segregation with increasing temperature

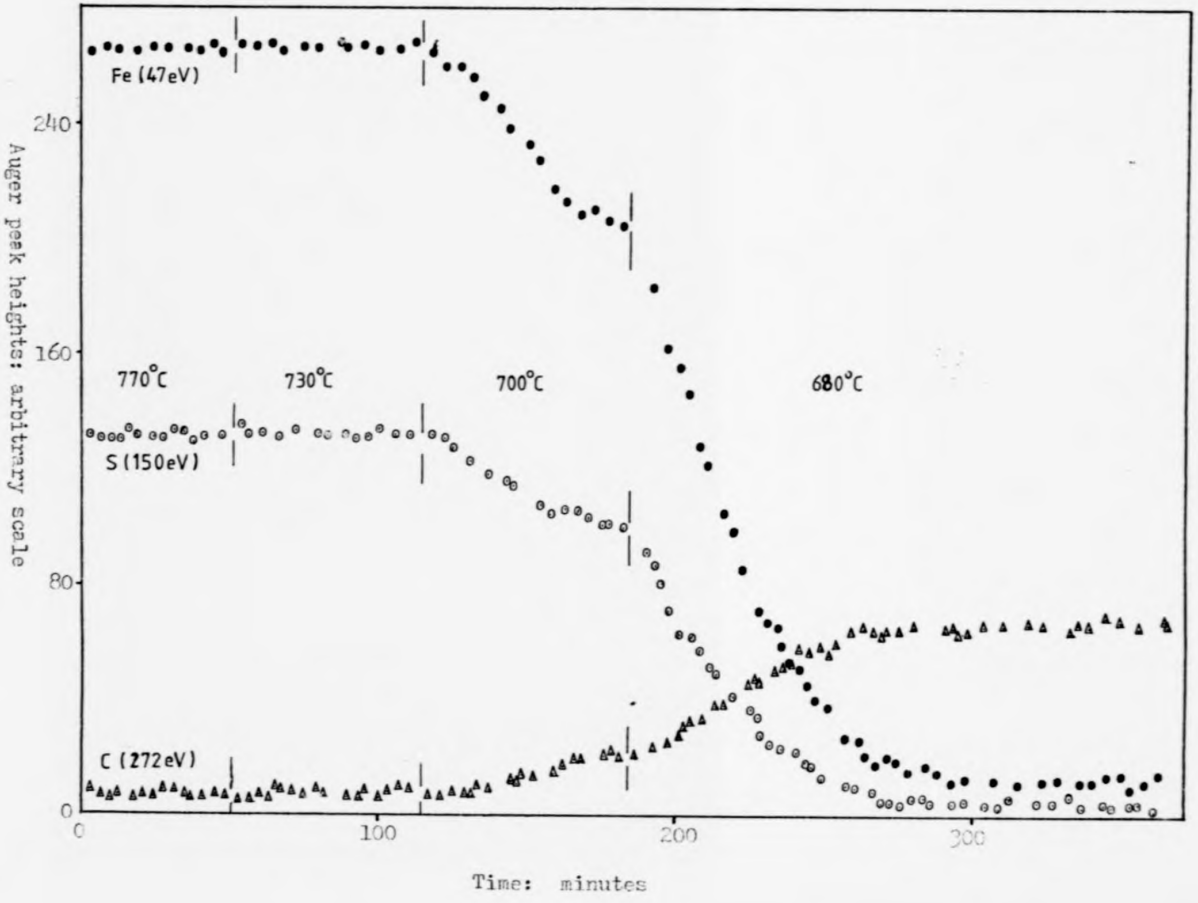

Fig. 4.3 Fe.87C: segregation with decreasing temperature

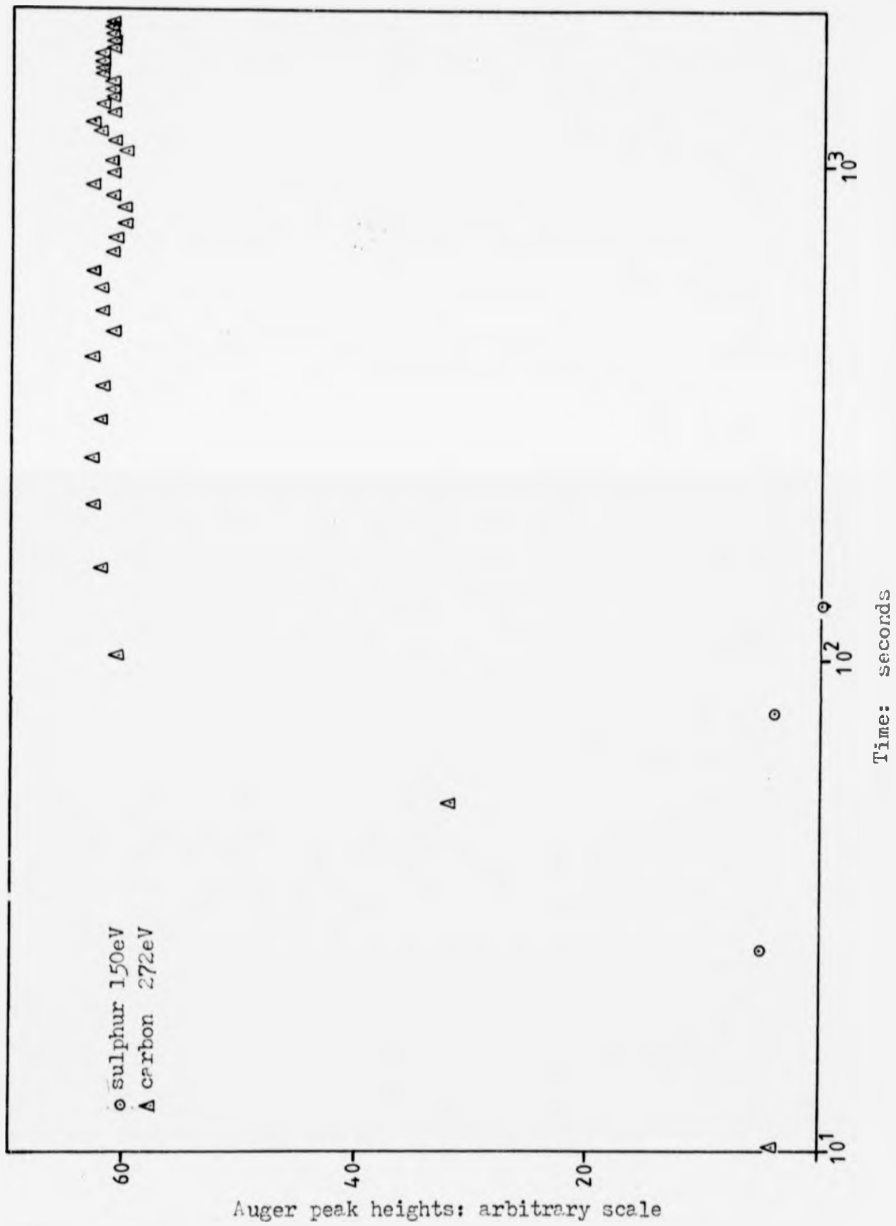

Fig. 4.4 Fe.27C: 700°C, fast heating, pearlitic sample

Fig. 4.5 Fe.87C: surface composition during low temperature cycling

The behaviour of argon at the surface was interesting. In the absence of surface carbon, 'heating' a sample produced a shortlived increase in the argon Auger signal as implanted argon atoms diffused to the surface and outgassed into the vacuum. When there was a strong carbon signal from the surface, however, the argon Auger peak became extremely resistant to outgassing heat-treatments. During some experiments there was still an argon Auger peak detectable after ten hours at 700°C. Another feature of these carbon-dominated surfaces was their resistance to ion bombardment. This introduced uncertainties into the 'depth-profiles' because the extent of the resistance varied from position to position on the surface, and the same area of the surface was not re-located exactly after each bombardment. The 'depth-profile' shown in Fig. 4.6. has a typical degree of scatter. It also shows an initial increase in the sulphur Auger signal upon bombardment. This was a common feature of 'depth-profiles' of carbon-covered surfaces.

'Transformations' upon cooling into this phase region were investigated in some detail because of the interesting features of the surface transformations that were observed. A sulphur-covered surface was obtained by 'fast heating' into the gamma phase. A subsequent 'transformation' at a constant temperature in the $\alpha+Fe_3C$ phase region resulted in the replacement of surface sulphur by carbon. Some results are now presented to illustrate the main features of these surface transformations.

In experiments near the eutectoid temperature there was an induction period, followed by a slow surface transformation as shown in an example at 700°C, Fig. 4.7. As the temperature of the transformation experiments was decreased towards 665°C, the rate of surface transformation

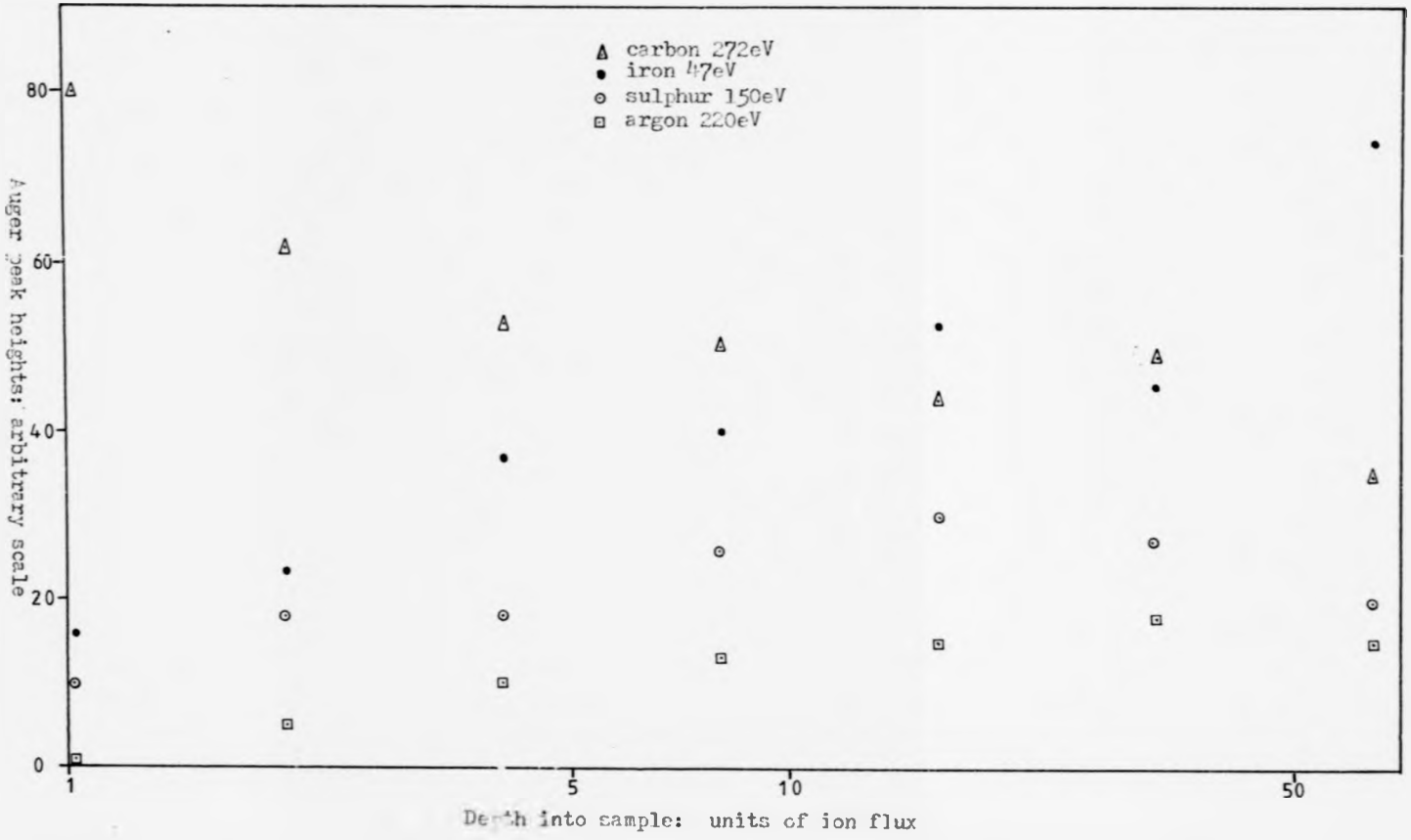

Fig. 4.6 Fe/C: Depth profile

Fig. 4.7 Fe.97C: isothermal transformation at 700°C

increased and the induction period disappeared. The transformations were sometimes single-stage and sometimes two-stage. Fig. 4.8 shows a two-stage result at 690°C. There were also variations in the rate of transformation in different areas of the surface. A result at 670°C, where four areas 100 μm apart were monitored sequentially, is shown in Fig. 4.9. At 665°C the surface transformation was at its fastest and was always a single-stage process. The example shown in Fig. 4.10 was the first of two consecutive experiments at this temperature, on the same area of the sample. In this case, there was no ion bombardment between the experiments, but the sample was heated back into the γ phase region to restore the surface coverage of sulphur before re-transforming. The two experiments gave almost identical results. At temperatures below 665°C the rate of surface transformation quickly became slower again. A result at 655°C is shown in Fig. 4.11.

4.1.3. The γ+Fe_3C phase region

'Heating' into this phase region produced the same strong carbon Auger peak as before, but the small sulphur Auger peak was no longer removed by equilibration. If a sample was maintained near the top of the alpha range until the sulphur peak had become very small and then 'transformed' into the γ+Fe_3C phase region, the sulphur Auger peak would increase slightly as shown in Fig. 4.12. There were still variations in composition between different areas of the surface. This was well illustrated when, at the end of the previous experiment, the temperature was 'incremented' from 740°C to 750°C whilst monitoring the composition at four points on the surface. As can be seen in Fig. 4.13, in two of the four areas the sulphur level increased while the carbon level declined.

Fig. 4.8 Fe.97C: isothermal transformation at 690°C

Fig. 4.9 Fe.87C: isothermal transformation at 670°C, four areas

Fig. 4.10 Fe.87C: isothermal transformation at 665°C

Fig. 4.10 Fe.87C: isothermal transformation at 665°C

Fig. 4.11 Fe.37C: isothermal transformation at 655°C

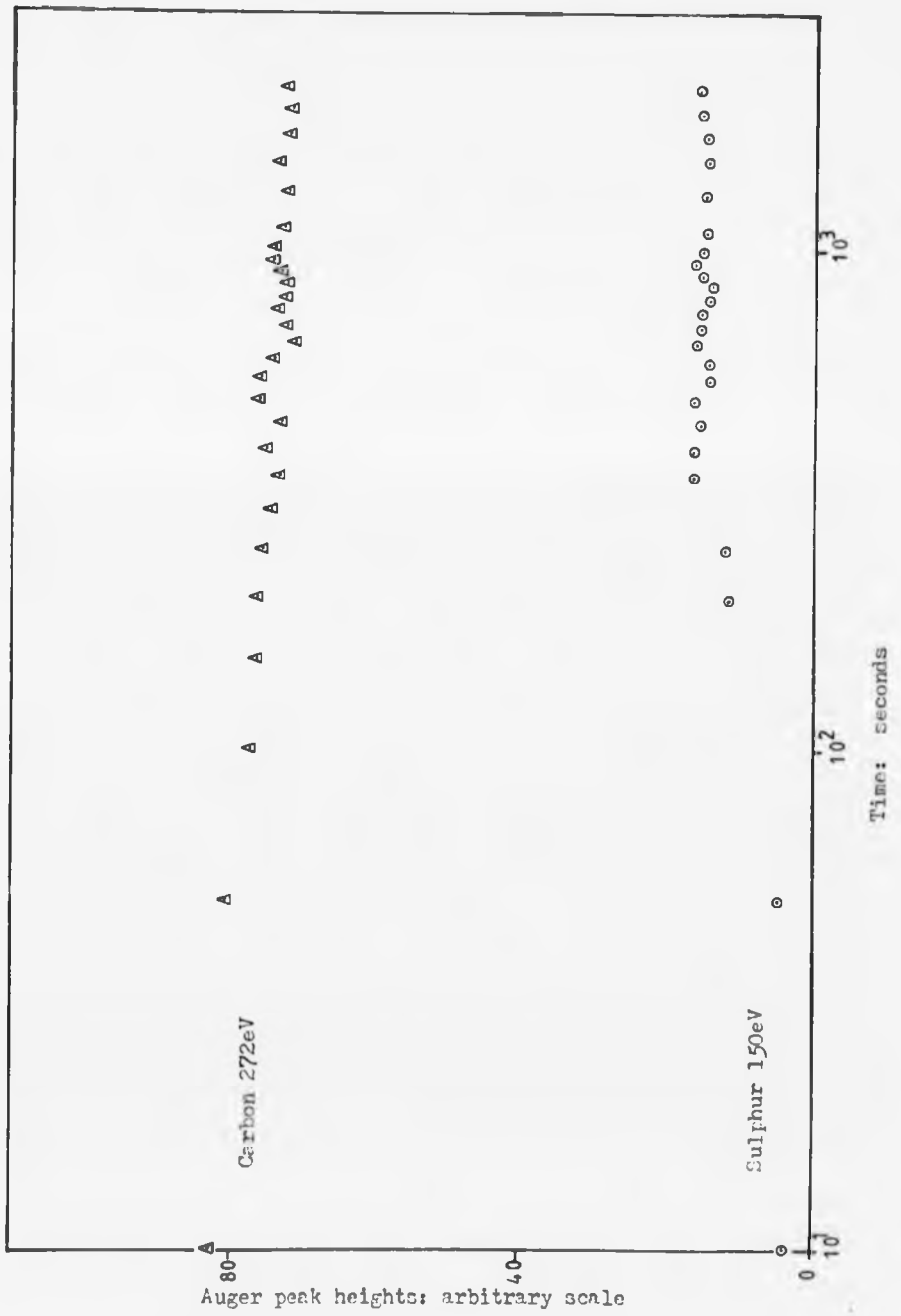

Fig. 4.12 Fe.37C: heating to 740°C from 700°C, 4 areas

Fig. 4.13 Fe.87C: heating to 750°C from 740°C, four areas

4.1.4. The γ phase region

Sulphur dominated surface segregation in this phase region. During 'heating' experiments, the rate of sulphur segregation was high and time dependences greater than $t^{1.7}$ were observed. If, however, the surface was initially covered with carbon as a result of an equilibration in the alpha range, the rate of sulphur segregation on 'transformation' into the gamma phase was reduced. 'Fast heating' directly into the gamma phase region could sometimes result in a small carbon Auger peak as shown in Fig. 4.14. When a sample was spheroidised in the UHV sample-heating stage and then given a 'superficial' ion bombardment, the surface behaviour upon subsequent 'heating' into the gamma phase was as shown in Fig. 4.15. The sulphur segregation showed evidence of near-surface depletion, but despite its slow rate of segregation there was only a small initial increase in the carbon level. The sulphur depletion probably arose from the spheroidisation heat-treatment, with prolonged holding in vacuo at 700°C resulting in evaporation of sulphur from the free surface. The 'superficial' ion bombardment would not have removed the sulphur depletion zone.

The effect of sulphur depletion can also be seen in Fig. 4.16. This was the result of direct 'heating' of a pearlitic sample to 780°C and is shown for comparison with Fig. 4.15. Once again, sulphur was slow to rise to saturation but in this case there was a large initial carbon Auger peak. The time dependence of the sulphur segregation may be shown up by plotting the logarithm of the fraction of surface coverage against log(time). This is shown for the present experiment in Fig. 4.17. It can be seen that the sulphur points are a good fit to a straight line of slope 0.5, indicating a $t^{\frac{1}{2}}$ dependence. During a

Fig. 4.14 Fe.37C: 760°C, fast heating, pearlitic sample

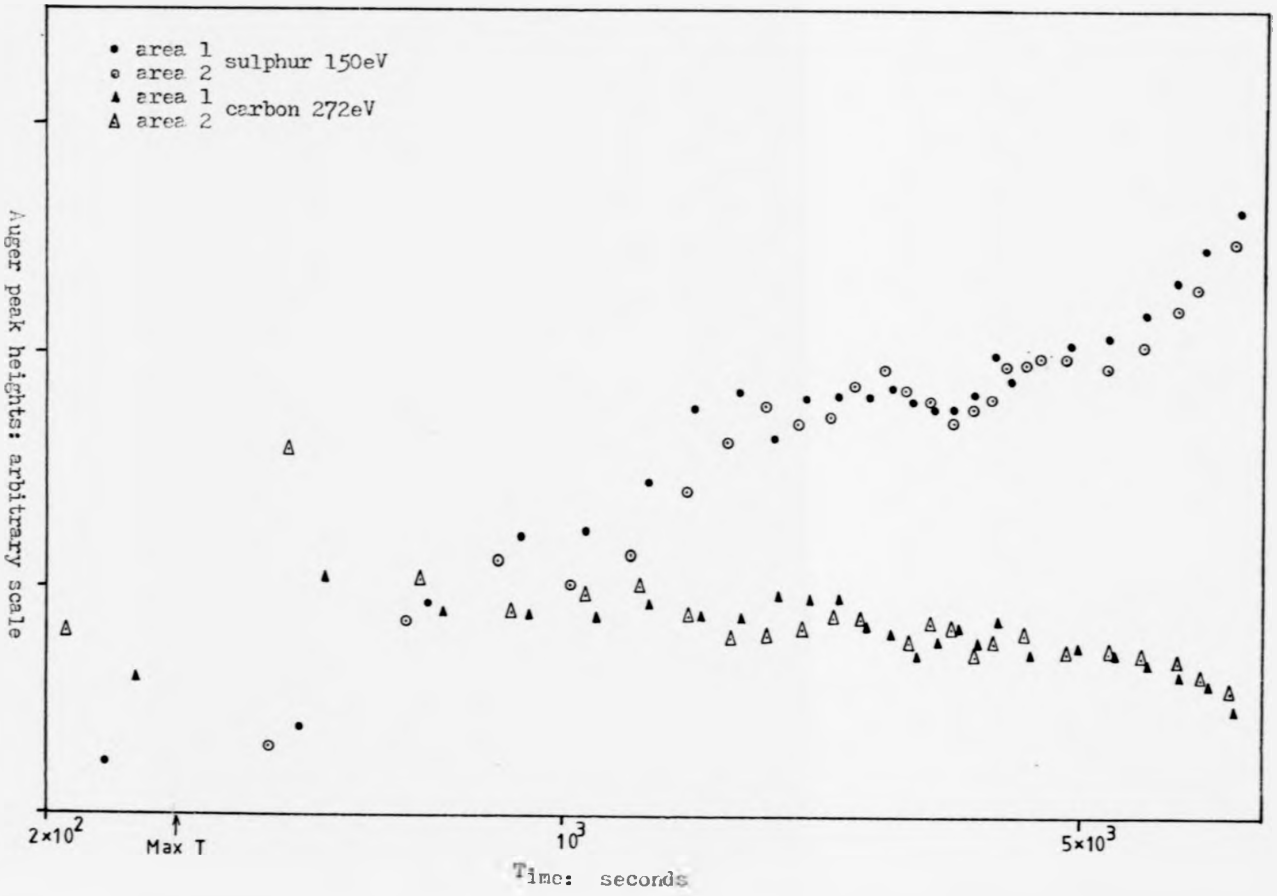

Fig. 4.15 Fe.97C; 790°C, spheroidised sample, two areas

Fig. 4.16 Fe.87C: 780°C, fast heating, pearlitic sample

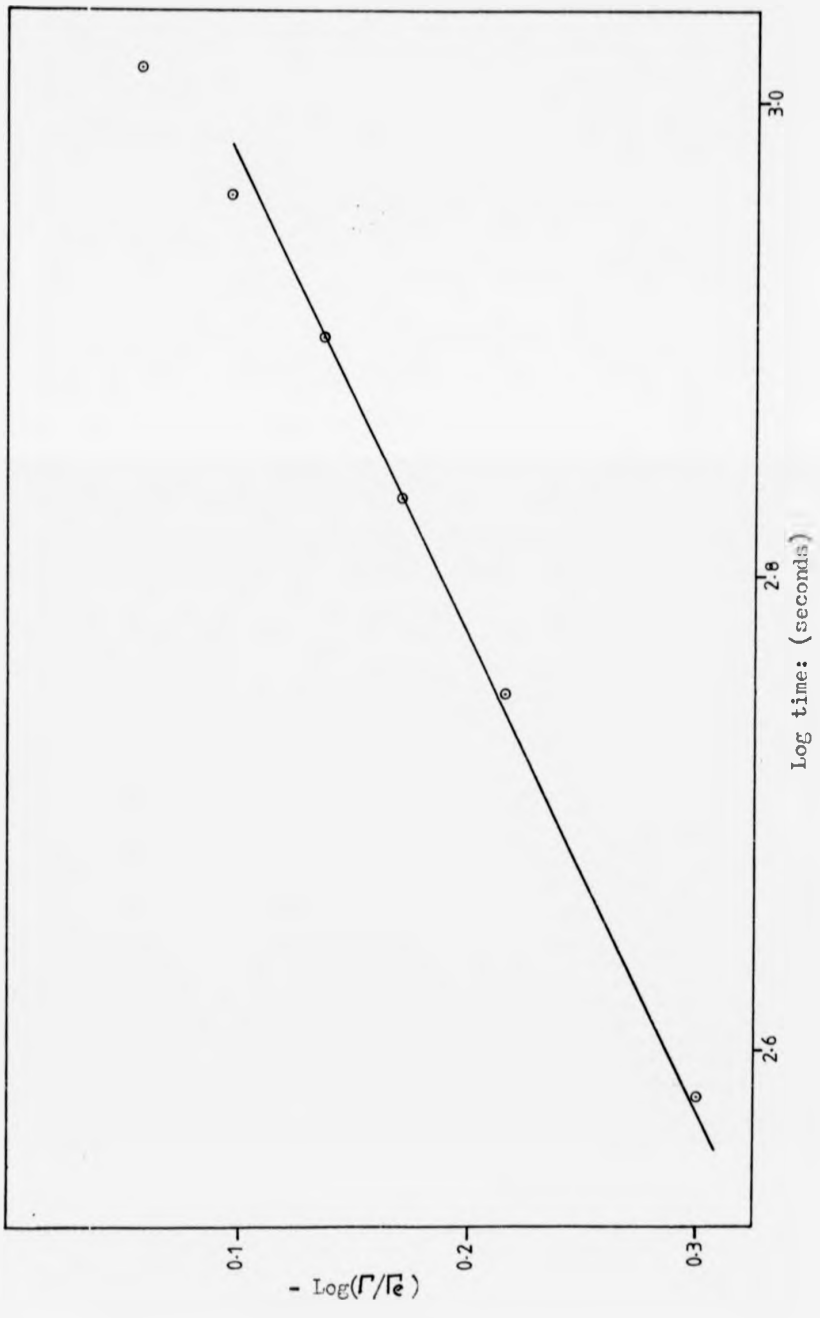

Fig. 4.17 Fe.87C: sulphur segregation at 780°C

another experiment, where a sulphur-depleted sample was 'heated' to 800°C (Fig. 4.18), the sulphur segregation rate also had a $t^{\frac{1}{2}}$ dependence as shown in Fig. 4.19.

The rate of change from a carbon-covered to a sulphur-covered surface upon 'transforming' a sample from the alpha range to the gamma phase was very fast. Even the high time-resolution of the computer-controlled analysis system was insufficient to follow the changes properly. The rate of change depended upon the length of the prior equilibration in the alpha range. Fig. 4.20 shows the result of a 'transformation' at 800°C after equilibrating the sample for five-hundred minutes at 700°C. This may be compared with the result of a similar 'transformation' after fifteen minutes at 700°C. The longer equilibration in the alpha range resulted in a slower rate of surface change. It is thought that the extent of any sulphur depletion produced by the long equilibration would have been small because there had initially been only a small sulphur peak, and this had disappeared after a few minutes.

Fig. 4.18 Fe.87C: 800°C, fast heating, pearlitic sample

Fig. 4.19 Fe.87C: sulphur segregation at 300°C

Fig. 4.20 Fe.87C: heating to 800°C after 500 minutes at 700°C

Fig. 4.21 Fe.87C: heating to 800°C after 15 minutes at 700°C

4.2. The Fe.65C alloy

4.2.1. General

Surface segregation on the Fe.65C alloy was generally similar to that of the Fe.87C alloy, but there were some detail differences. The rate of increase of the carbon level upon 'heating' in the $\alpha+Fe_3C$ phase region was slower than on the hyper-eutectoid alloy. When samples were 'transformed' from the $\alpha+Fe_3C$ to the $\alpha+\gamma$ phase region, there was a more distinct change in the carbon and sulphur levels and carbon often began to disappear while the temperature was still below the equilibrium graphite-dissolution value of 738°C. Despite this early dissolution, once carbon had been allowed to reach a high level at the surface it was difficult to remove; even at temperatures well into the gamma range. In those areas of the surface which appeared to favour carbon segregation, the initial sulphur Auger peak disappeared steadily upon equilibration in the $\alpha+Fe_3C$ phase region and the carbon Auger peak was stable at temperatures up to 815°C. The general behaviour is shown in Fig. 4.22 where the sample had been 'heated' to 690°C and then taken in steps into the gamma phase. The results from the individual phase regions, which follow, have been restricted to those cases where a novel type of experiment was undertaken or to those results which showed sustantially different behaviour to the Fe.87C alloy.

4.2.2. The $\alpha+Fe_3C$ phase region

The isothermal 'transformations' in this phase region were similar to those on the Fe.87C alloy except that the surface compositional changes required longer times to go to completion. The temperature of maximum surface-transformation rate was again around 670°C. It had been surmised that the induction period in the

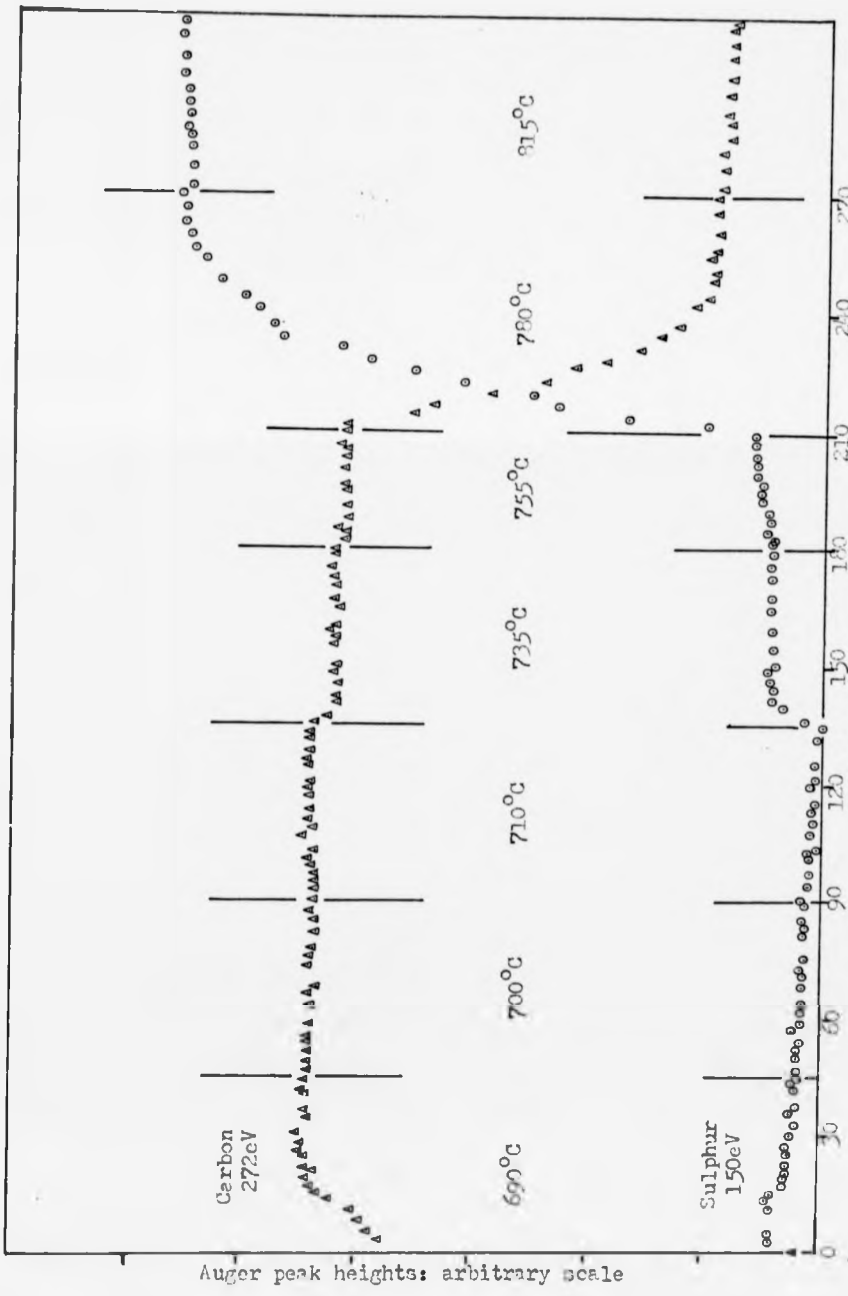

Fig. 4.22 Fe.65C: segregation with increasing temperature

700°C result on the hyper-eutectoid alloy might have been due to the time delay before the bulk transformation reaction occurred (Fig. 2.4). The equivalent transformation on the hypo-eutectoid alloy gave a similar result. To test this hypothesis, a sample of Fe.65C was taken through the following heat treatment. Instead of cooling to the transformation temperature, the sample was cooled directly to room temperature. This allowed the bulk transformation to take place while 'freezing-in' the high-temperature surface composition. The sample was then reheated to 700°C and the surface compositional changes monitored as before. The result is shown in Fig. 4.23. The rate of surface transformation was slow at first but then increased until it was faster than had been observed upon direct cooling to 700°C.

Another aspect of surface transformation that was studied was its dependence upon the length of the prior austenitisation heat treatment. Figs. 4.24 and 4.25 show surface transformations at 670°C after 150 minute and 15 minute austenitisations respectively. The surface transformation after the short austenitisation had an induction period but then required a shorter time to go to completion.

4.2.3. The $\alpha+\gamma$ phase region

'Heating' directly into this phase region, Fig. 4.26, produced a carbon dominated surface with a small sulphur Auger peak which increased slowly with time. This heat treatment was repeated after a 'hot' bombardment to deplete sulphur in fast sub-surface diffusion paths. The result is shown in Fig. 4.27. There was an induction period before sulphur appeared. A logarithmic plot of its initial rise is shown in Fig. 4.28. It can be seen that the sulphur segregation rate had an initial $t^{\frac{1}{2}}$ dependence.

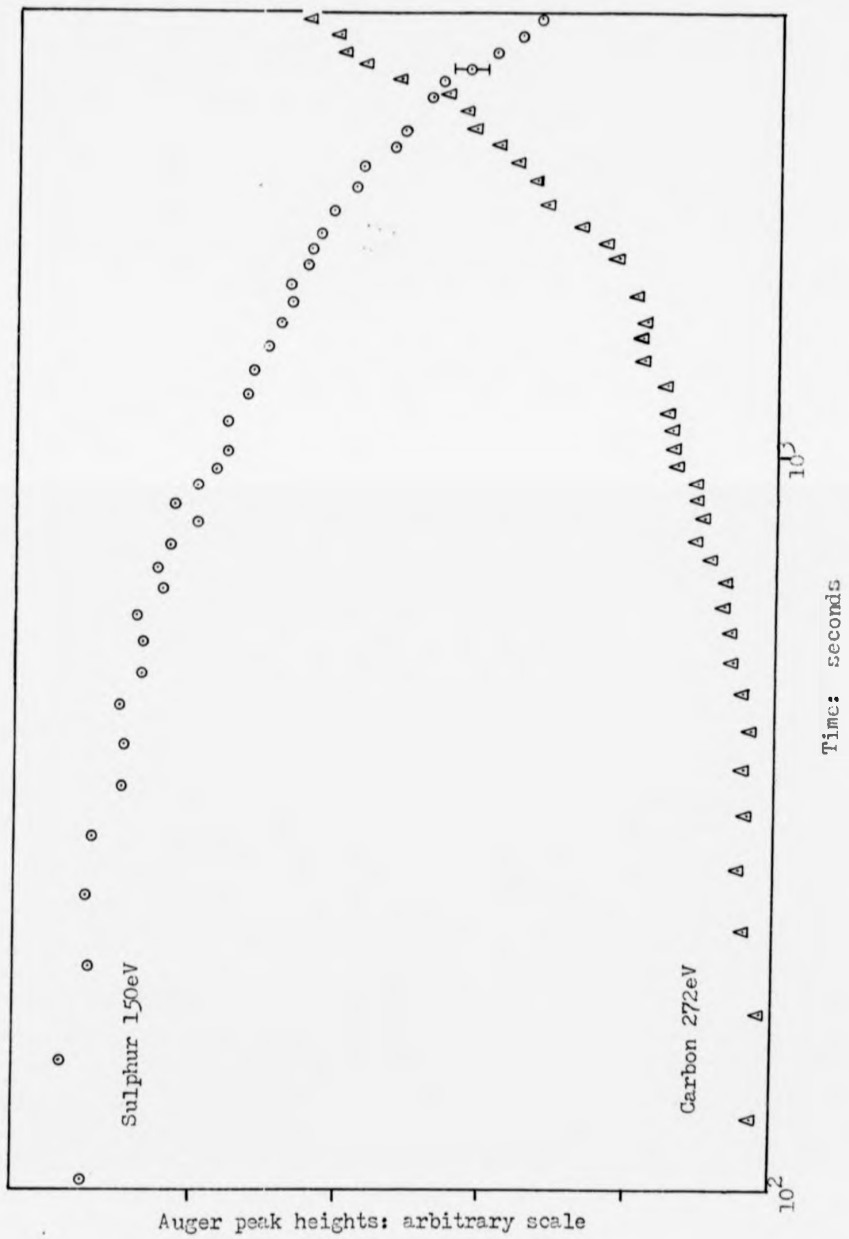

Fig. 4.23 Fe.65C: reheat to 700°C after austenitisation and fast cool to room temperature

Fig. 4.24 Fe.65C: isothermal transformation at 670°C after a long austenitisation

Fig. 4.25 Fe.65C: isothermal transformation at 670°C after a short austenitisation

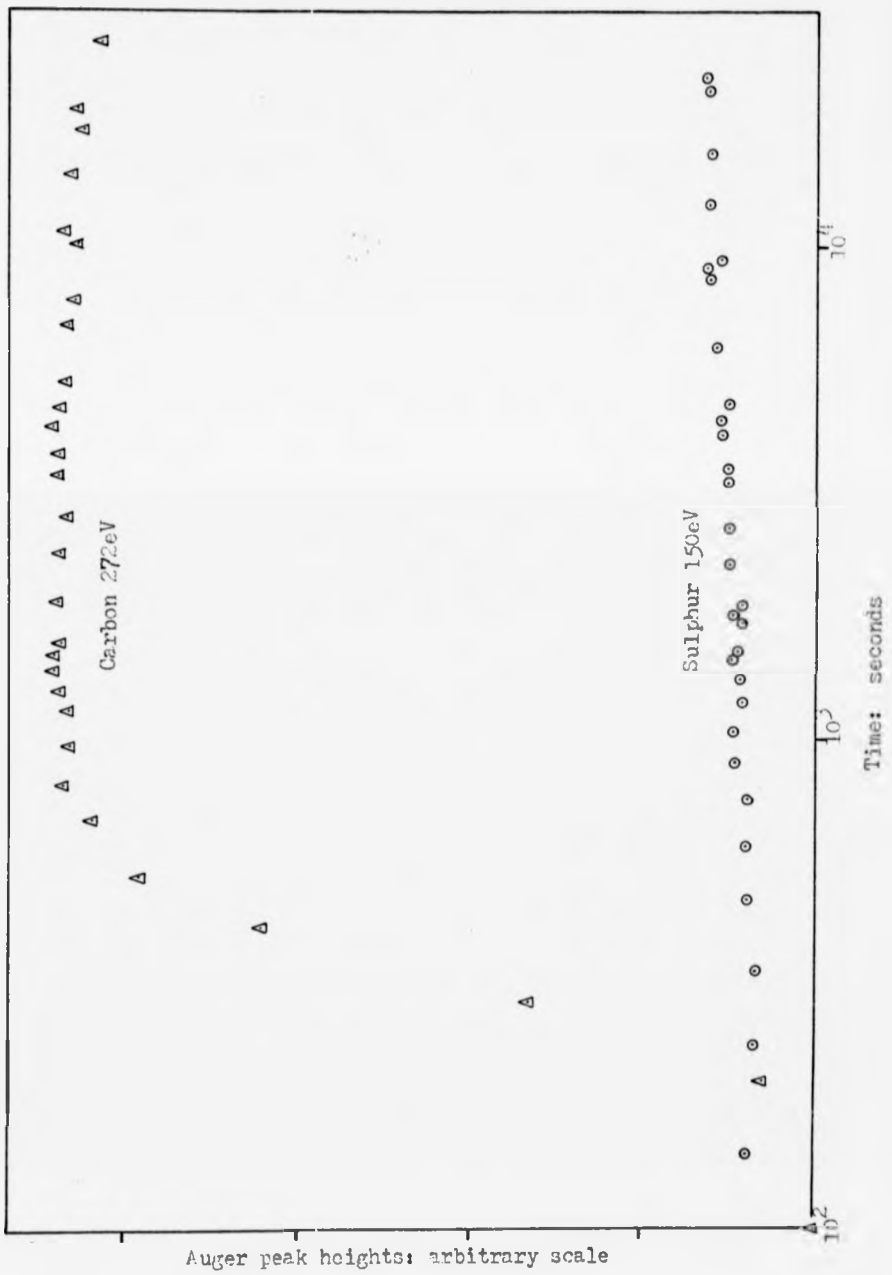

Fig. 4.26 Fe.65C: 730°C, fast heating, pearlitic sample

Fig. 4.27 Fe.65C: 735°C, strong sulphur depletion

Fig. 4.28 Fe.65C: sulphur segregation at 735°C

4.2.4. The δ phase region

'Fast heating' into the gamma phase produced a sulphur covered surface without the segregation of any carbon. Fig. 4.29 shows a result of this type. The sulphur segregation rate had a maximum time dependence in excess of t^2. The segregation rate was still as fast if 'slow heating' was employed but there was a transient carbon Auger peak as shown in Fig. 4.30. The 'dip' in the sulphur level was characteristic of this type of experiment. If a 'hot' bombardment had been used in order to deplete sulphur then the result of 'fast heating' was as shown in Fig. 4.31. The segregation of sulphur was sufficiently delayed for a strong and persistent carbon Auger peak to result. A logarithmic plot of the sulphur time-history is shown in Fig. 4.32. The 'hot' bombardment produced a linear time dependence.

When a 'hot-bombarded' sample was given a 'slow heating' into the gamma phase, it produced the result shown in Fig. 4.33. This was the only appearance by phosphorus at the surface of the plain-carbon alloys: indeed, it was the only appearance by any element other than carbon, sulphur and argon. The effect of spheroidisation of cementite was studied in a slightly different way on this alloy. Both the time and temperature of the spheroidisation heat-treatment were the same as before, but it was carried out on a piece of the stock alloy before the sample was machined out and inserted into the UHV system. It can be seen from Fig. 4.34 that there was no longer any evidence of sulphur depletion. The initial high carbon Auger signal could not be removed by ion bombardment, and there was still a resistant carbon Auger peak after a considerable time at 800°C.

Fig. 4.29 Fe.65C: 780°C, fast heating, pearlitic sample

Fig. 4.30 Fe.65C: 730°C, slow heating, pearlitic sample

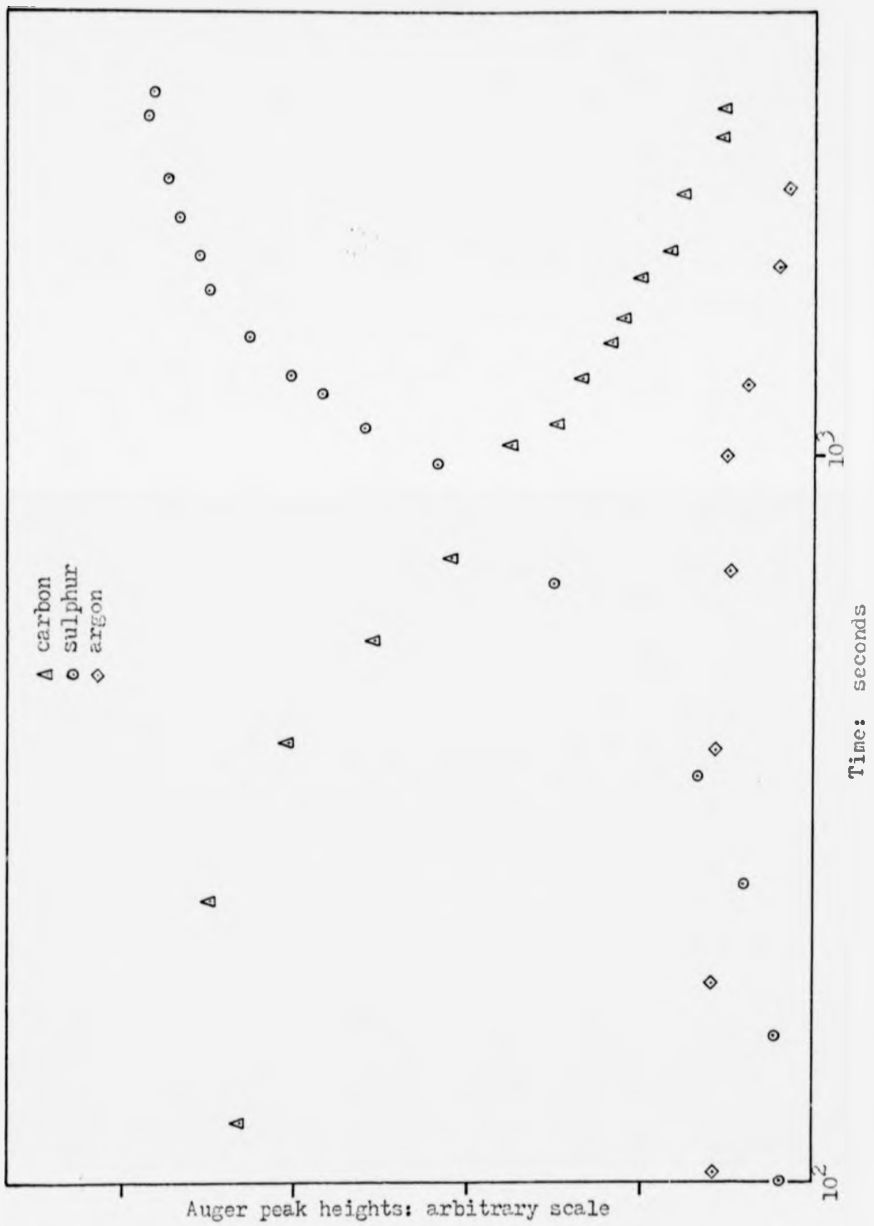

Fig. 4.31 Fe.65C: 730°C, fast heating, strong sulphur depletion

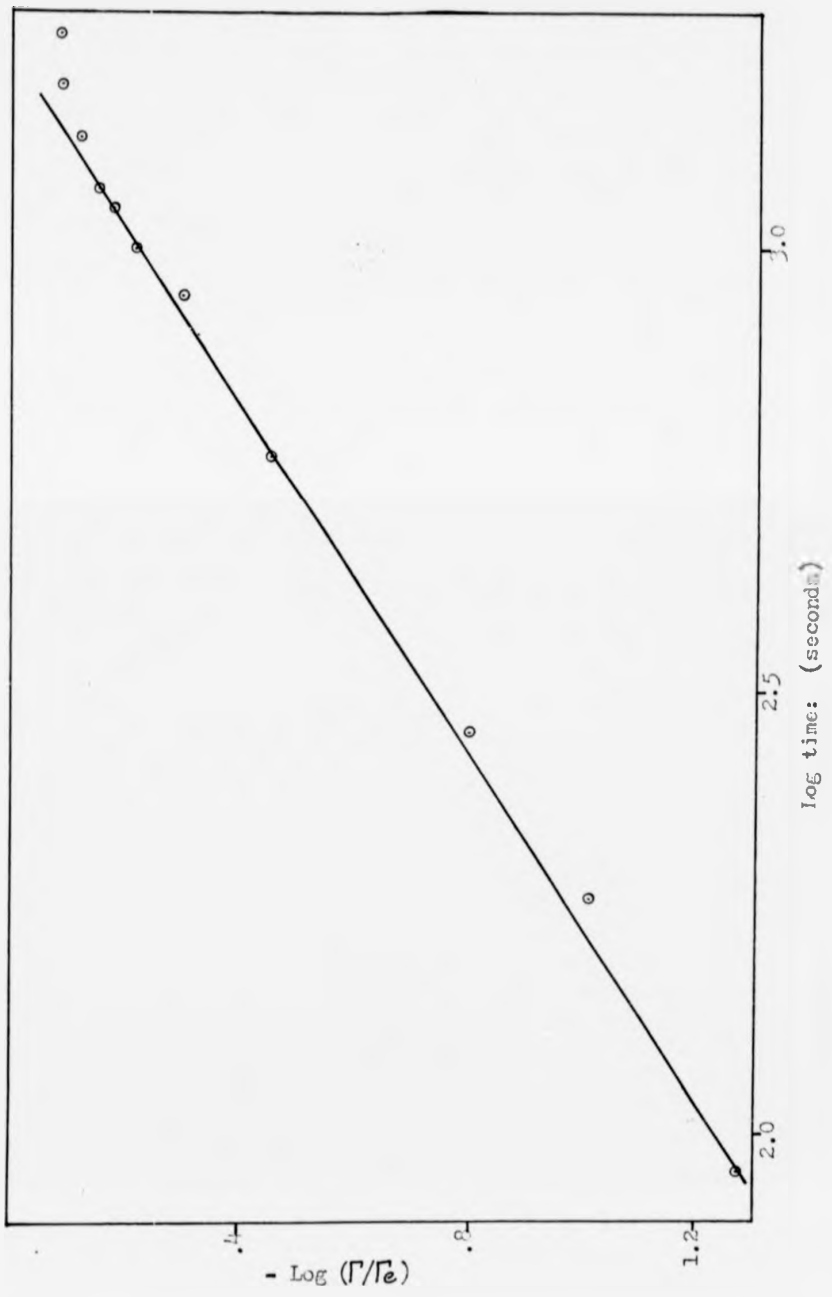

Fig. 4.32 Fe.65C: sulphur segregation at 780°C

Fig. 4.33 Fe.65C: 770°C, slow heating, sulphur depletion

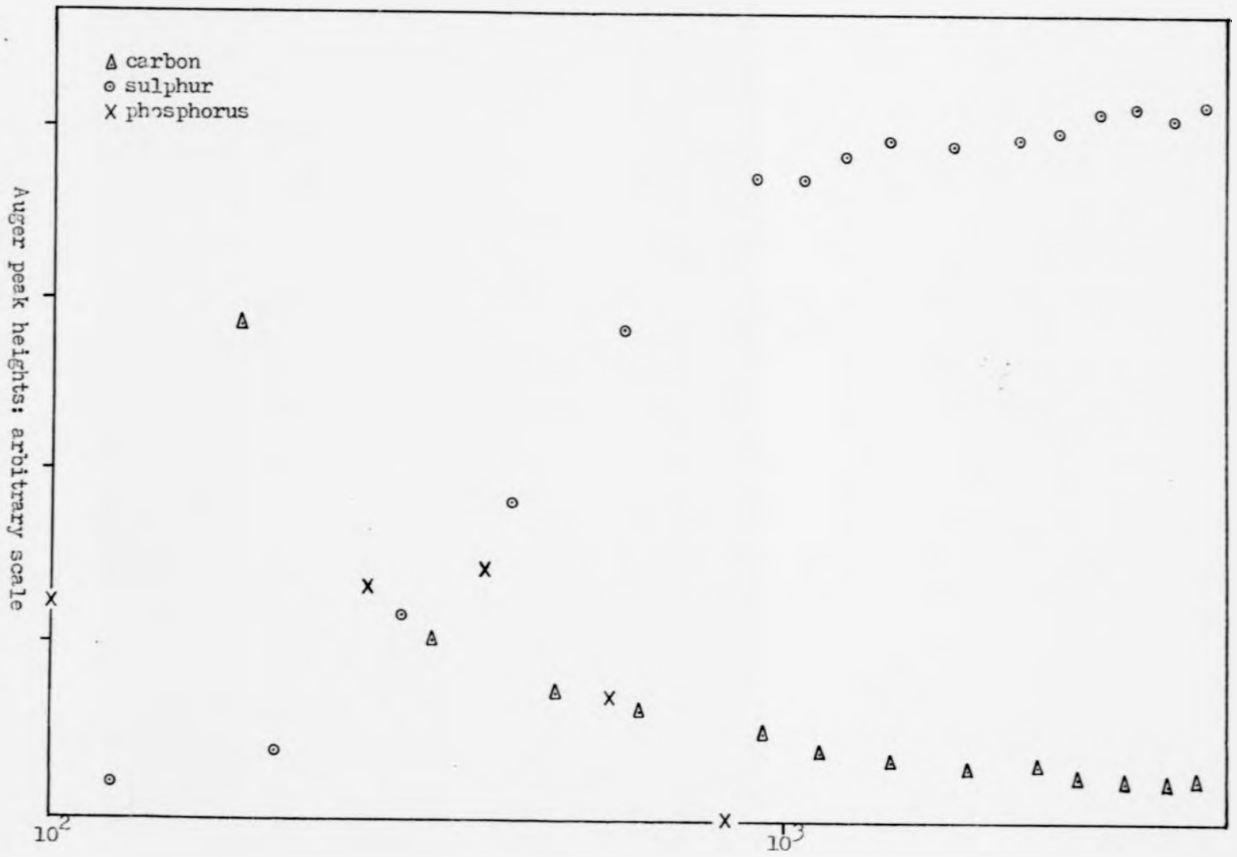

Fig. 4.33 Fe.650: 770°C, slow heating, sulphur depletion

Fig. 4.34 Fe.65C: 800°C, spheroidised sample

4.3. The FeCr alloy

4.3.1. General

On this alloy there was no strong segregation of carbon to the surface. Consequently, sulphur segregation was the dominant feature of surface behaviour in all phase regions unless there was near-surface sulphur depletion. Undepleted sulphur segregation was very fast and a $t^{\frac{1}{2}}$ dependence was observed on one occasion. Transient segregation of other elements occurred when sulphur was depleted, the 'heating' rate was very slow or the temperature of the experiment was below about 600°C. Surface enhancements of phosphorus, carbon, chromium and nitrogen were observed. All except chromium disappeared by the time that sulphur segregation reached saturation coverage.

Fig. 4.35A is an Auger spectrum of a clean surface of this alloy. The positions of the chromium peaks are indicated, but were too small to be distinguished on clean surfaces. Auger spectra from a low temperature experiment are shown in the other parts of this figure. Fig. 4.35B is a spectrum taken soon after the equilibration temperature was reached. Auger peaks due to phosphorus, carbon, nitrogen and chromium appeared as transients. The sulphur Auger peak continued to grow until it reached the state shown in Fig. 4.35C. The chromium Auger peaks were still occasionally visible above the noise level.

Although three regions of the equilibrium phase diagram were accessible to the heating stage, experiments were only performed in two of them. Surface coverages of carbon were calculated on the assumption that it was present at the surface as a segregant rather than a precipitate. All the results presented below are from experiments where there was near-surface depletion of sulphur.

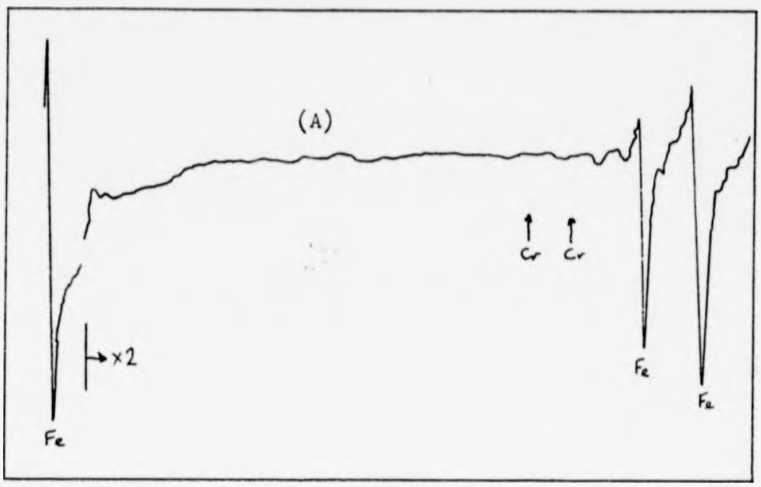

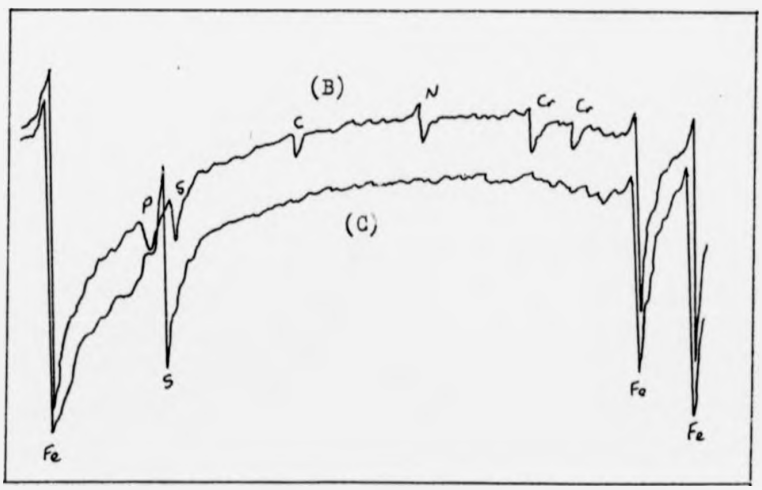

Fig. 4.35 FeCr: Auger spectra of (A) clean surface
(B) transient segregation
(C) final segregation

4.3.2. The α+$(Fe,Cr)_3C$ phase region

A typical result illustrating transient segregation is shown in Fig. 4.36. Approximate lines are included to guide the eye. Such transient segregations were present at low temperatures anyway but they were enhanced by sulphur depletion. All the elements detected at the surface exhibited oscillations in their time-histories. If the individual surface coverages of the interstitial elements are added together, the resulting total surface coverage has a maximum value of about 1.05. This apparent limit to the total surface coverage can also be seen to apply in the result at 650°C which is shown in Fig. 4.37. The rise in the sulphur level did not exhibit oscillations but these were still a feature of the other elements' time-histories. At the point where phosphorus reached its maximum level, and the approximate total interstitial coverage reached 0.95, the sulphur segregation rate increased and the other elements went into a rapid decline. The experiment was stopped before all the phosphorus had disappeared. The sulphur rate-change, from a $t^{\frac{1}{2}}$ to a t^{1} dependence, shows up clearly in the logarithmic plot of its time-history shown in Fig. 4.38. A 'depth-profile' taken after this experiment, Fig. 4.39, showed that both sulphur and phosphorus were comparatively poorly localised at the surface.

Fig 4.40 shows the effect of 'heating' to 720°C. A curve corresponding to the total phosphorus-plus-sulphur coverage is included in this figure. It shows that their total surface coverage had a maximum value close to unity. The carbon Auger peak disappeared at about the time that this maximum was achieved. Sulphur had a $t^{1.4}$ dependence throughout this experiment (Fig. 4.41). Phosphorus segregation exhibited a $t^{\frac{1}{2}}$ dependence as shown in Fig. 4.42. The

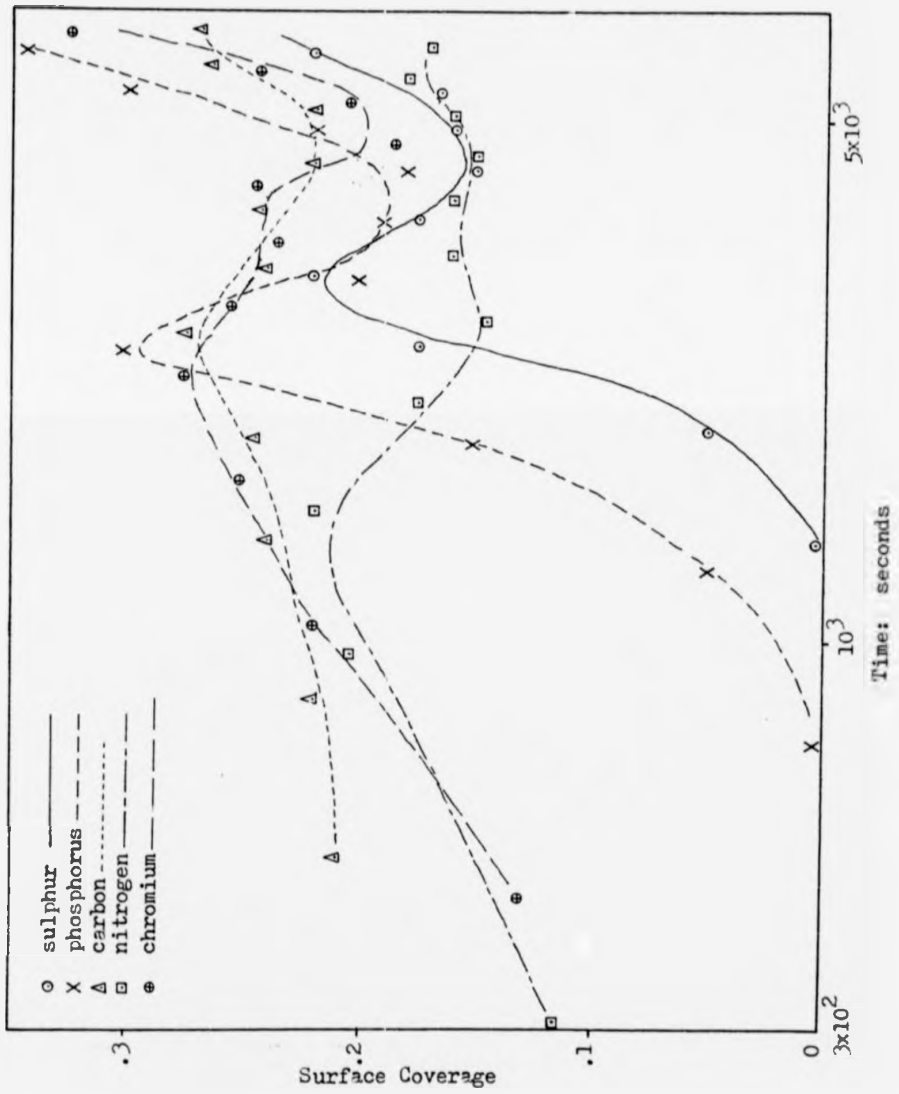

Fig. 4.36 FeCr: transient segregation at 600°C

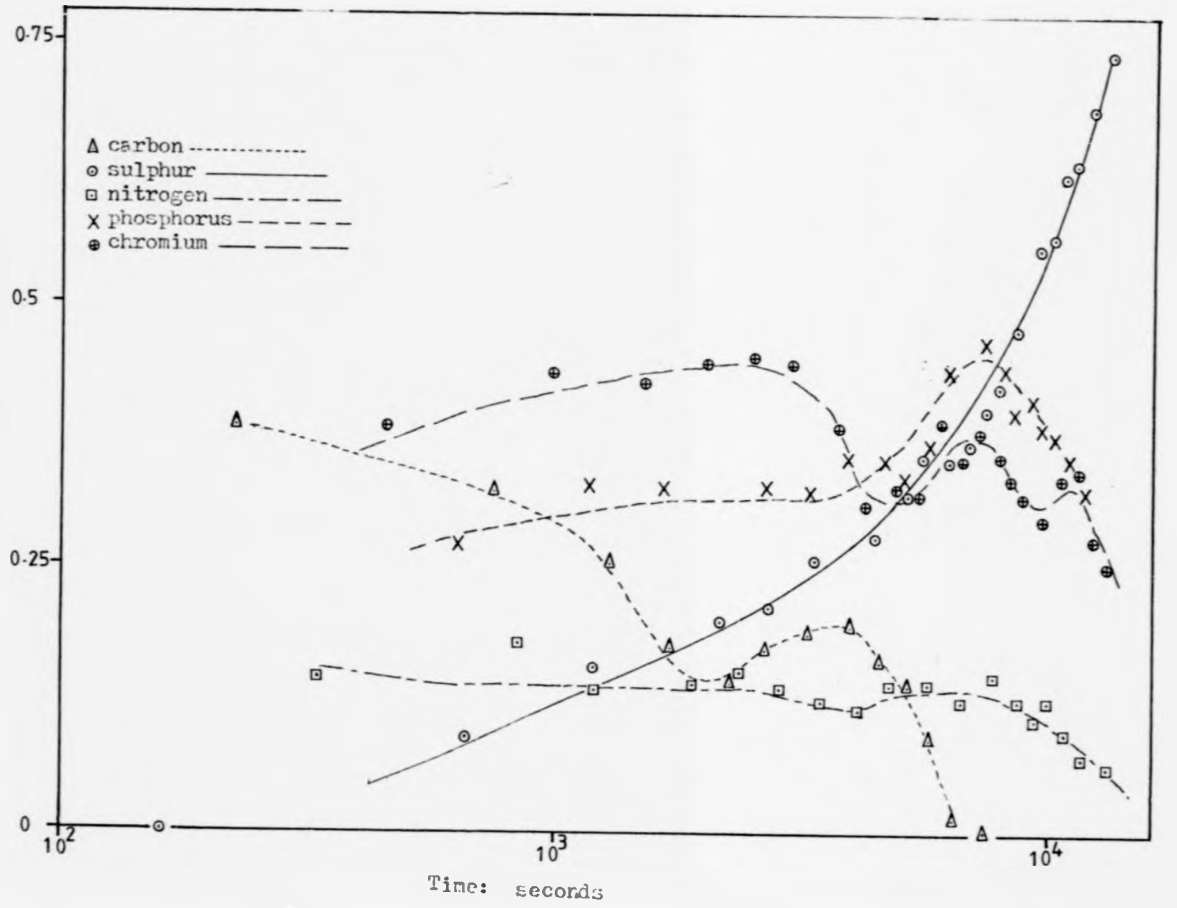

Fig. 4.37 FeCr: transient segregation at 650°C

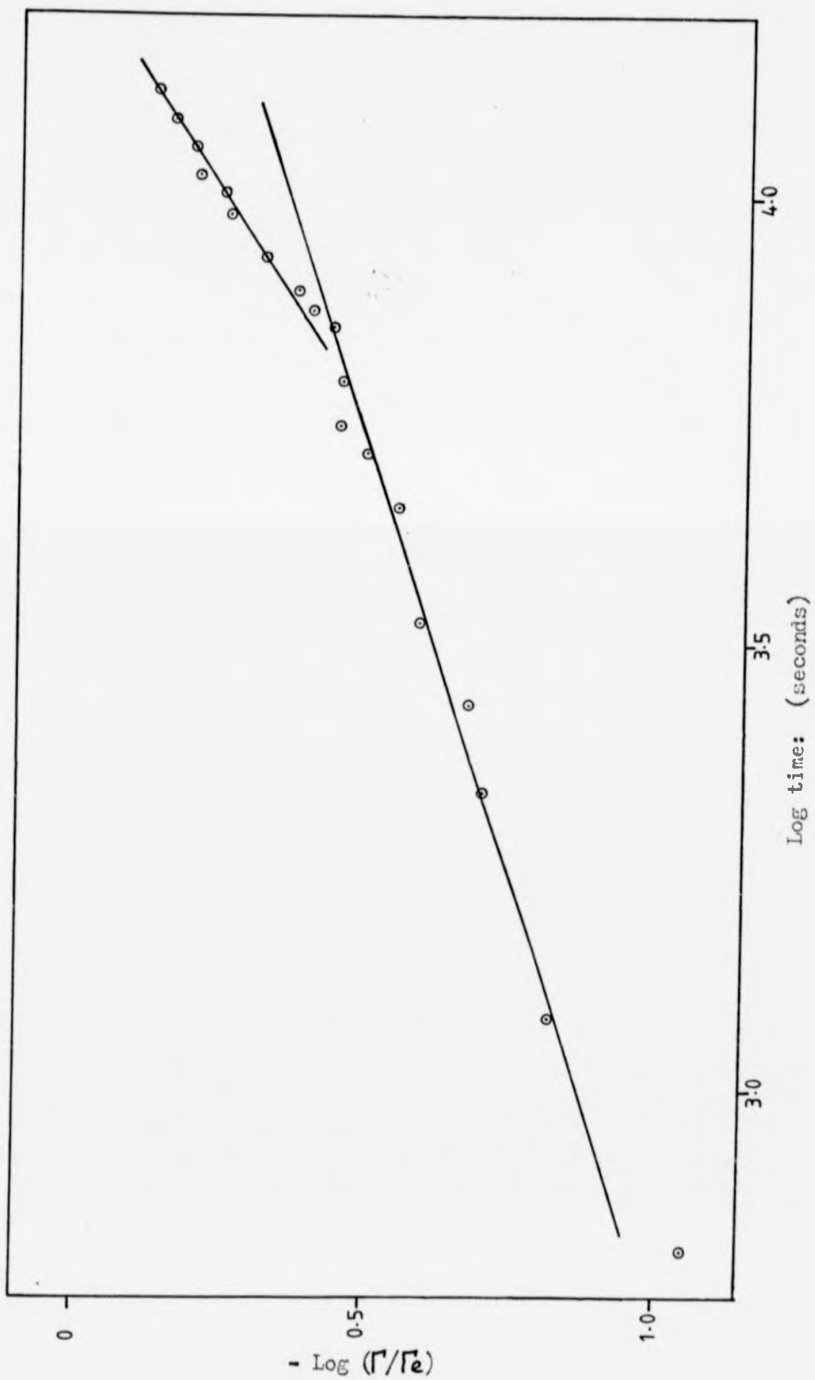

Fig. 4.18 FeCr: sulphur segregation at 650°C

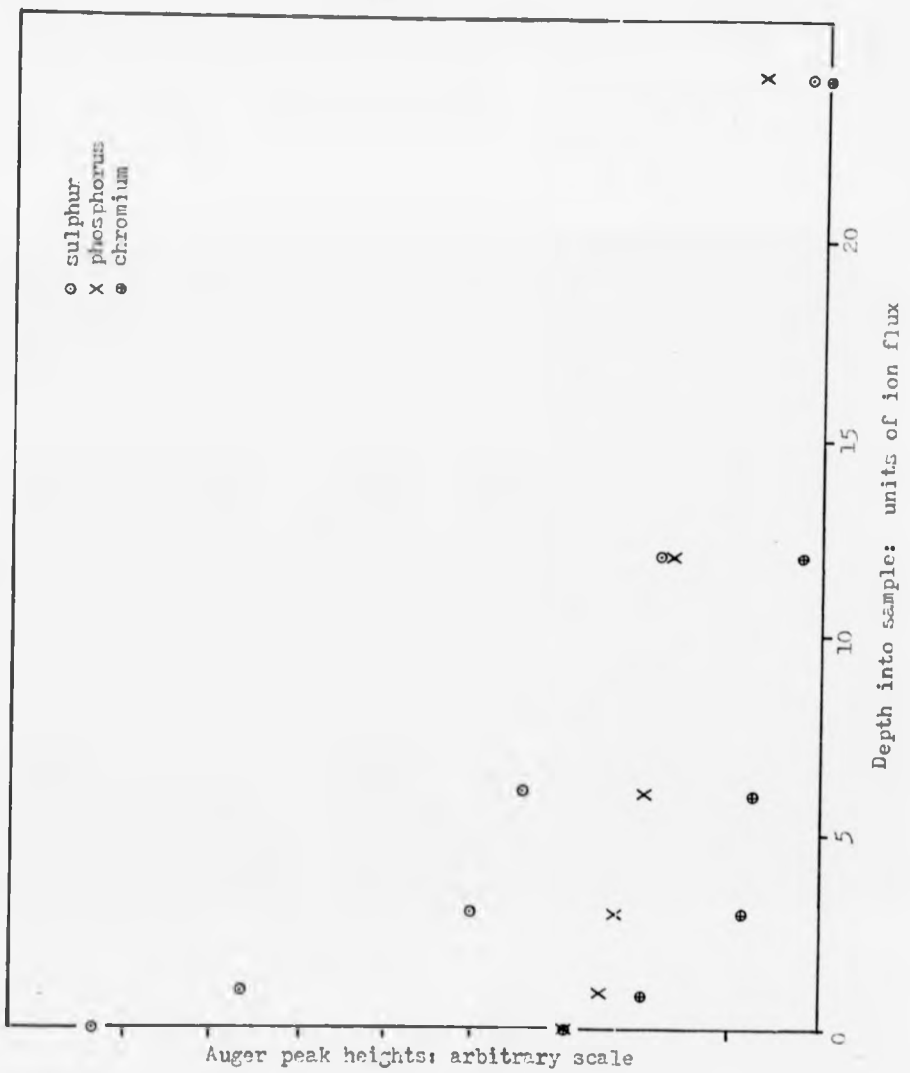

Fig. 4.39 FeCr: depth profile after experiment at 650°C

Fig. 4.40 FeCr: transient segregation at 720°C

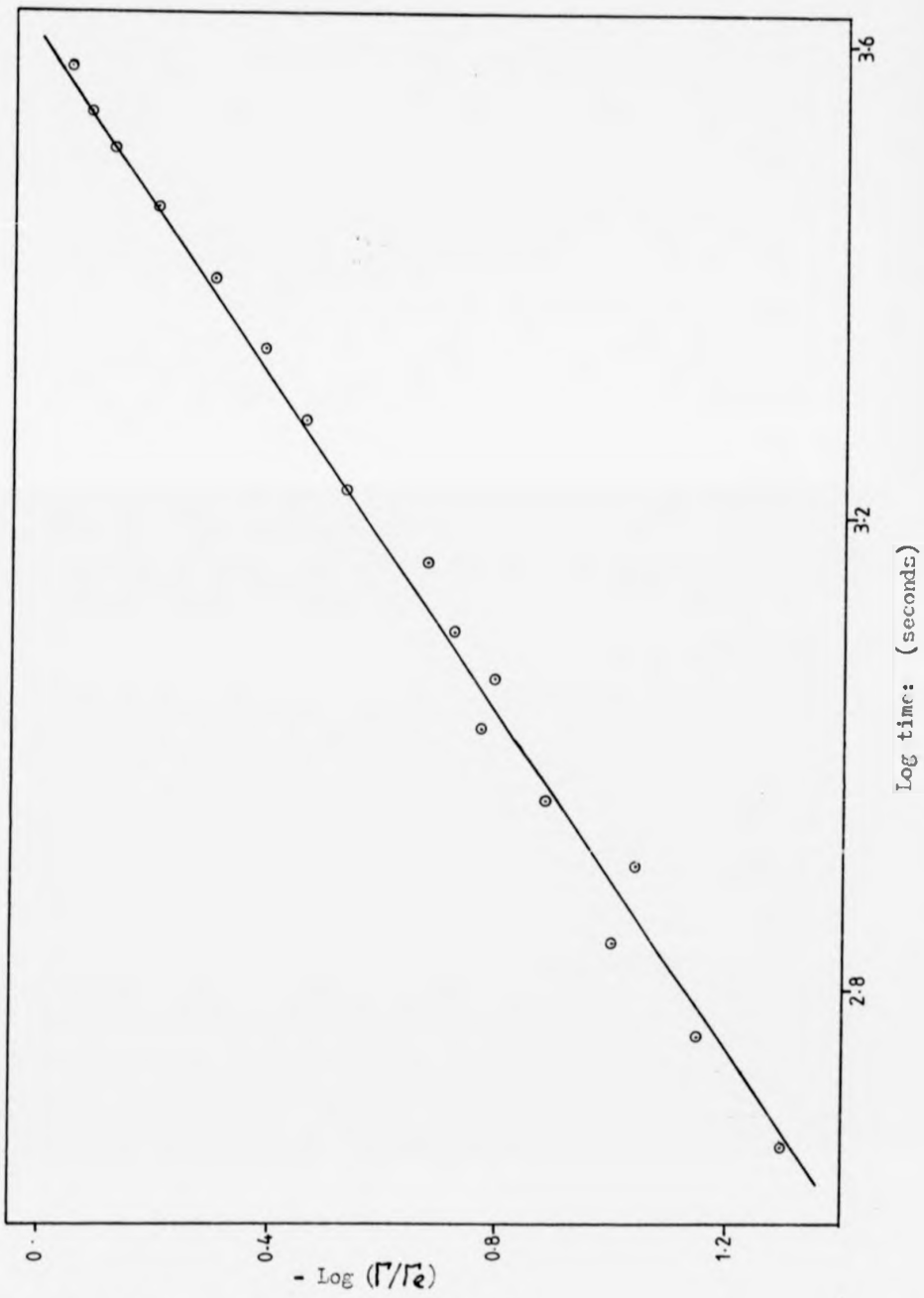

Fig. 4.41 FeCr: sulphur segregation at 720°C

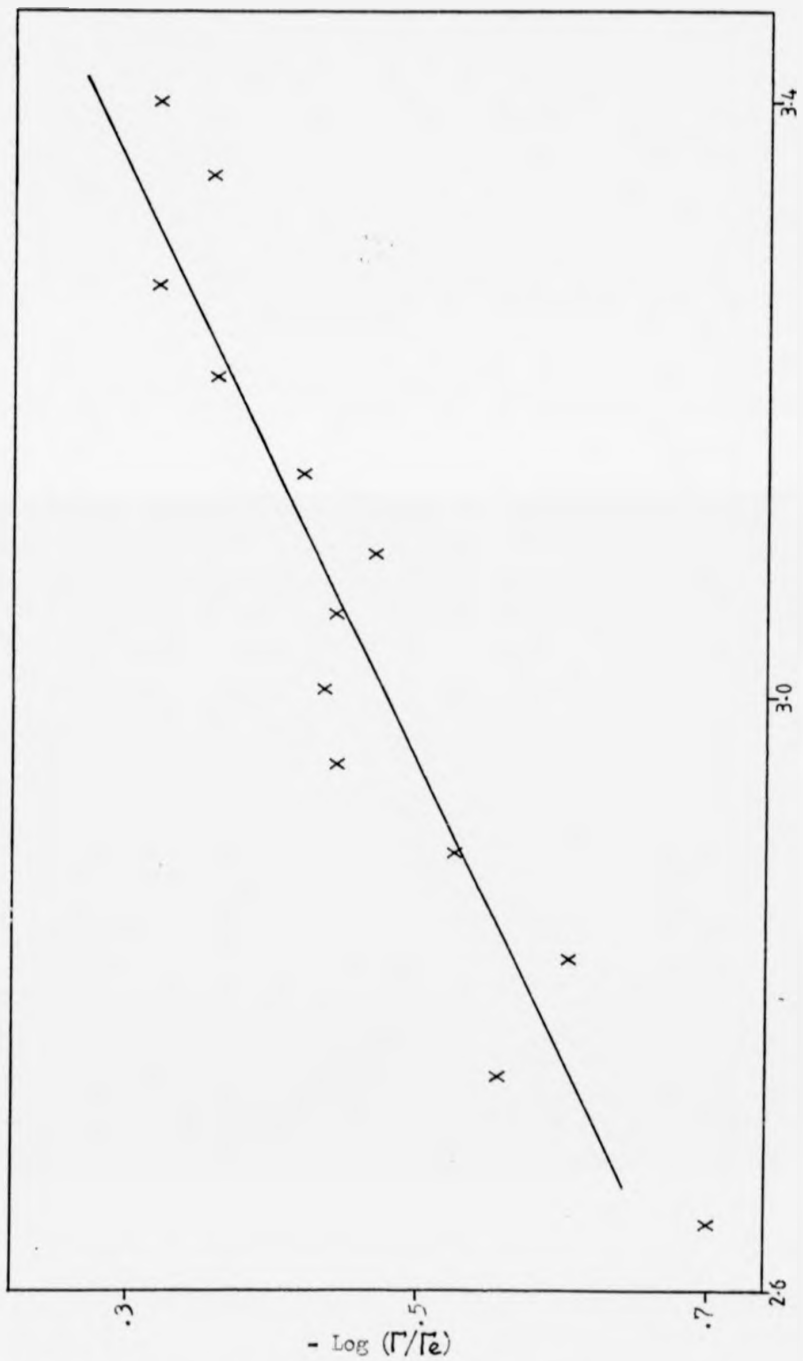

Fig. 4.42 FeCr: phosphorus segregation at 720°C

long-term behaviour of sulphur and chromium during this experiment has been plotted separately in Fig. 4.43. As the sulphur level approached saturation the chromium level began to rise. The sulphur level fell sharply to a lower, but fairly stable value shortly after it had reached saturation. At this time, the chromium concentration reached the highest level ever observed at a sulphur-covered surface. A 'depth-profile' taken at the end of this experiment is shown in Fig 4.44. The sulphur profile was broader than usually observed and the chromium level did not decrease much with depth into the surface.

4.3.3. The $\alpha+\gamma$ phase region

With the exception of phosphorus, the maximum level of the transient segregants was small on sulphur-depleted samples 'heated' into this phase region. A result from an experiment where a sample was 'heated' to 795°C is shown in Fig 4.45. The chromium level passed through an early maximum. Phosphorus was next to reach a maximum but shortly afterwards its level declined rapidly to zero as the sulphur arrival rate increased. There was also a minimum in the chromium concentration at this time. The change in the sulphur segregation rate shows up clearly in Fig. 4.46. The two lines drawn through the results have slopes of 1.0 and about 4. A 'depth-profile' was also taken after this experiment and is shown in Fig. 4.47. Error bars are included in this figure to show that the initial increase in the chromium level was a significant result. The sulphur saturation level in these experiments did not show any sign of the effect of evaporation from the surface. A higher temperature result did, however, result in a sulphur level which passed through a maximum and then slowly declined.

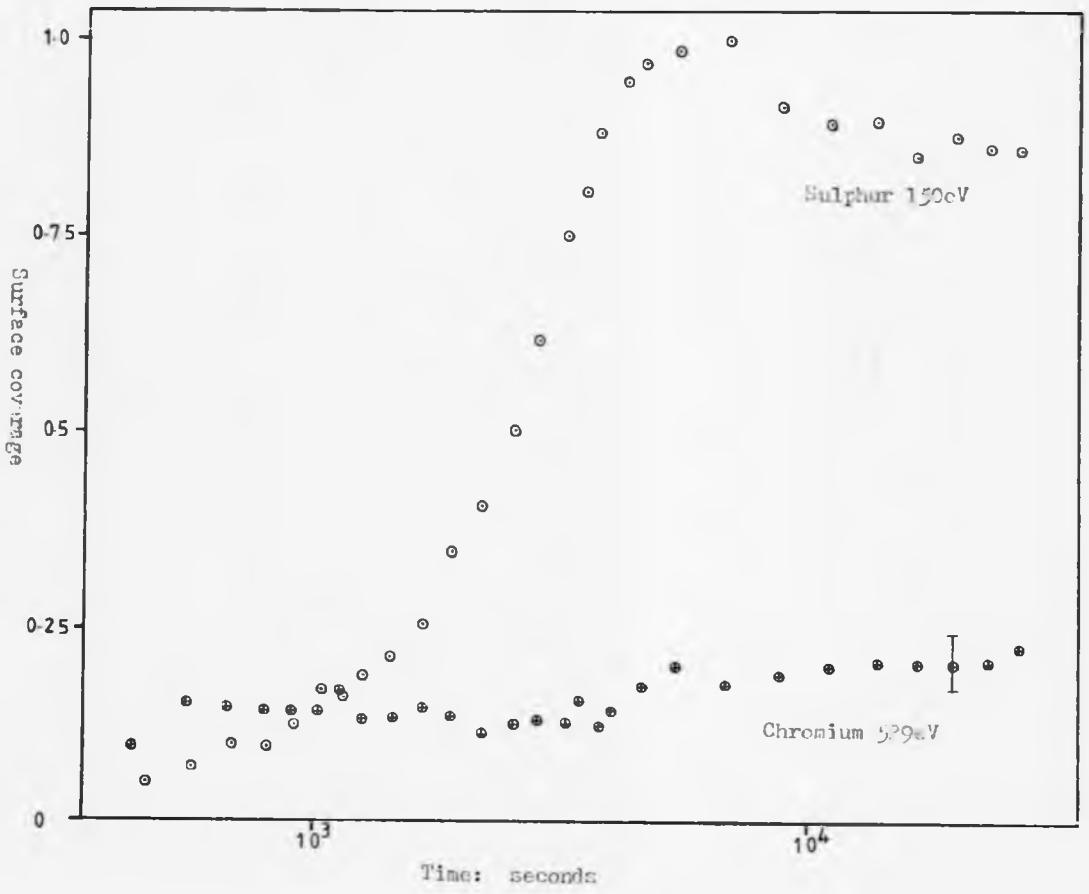

Fig. 4.43 FeCr: long term segregation at 720°C

Fig. 4.44 FeCr: depth profile after experiment at 720°C

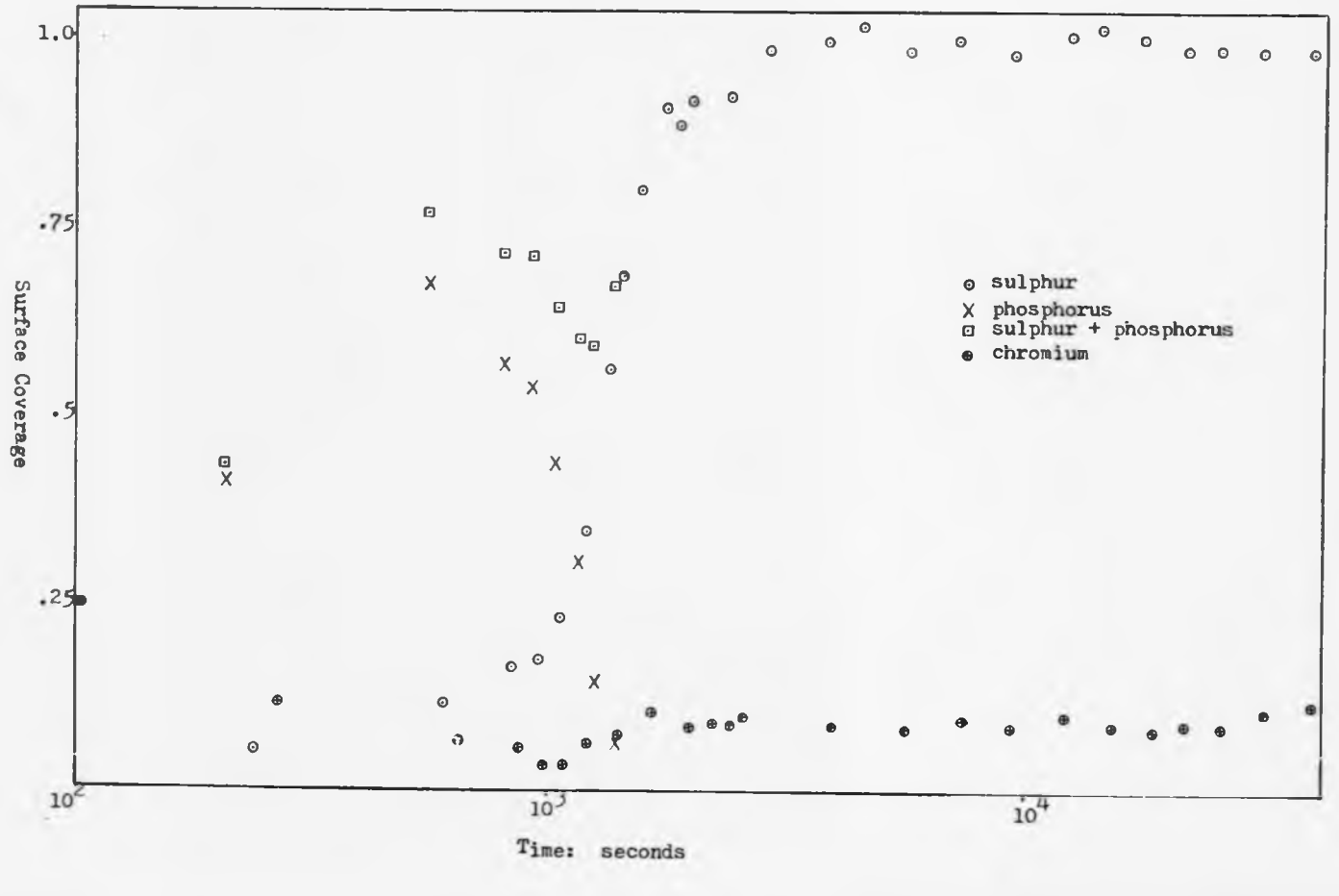

Fig. 4.45 FeCr: segregation at 795°C

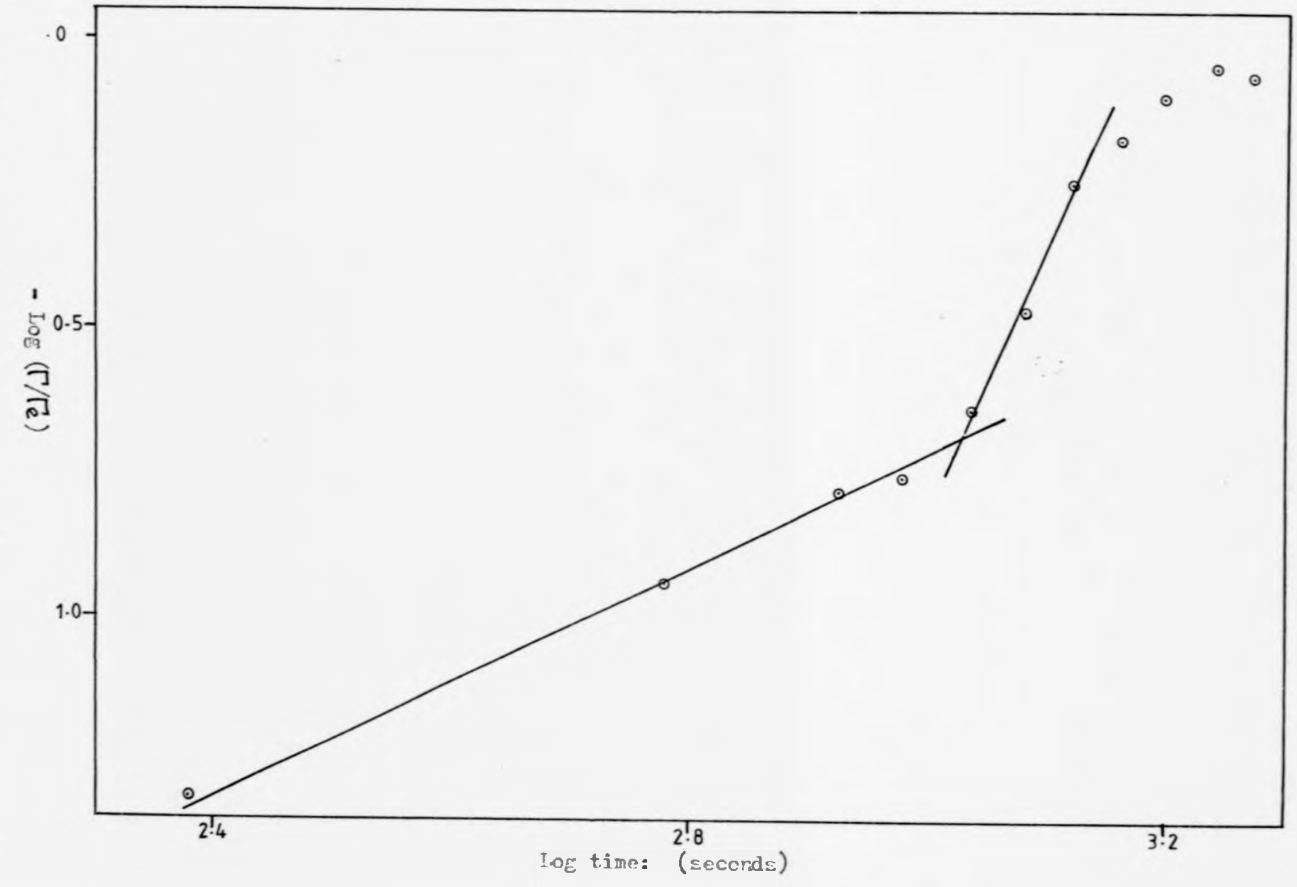

Fig. 4.46 FeCr: sulphur segregation at 795°C

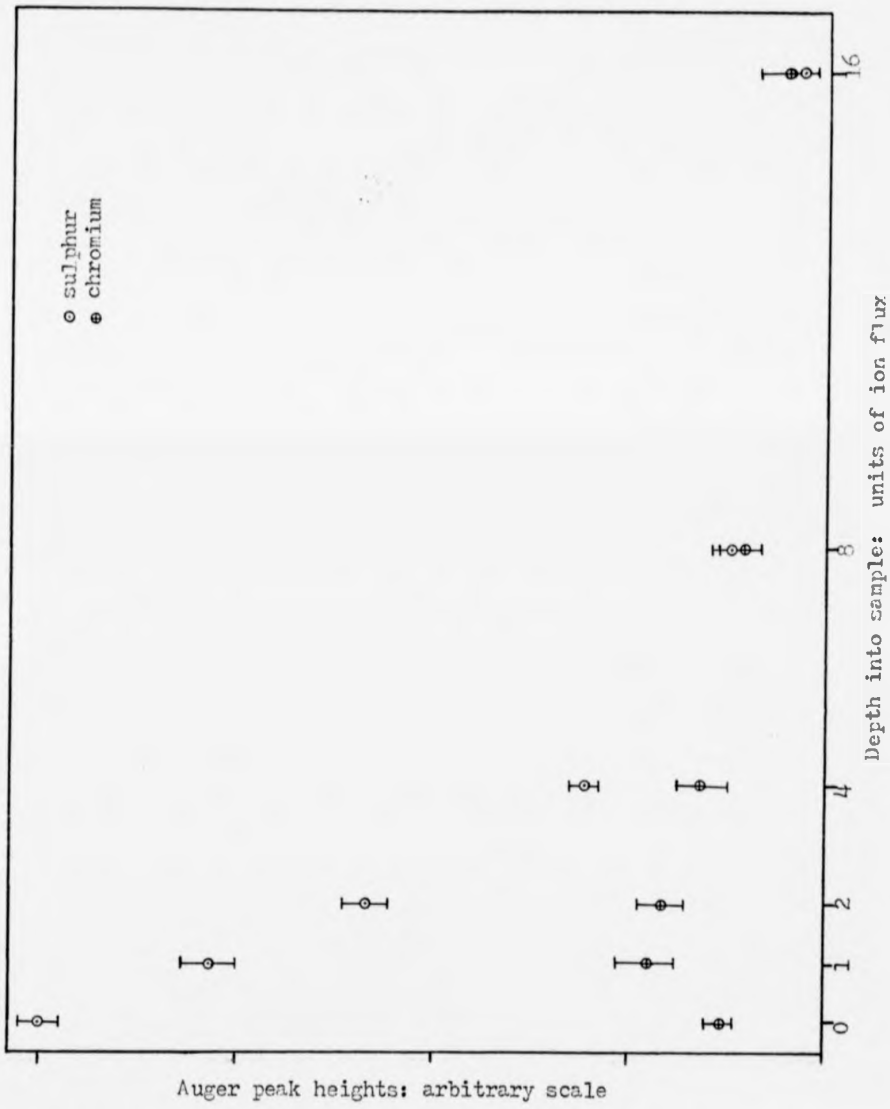

Fig. 4.47 FeCr: depth profile after experiment at 795°C

4.4. The FeCrC alloy

4.4.1. General

The increased carbon content of this alloy relative to the FeCr alloy produced a new, three-phase region: $\alpha+\gamma+(Fe,Cr)_3C$. The results in all phase regions were broadly similar to those obtained on the FeCr alloy, except that the carbon Auger peak was more persistent. There was no evidence of unusual behaviour by chromium. Apart from the first figure, all the results presented below are from sulphur-depleted samples.

4.4.2. The $\alpha+(Fe,Cr)_3C$ phase region

'Heating' an undepleted sample to 600°C produced the result shown in Fig. 4.48. The sulphur segregation rate had a maximum $t^{3.5}$ dependence. The sulphur coverage began to level off when it was just short of saturation. At the same time, there was a persistent carbon Auger peak at a low level. Sulphur did not reach saturation until the carbon peak had disappeared. Segregated carbon is known to be easily displaced by sulphur, so this could be an indication that the carbon was present as resistant graphite islands (Grabke et al (1975)). Fig. 4.49 shows another result at the same temperature, but on a sulphur-depleted sample. Phosphorus and carbon were the first elements to appear. The carbon Auger peak disappeared when the phosphorus-plus-sulphur coverage reached unity. Both the sulphur and phosphorus segregation rates exhibited $t^{\frac{1}{2}}$ dependences. At 685°C, Fig. 4.50, phosphorus segregation still had a $t^{\frac{1}{2}}$ dependence but that of sulphur was linear with time. The first maximum in the phosphorus-plus-sulphur coverage was less than unity and the carbon Auger peak persisted until sulphur reached saturation coverage on its own.

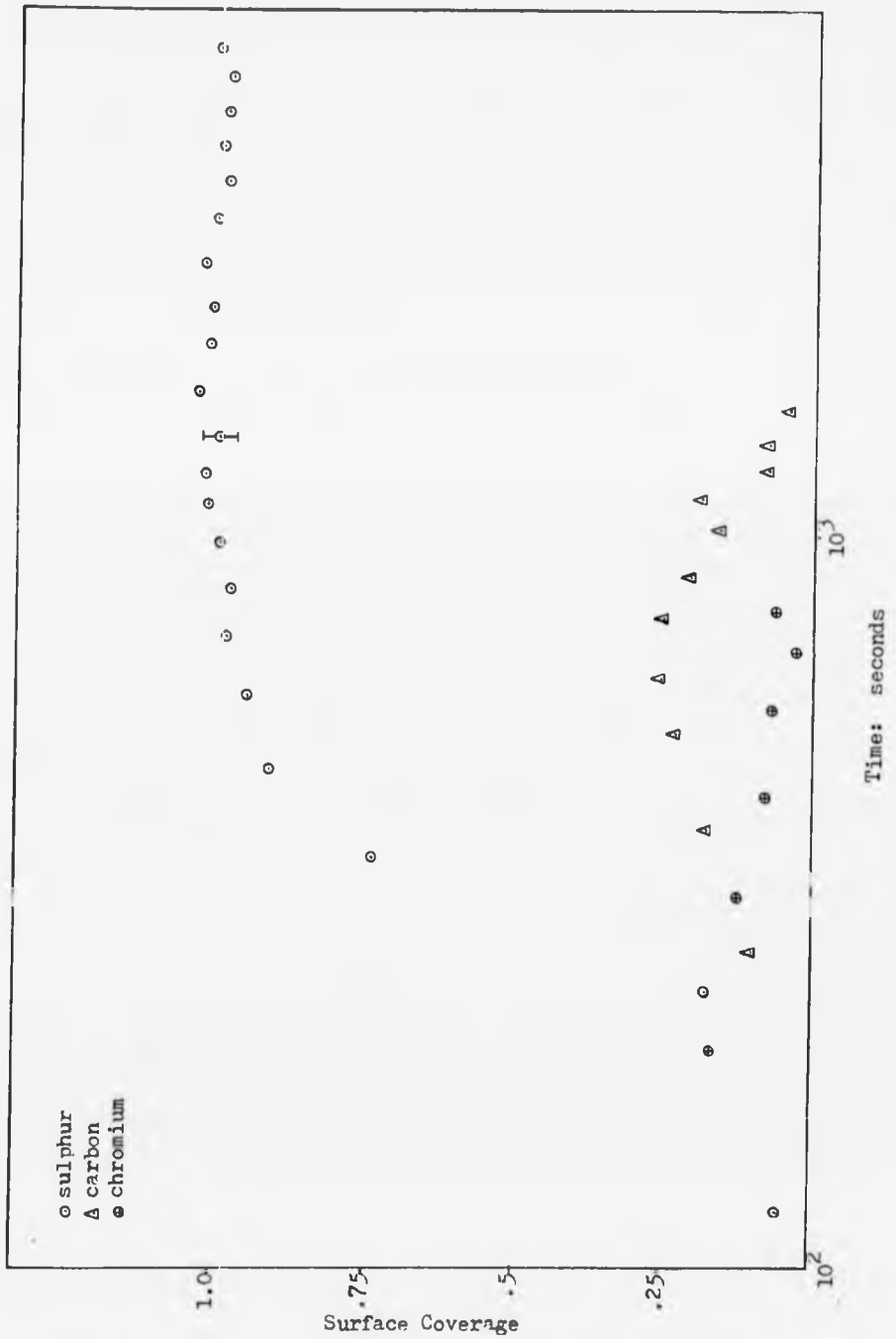

Fig. 4.48 FeCrC: segregation at 600°C, no sulphur depletion

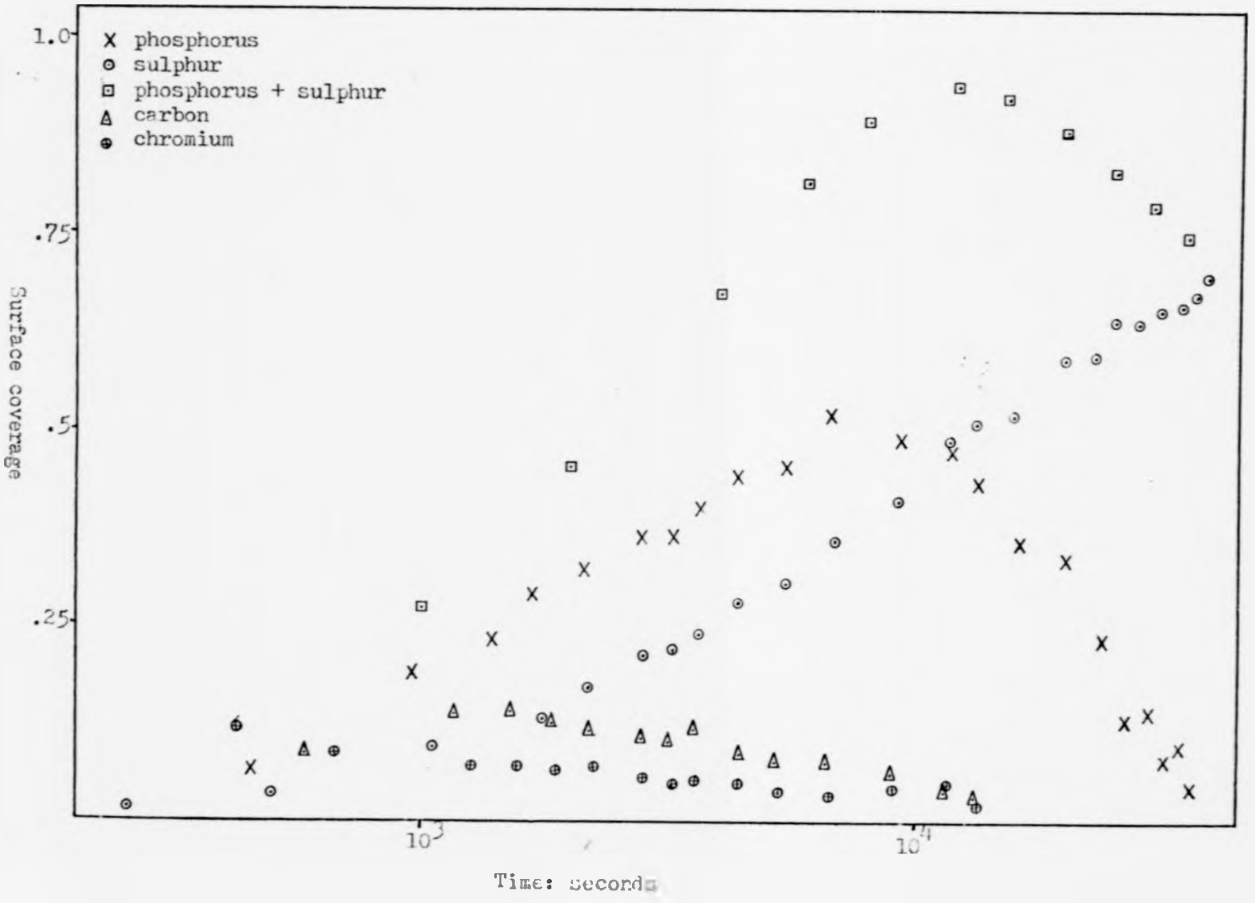

Fig. 4.49 FeCrC; transient segregation at 600°C

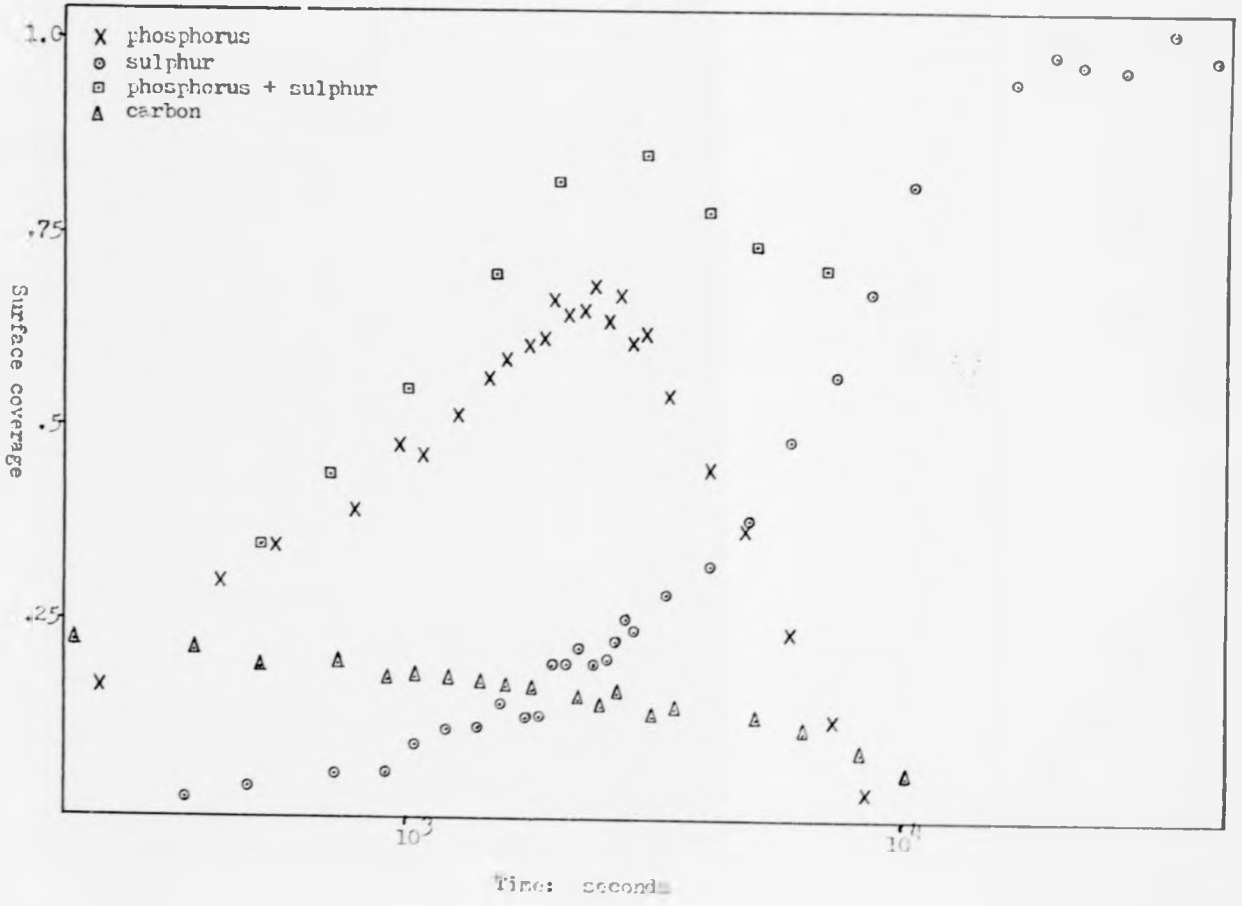

Fig. 4.50 FeCrC: segregation at 685°C

4.4.3. The $\alpha+\gamma+(Fe,Cr)_3C$ phase region

In this phase region, carbon and chromium were generally present at lower levels. An interesting feature of an experiment at 740°C was the persistence of the phosphorus level. Fig. 4.51 shows how it approached saturation very quickly and then went into a gradual decline. A logarithmic plot of the sulphur time-history is shown in Fig 4.52. There was a gradual change in the arrival rate from a $t^{\frac{1}{2}}$ to a t^1 dependence. At 760°C, Fig. 4.53, 'heating' produced a phosphorus level that was not as high as at 740°C but still showed the same slow rate of decline. Fig. 4.54 shows that there was again a change in the sulphur segregation rate, but that it was an abrupt change this time. A logarithmic plot of the phosphorus time-history is shown in Fig. 4.55. It can be seen that the rate of disappearance of phosphorus increased at the same time that the sulphur arrival rate increased. The straight line drawn in this figure has a slope of 0.5.

4.4.4. The $\gamma+(Fe,Cr)_3C$ phase region

Once again the pattern of segregation was similar, and only three results are presented. These are from three consecutive experiments at the same temperature on the same sample (although not on exactly the same area of that sample). Between each pair of experiments the sample was given a 'superficial' ion bombardment. The result of the first experiment is shown in Fig. 4.56, and the logarithmic plot in Fig. 4.57 shows that the sulphur segregation rate had a linear time dependence. The two subsequent results are shown in Figs. 4.58 and 4.59. In each case the sulphur segregation rate had the same t^1 dependence. Phosphorus segregated more strongly each time, and there were also small carbon and chromium Auger peaks.

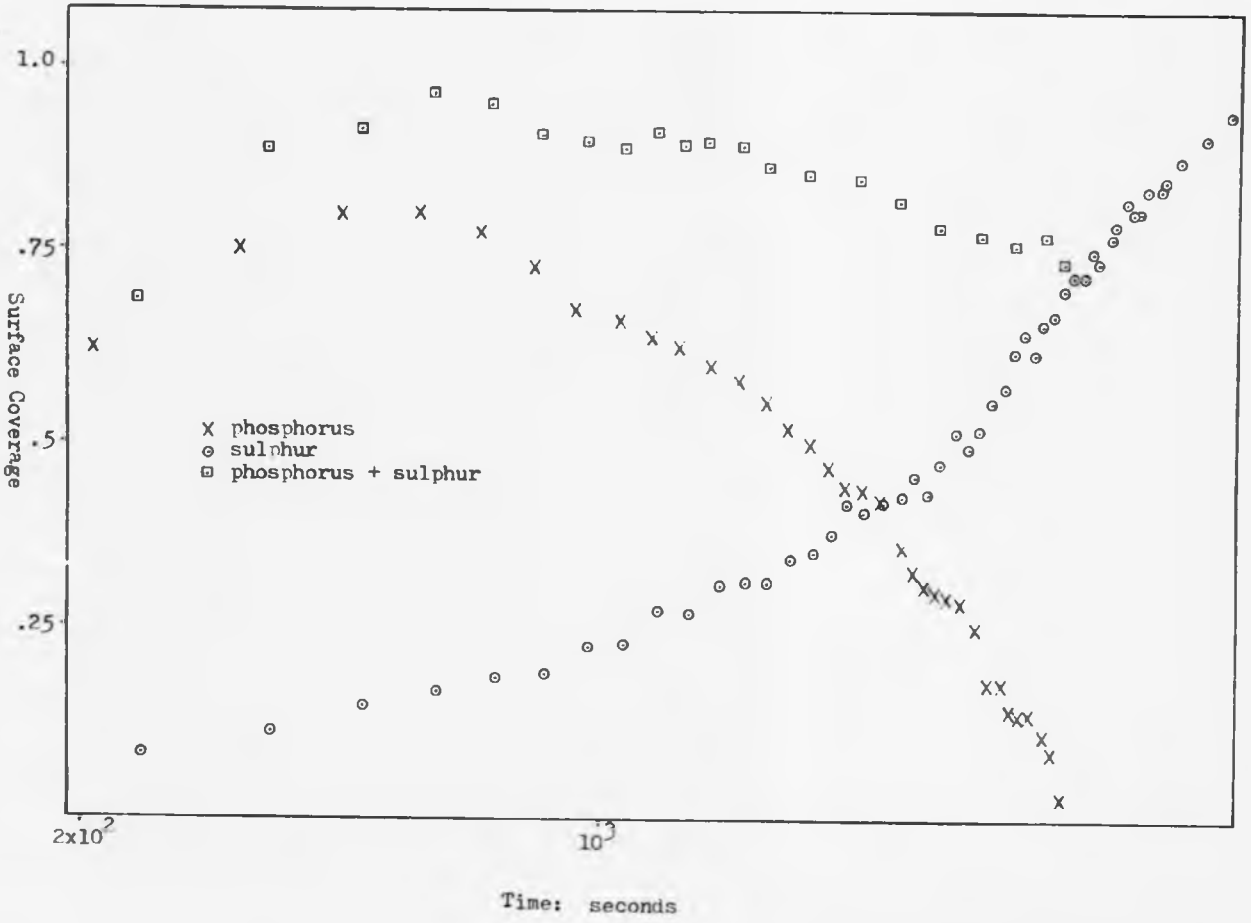

Fig. 4.51 FeCrC: segregation at 740°C

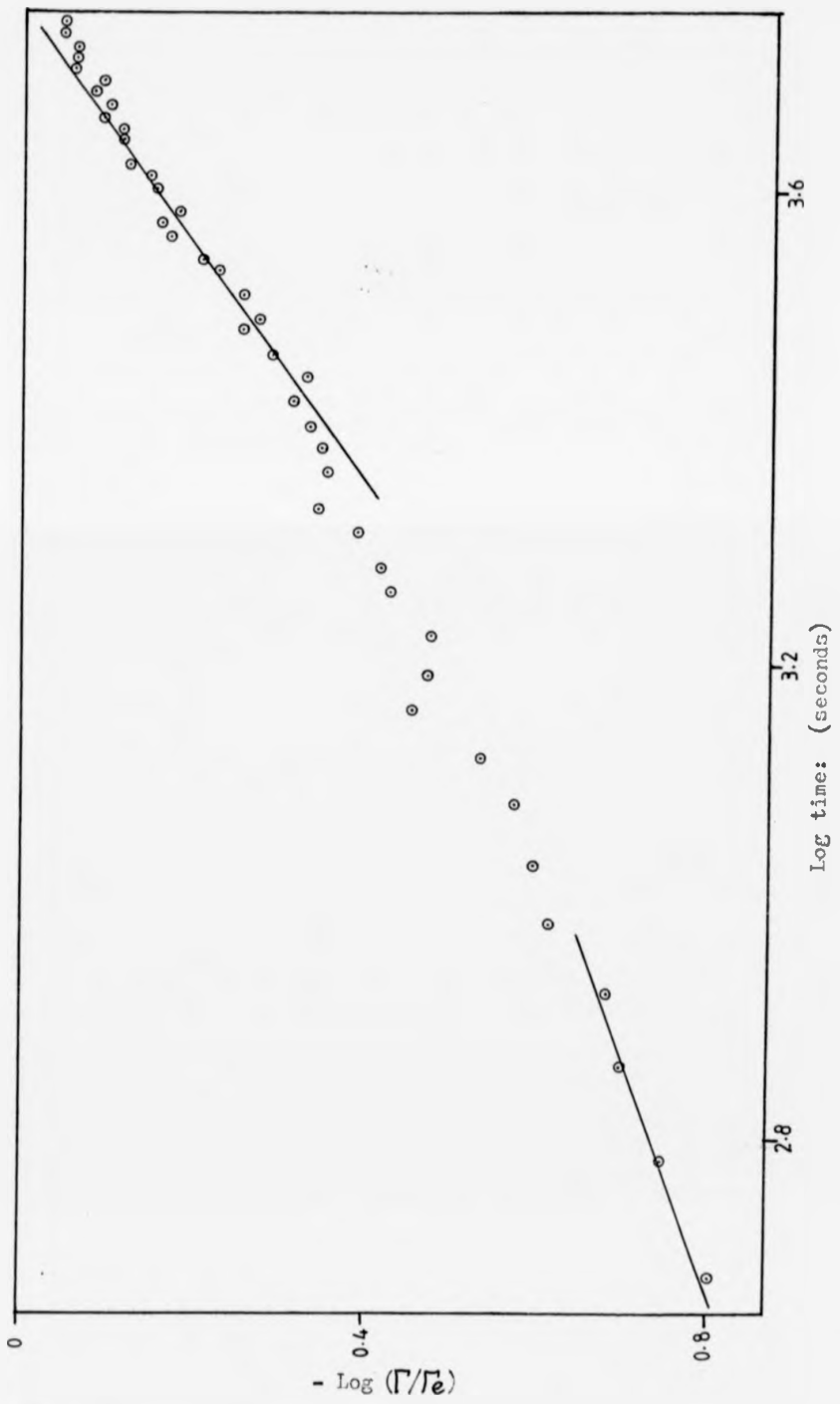

Fig. 4.52 FeCrC: sulphur segregation at 740°C

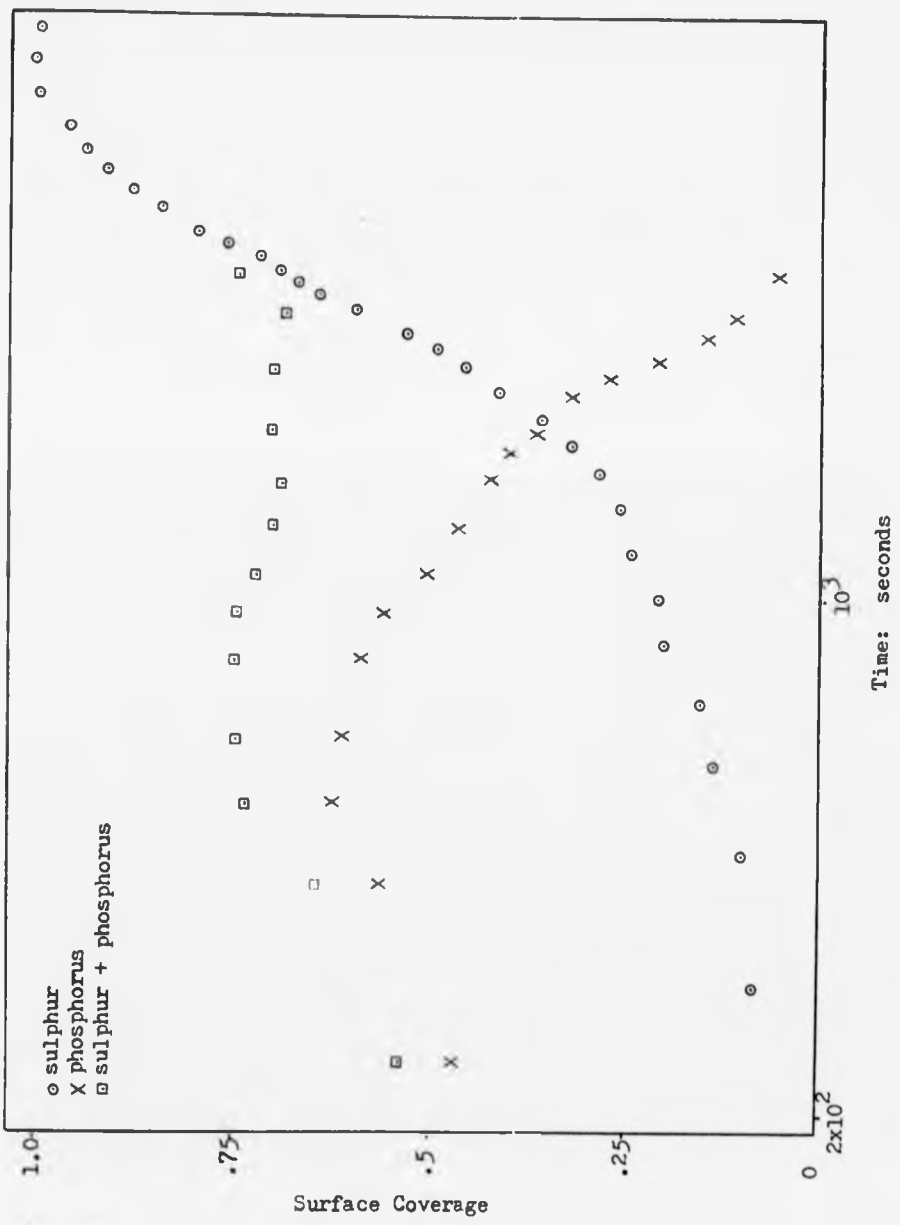

Fig. 4.53 FeCrC: segregation at 760°C

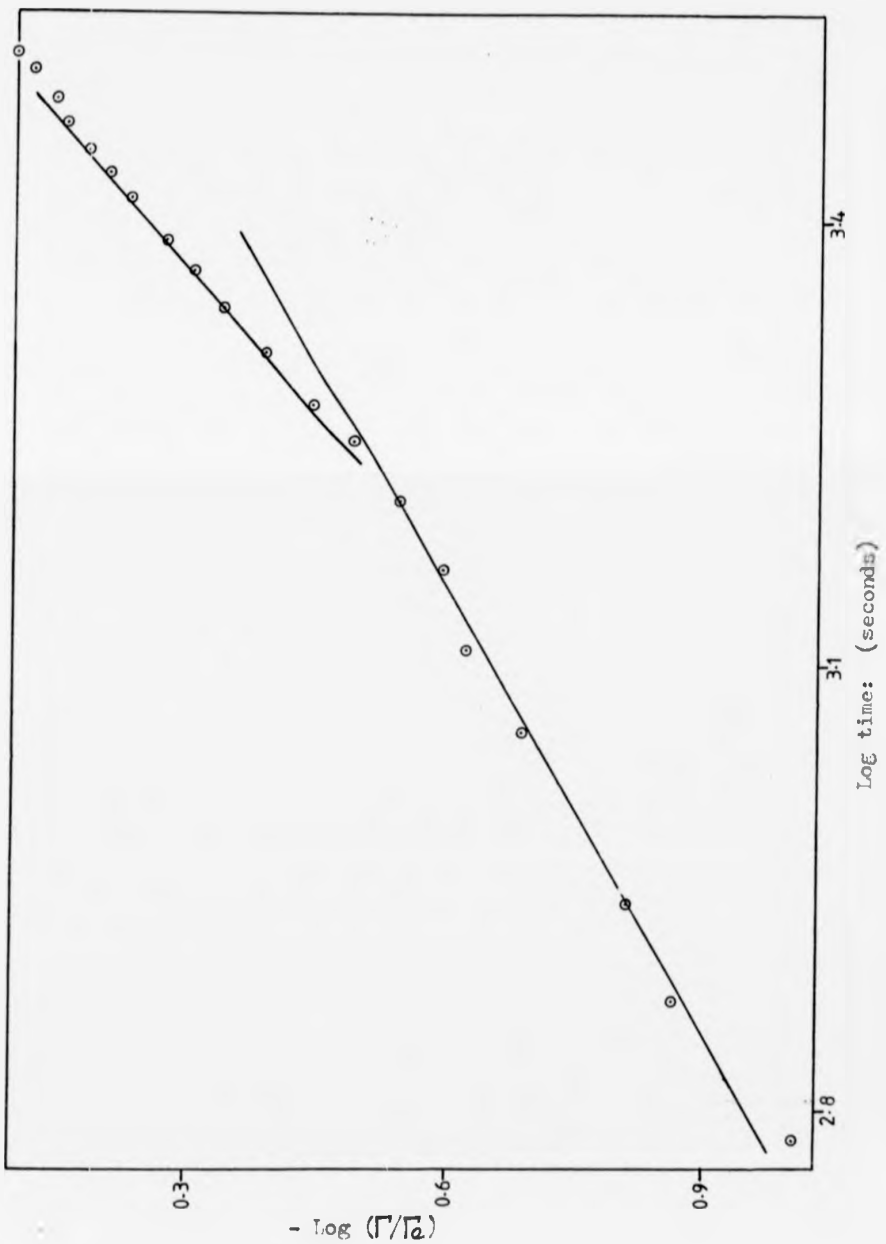

Fig. 4.54 FeCrC: sulphur segregation at 760°C

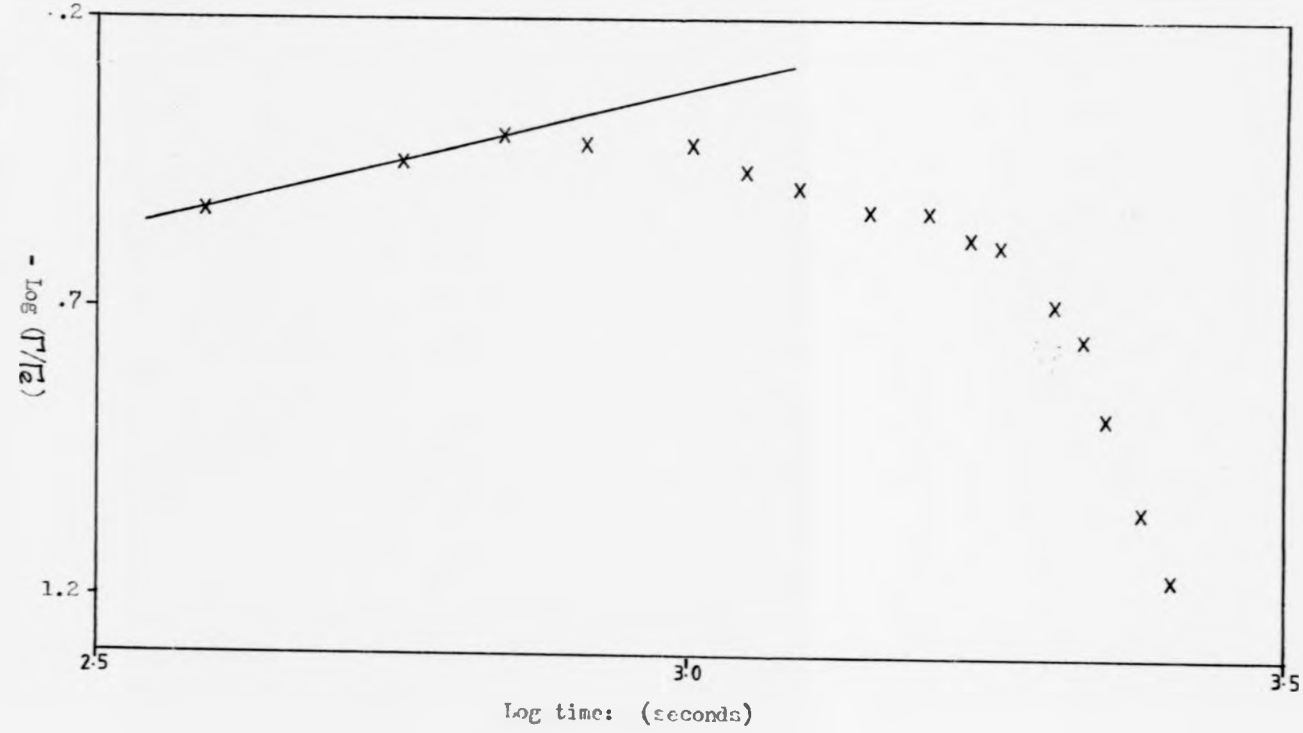

Fig. 4.55 FeCrC: phosphorus segregation at 760°C

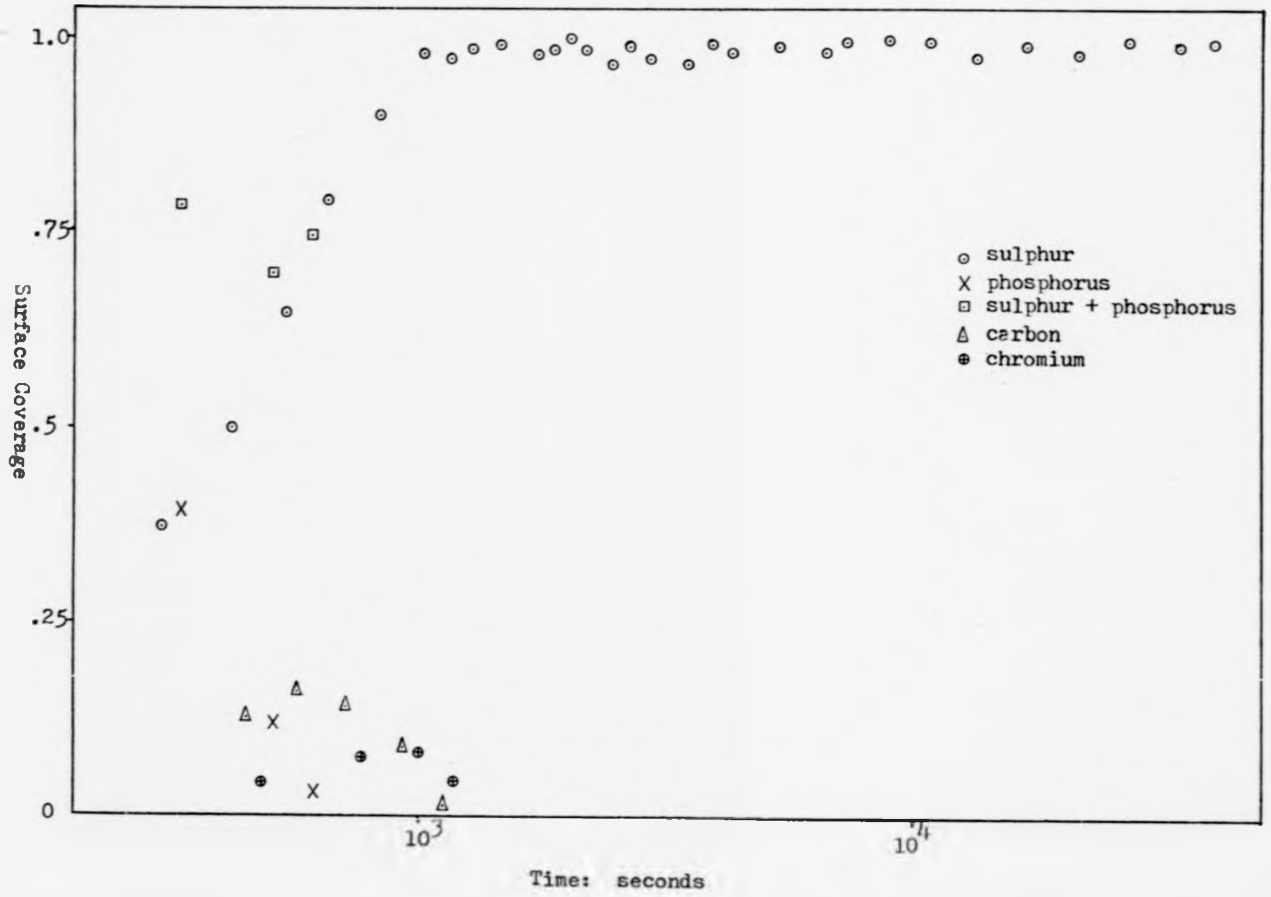

Fig. 4.56 FeCrC: segregation at 775°C

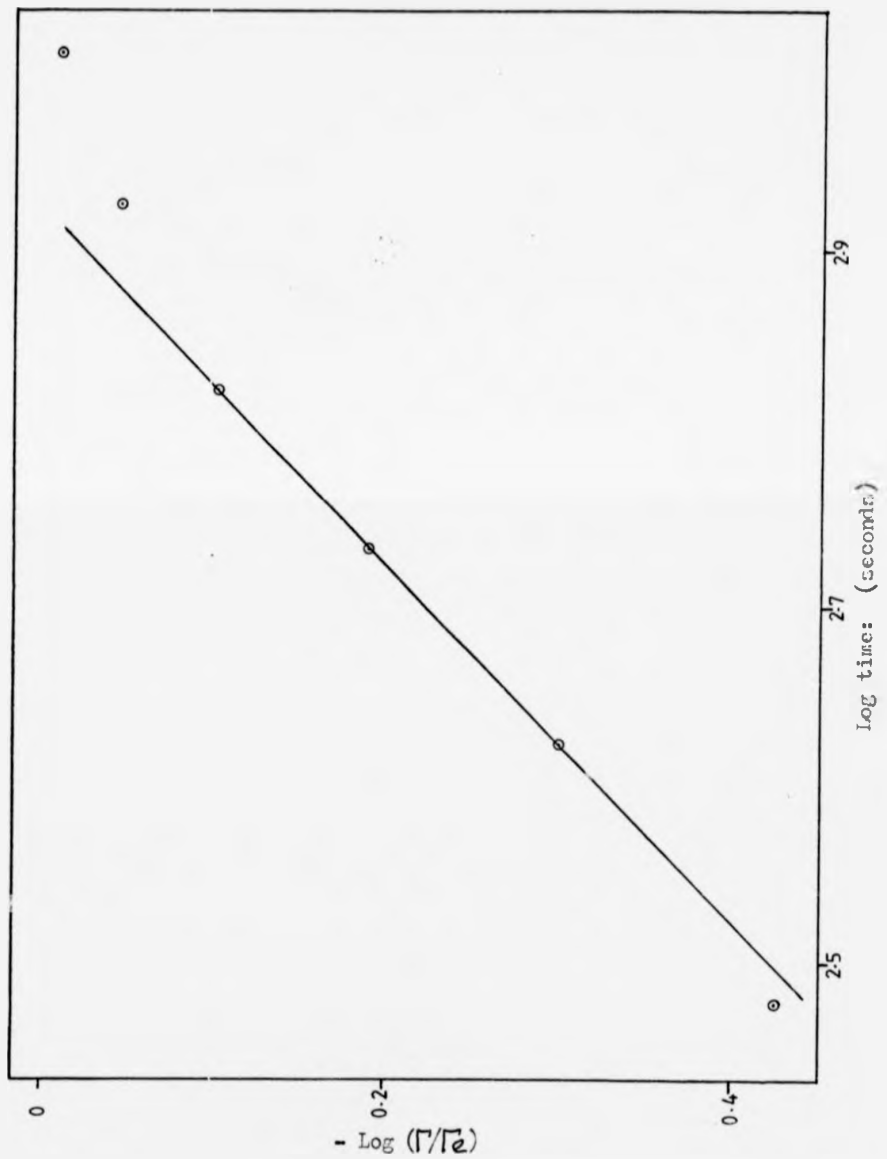

Fig. 4.57 FeCrC: sulphur segregation at 775°C

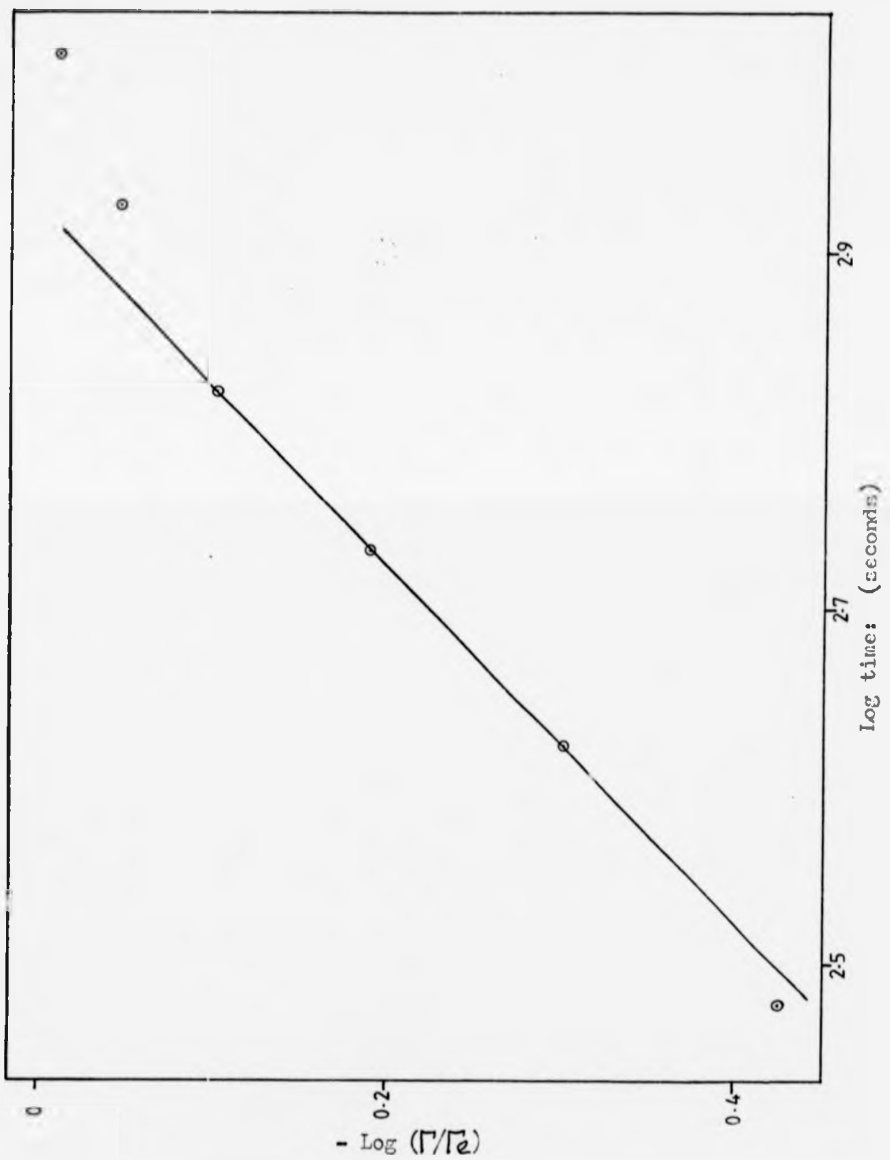

Fig. 4.57 FeCrC: sulphur segregation at 775°C

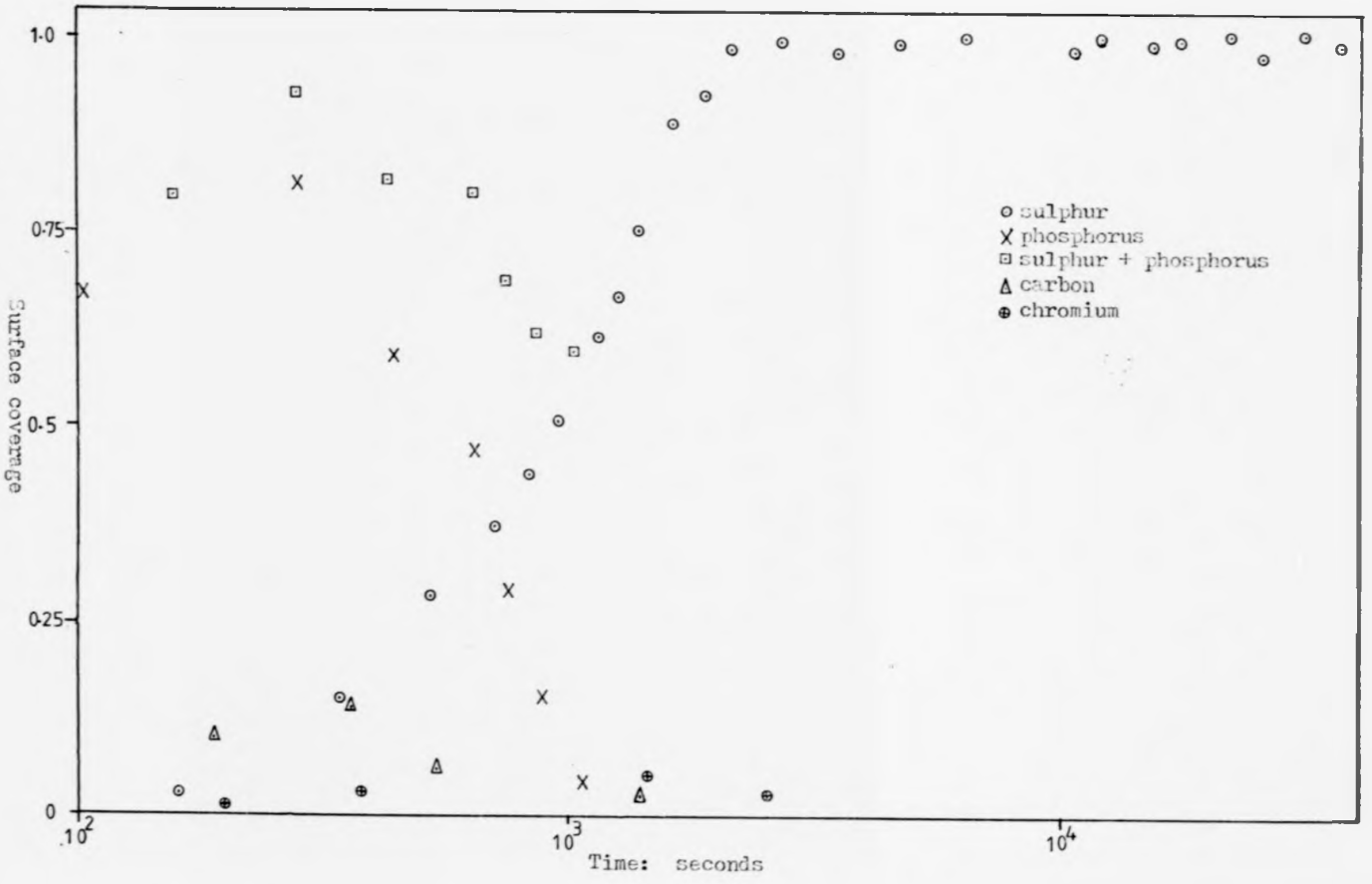

Fig. 4.58 FeCrC: segregation at 775°C

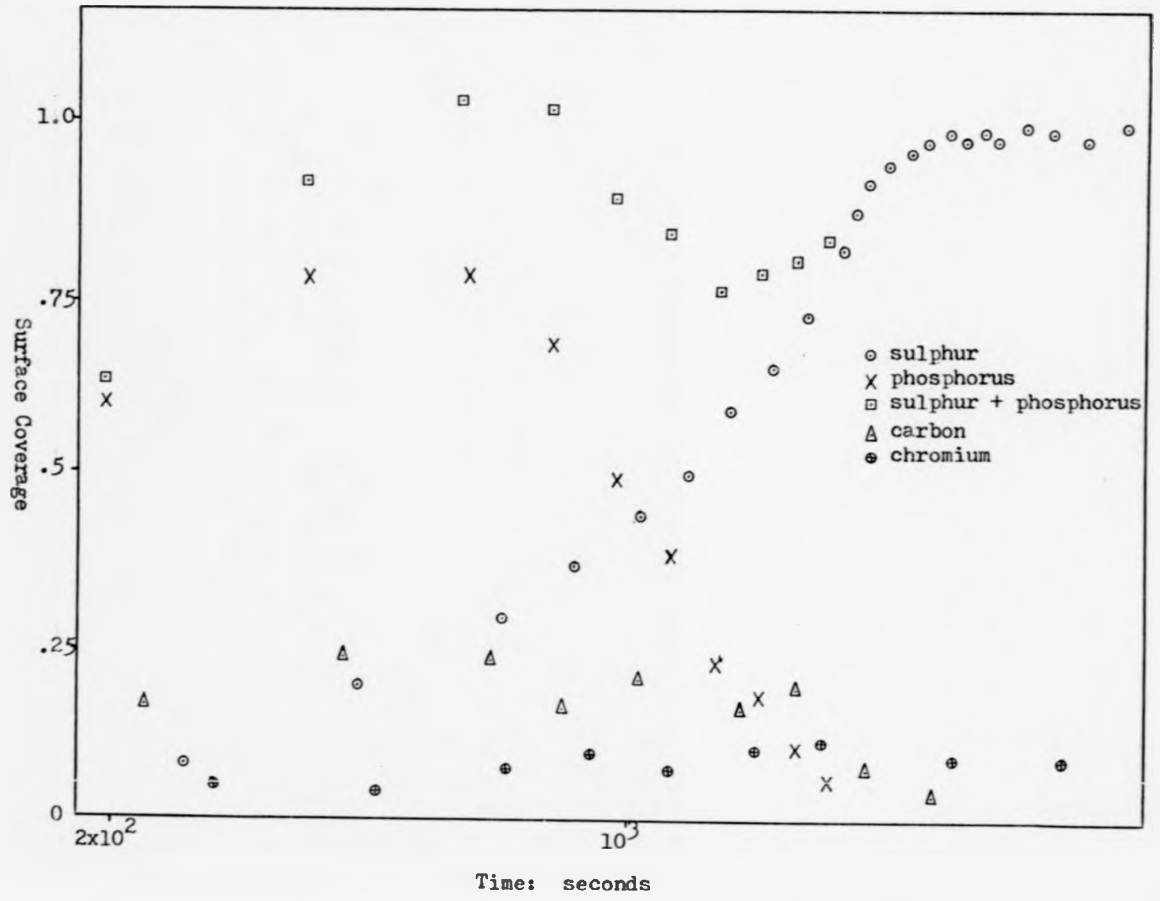

Fig. 4.59 FeCrC: segregation at 775°C

4.5. The commercial HCC alloy

4.5.1. General

Samples of this alloy gave very variable results. Surface enhancements of sulphur, phosphorus, carbon, nitrogen and chromium were observed. Manganese had been added to the commercial alloy to 'tie-down' the sulphur, and so phosphorus segregation became much more important. While sulphur segregation did still occur, its level was unpredictable and it never reached saturation coverage. All surface segregation was now transient and it was possible to maintain a sample which had near-surface depletion at 700°C for several hours before any surface segregation occurred. Of the elements detected, only nitrogen had not been observed on the FeCrC pure analogue of HCC. No consistent time-dependences of segregation were observed.

4.5.2. The $\alpha+(Fe,Cr)_3C$ phase region

Fig. 4.60 shows a typical result of 'heating' to 650°C. Phosphorus was the major segregant and it approached saturation coverage soon after the start of the experiment. There was an initially strong carbon Auger peak and a smaller peak in the chromium concentration. Sulphur segregation was persistent, but only at a very low level. There was some segregation of nitrogen at this temperature but its level was low and irregular and it was not plotted in the figure.

4.5.3. The $\alpha+\gamma+(Fe,Cr)_3C$ phase region

In the result at 740°C which is shown in Fig. 4.61, the sulphur segregation was stronger. It was, however, still transient and at a lower level than phosphorus. While the phosphorus segregation was similar to that shown in the previous figure, carbon was present at a higher level than before. Nitrogen and chromium also segregated.

Fig. 6.60 HCC: segregation at 650°C

Fig. 4.61 HSC: segregation at 740°C

4.5.4. The γ+$(Fe,Cr)_3C$ phase region

At the end of the previous experiment the temperature was raised to 'transform' the sample into this phase region. The result is shown in Fig. 4.62. Phosphorus only reappeared briefly but there was a strong resurgence in the sulphur segregation to about half saturation coverage. Carbon and nitrogen eventually disappeared. This may be compared with the result of direct 'heating' into this phase region as shown in Fig. 4.63. The carbon, nitrogen and chromium signals were very small and are not shown in the figure. Both sulphur and phosphorus segregated quite strongly but both were transient. The rise in the sulphur level was erratic. Oscillations in the levels of surface segregants were common to all alloys at low temperatures but on the HCC alloy they could occur at all temperatures.

REFERENCES for Chapter Four

Grabke H.J., Tauber G. & Viefhaus H., Scripta Met. 9(1975)1181

McDonnell L., Powell B.D. & Woodruff D.P., Surface Science 40(1973)669

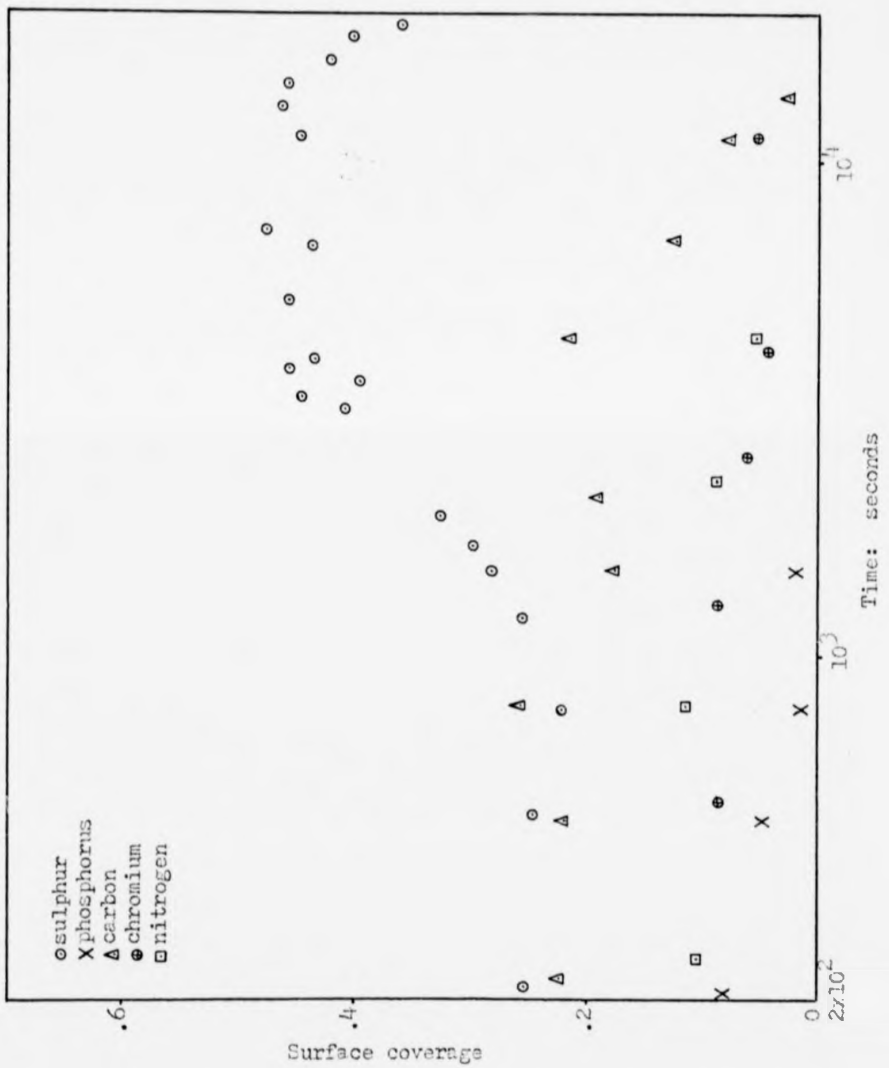

Fig. 4.62 HCC: segregation at 800°C after heating from 740°C

Fig. 4.63 MCC: segregation at 790°C

CHAPTER FIVE DISCUSSION

Surface enhancements of six elements were observed on the pure alloys: sulphur, phosphorus, nitrogen, chromium, carbon and argon. Of these, the first four are considered to have been present as segregants and their behaviour is discussed in the first section of this chapter: surface segregation. It is thought that carbon was present as a three-dimensional graphite precipitate and so it is dealt with in the second section: surface precipitation. The presence of significant amounts of argon at the surface was always associated with graphite precipitation and it is therefore discussed in the same section. The results from the commercial HCC samples are considered separately in the third section of this chapter.

5.1. Surface segregation

The four segregants; sulphur, phosphorus, nitrogen and chromium are considered in order below. A fifth sub-section contains a discussion of the observed site-competition between sulphur and phosphorus.

5.1.1. Sulphur

Many workers have reported details of surface segregation of sulphur on ferrous alloys. Most of these results have, however, been limited to descriptions of the circumstances under which the segregation occurred, the levels obtained or the surface structure of the segregated layer. In some cases, sulphur segregation had suppressed some other segregation that was being studied, and so it had to be removed by additions of manganese to the alloys. Grabke et al (1977) found that the saturation level of sulphur on iron (100) surfaces was independent of temperature within the alpha range and corresponded to a c(2x2) structure: 23% of a close-packed monolayer. In addition, sulphur had in time displaced all other

segregated atoms from the surface, including carbon. In the present work, sulphur segregation did indeed dominate surface segregation but the precipitation of graphite obtruded under some conditions. Sulphur usually reached saturation coverage, even when depleted near the surface. Saturation levels lay between 42% and 57% of a close-packed monolayer, varying from experiment to experiment in an apparently random fashion. There did not appear to be any correspondence with temperature or past thermal history. This range of saturation levels was probably due to the inherent variability of surface orientation that is present with polycrystalline samples. There was no evidence of evaporation from the free surface at temperatures below about 820°C. Depth profiles showed that sulphur was well localised at the surface once saturation coverage had been achieved.

On the plain-carbon alloys, sulphur segregation was in direct competition with graphite precipitation. The question of whether graphite overgrew sulphur or displaced it from the surface is discussed in the next section. The course of the competition depended upon such factors as the rate of heating, because sulphur segregation began at a lower temperature than graphite precipitation, and the area of the surface examined because of the dependence of graphite growth on surface orientation. This competition between sulphur and graphite precluded the segregation of other elements to the surface of the plain-carbon alloys; except for one occasion when phosphorus made a transient appearance (Fig. 4.33). This one case may be explained in terms of the slow rate of heating used, which favoured sulphur segregation, together with strong sulphur depletion which allowed phosphorus to reach the surface in its place. On the two alloys that contained chromium the same strong precipitation of

graphite did not occur, although there was at times a small carbon Auger peak. It is not known whether this peak originated from segregated or precipitated carbon.

The kinetics of sulphur segregation to the free surface have received very little attention. In the present work, saturation coverage was achieved very quickly, provided that sulphur was not depleted near the surface. In experiments on undepleted samples, the sulphur arrival rate was found to have a time dependence which lay in the range $t^{1.3}$ - t^{5}. This type of behaviour will be considered later in this section. In some of the experiments where sulphur had been depleted the segregation rate exhibited a $t^{\frac{1}{2}}$ dependence, at least initially. This behaviour was visible as linear regions of slope 0.5 in the log(coverage) versus log(time) plots of the experimental results (see Fig. 4.17 for example). This was the behaviour predicted in the analysis of the segregation process by Rowlands & Woodruff. Accordingly, bulk to surface diffusion coefficients were calculated from the intercepts on the log(time) axis using the method described in section four of Chapter Two. These coefficients are plotted against the reciprocal of experimental temperature in Fig. 5.1, for alpha-phase diffusion and Fig. 5.2, for gamma-phase diffusion. Also plotted in these figures are lines corresponding to values of the lattice diffusion coefficient of sulphur taken from the literature. All these lines are extrapolations from measurements made at higher temperatures than the experiments conducted here, and all but one refer to diffusion in unalloyed iron samples.

When using polycrystalline samples there is a possibility that the observed bulk to surface diffusion coefficients may contain contributions from grain boundary diffusion as well as lattice diffusion.

graphite did not occur, although there was at times a small carbon Auger peak. It is not known whether this peak originated from segregated or precipitated carbon.

The kinetics of sulphur segregation to the free surface have received very little attention. In the present work, saturation coverage was achieved very quickly, provided that sulphur was not depleted near the surface. In experiments on undepleted samples, the sulphur arrival rate was found to have a time dependence which lay in the range $t^{1.3}$ - t^{5}. This type of behaviour will be considered later in this section. In some of the experiments where sulphur had been depleted the segregation rate exhibited a $t^{\frac{1}{2}}$ dependence, at least initially. This behaviour was visible as linear regions of slope 0.5 in the log(coverage) versus log(time) plots of the experimental results (see Fig. 4.17 for example). This was the behaviour predicted in the analysis of the segregation process by Rowlands & Woodruff. Accordingly, bulk to surface diffusion coefficients were calculated from the intercepts on the log(time) axis using the method described in section four of Chapter Two. These coefficients are plotted against the reciprocal of experimental temperature in Fig. 5.1, for alpha-phase diffusion and Fig. 5.2, for gamma-phase diffusion. Also plotted in these figures are lines corresponding to values of the lattice diffusion coefficient of sulphur taken from the literature. All these lines are extrapolations from measurements made at higher temperatures than the experiments conducted here, and all but one refer to diffusion in unalloyed iron samples.

When using polycrystalline samples there is a possibility that the observed bulk to surface diffusion coefficients may contain contributions from grain boundary diffusion as well as lattice diffusion.

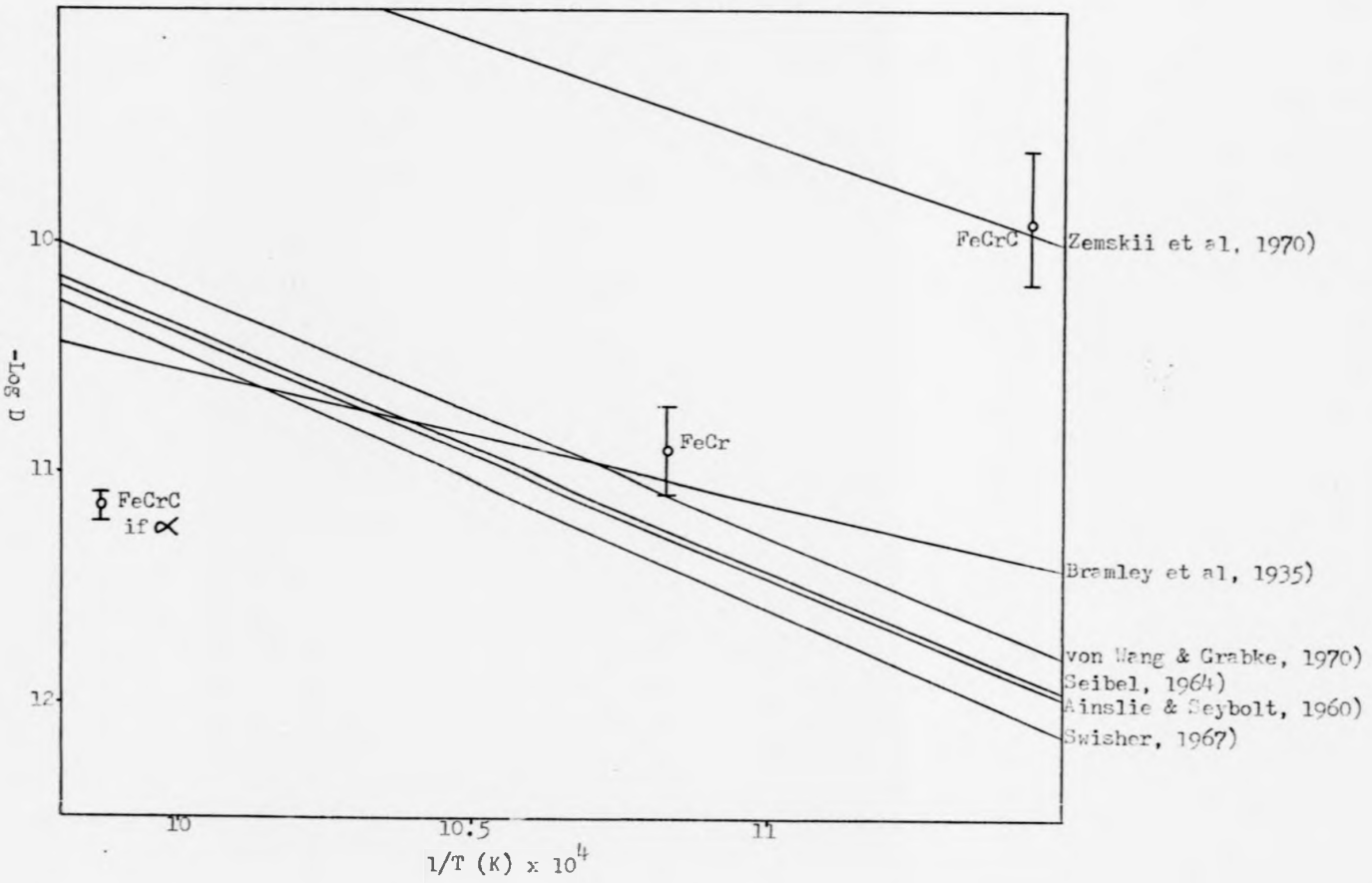

Fig. 5.1 ∝ phase sulphur diffusion data

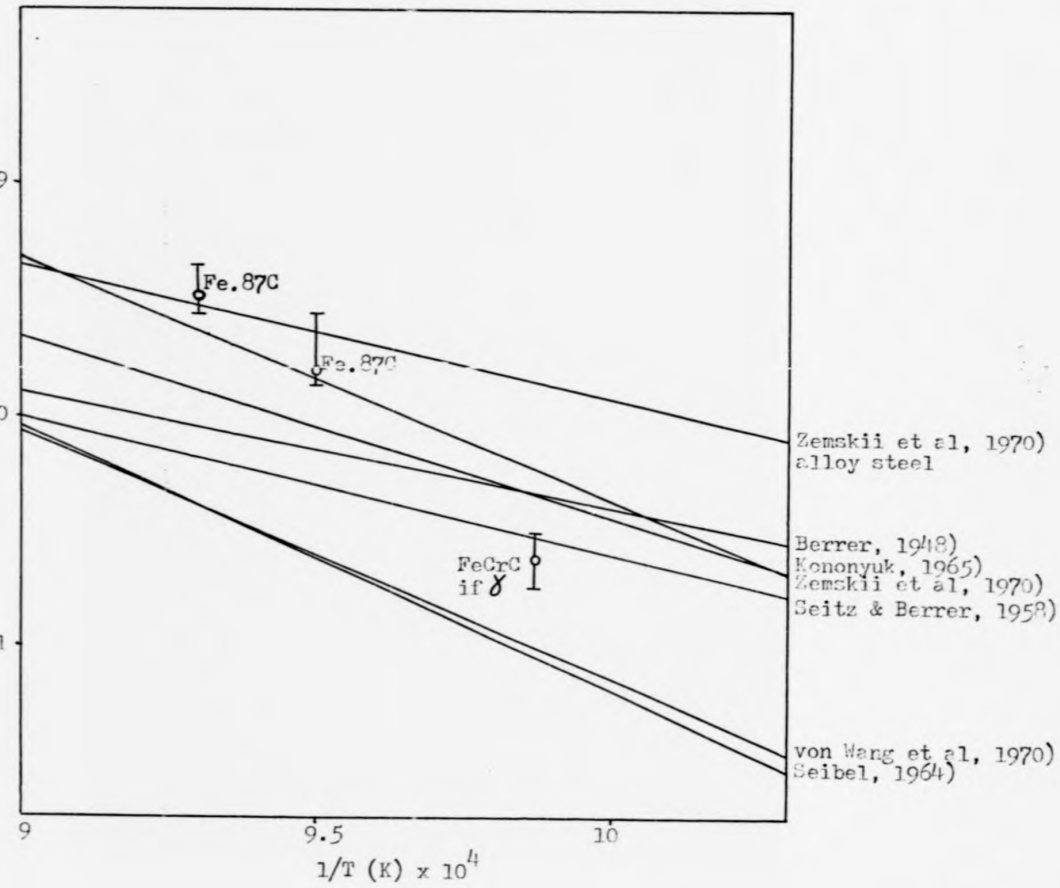

Fig. 5.2 γ phase sulphur diffusion data

Grain boundary diffusion is characterised by a substantially lower activation energy than is diffusion through the lattice. As the experimental temperature is decreased, therefore, the contribution to the total arising from boundary diffusion falls more slowly than that from lattice diffusion and so becomes more important to the observed segregation kinetics. The over-estimation of the lattice diffusion coefficient that results from a grain boundary contribution may be minimised by depleting all the fast diffusion paths of the segregant before an experiment is begun. The fast diffusion paths may be depleted by ion bombardment of the surface with the sample held at a temperature high enough for segregation to occur, but low enough for the grain boundary contribution to be large. While the diffusion coefficients calculated here were obtained from sulphur-depleted samples, there is still a possibility that they are over-estimations, particularly at the lowest temperatures. The result at 600°C on the FeCrC alloy probably contained a grain-boundary contribution as it was nearly two orders of magnitude above the main grouping of literature values. In another of these experiments, at 650°C on the FeCr alloy, the result lay very close to the extrapolated lines. The remaining result in Fig. 5.1 was at 740°C in the three phase $\alpha+\gamma+(Fe,Cr)_3C$ region of the FeCr alloy. This offered the possibility of diffusion in both alpha and gamma iron, or perhaps some mixture of the two. Consequently, the diffusion coefficient from this result was also calculated assuming gamma-phase diffusion and plotted in Fig. 5.2. It can be seen that in Fig. 5.1 this result was rather low, while in Fig. 5.2 it lay within the spread of the literature values. The highest temperature results, both from the Fe.87C alloy, also lay close to the extrapolated literature values.

The close relationship between these results and the values of the lattice diffusion coefficient reported in the literature shows the potential usefulness of the AES-based technique, as well as confirming the validity of Rowlands & Woodruff's interpretation of surface segregation kinetics. When calculating diffusion coefficients by this method, however, it is essential to know the segregant's solid solubility as accurately as possible as the results depend upon its square. For the present case, a solid solubility curve for sulphur in an unalloyed low-carbon steel is shown in Fig. 5.3. This was compiled from the data of Ainslie & Seybolt (1960), Hager & Elliot (1967), Rosenqvist & Dunicz (1952) and Turkdogan et al (1955). It was necessary to extrapolate some of the data in order to obtain the gamma-phase portion of the curve. This base-curve was modified to take into account the effects of the carbon and chromium contents of each of the pure alloys. Morris & Buehl (1950) found that in liquid iron a 1% addition of carbon reduced the sulphur content by 25%. The solid solubility of sulphur in iron is also reduced by chromium, which has the additional effect of raising the alpha to gamma transition temperature. Sawle (1974) has made a calculation of the effect of chromium additions, based on the data of Hager & Elliot. It is estimated that an addition of 1.5% chromium would produce a 10% reduction in the sulphur solubility. The error bars in Figs. 5.1 and 5.2 reflect the uncertainties in the solid solubility.

Even when the free-sulphur concentration in the bulk is known, care must be taken to ensure that experimental factors do not produce an effective level at the surface which is different to the true bulk level. Fig. 5.4 illustrates a sequence of events which could lead to a reduction in the near-surface sulphur concentration,

Fig. 5.1 Solid solubility of sulphur in iron - low carbon alloy

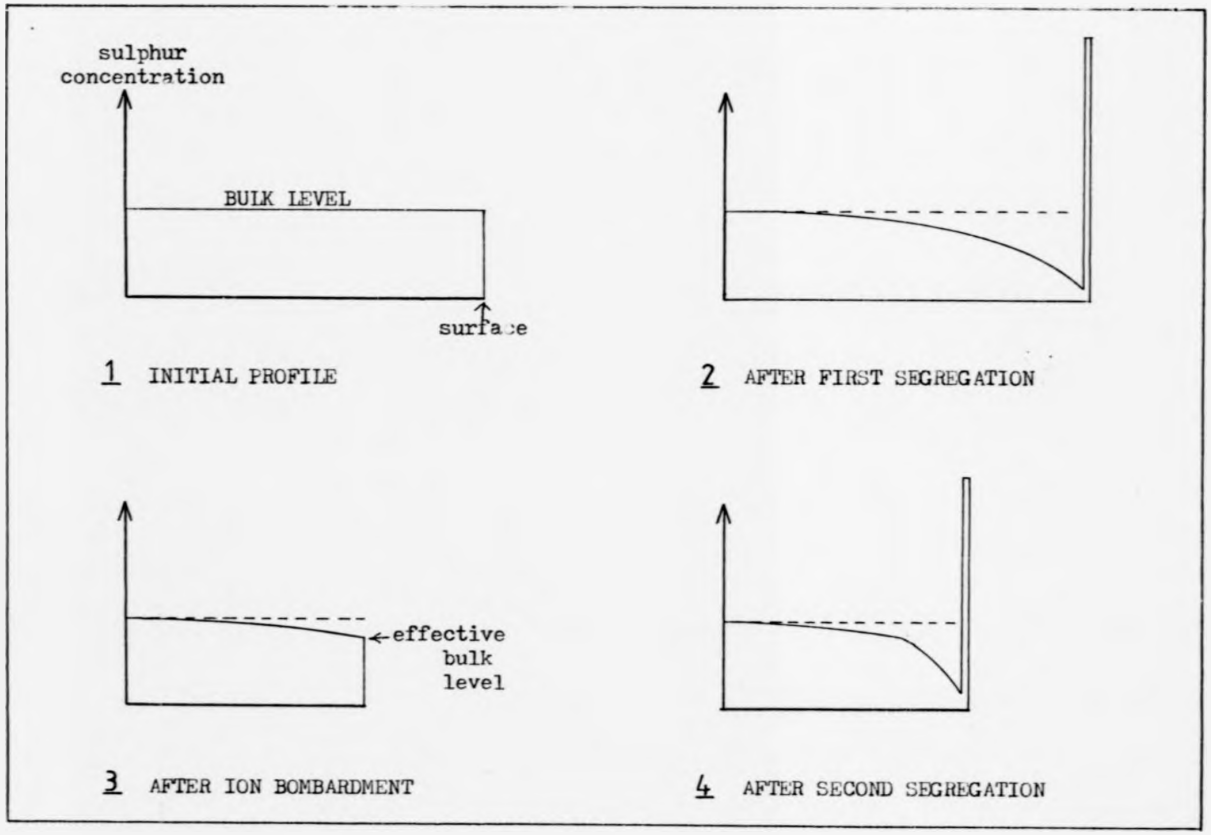

Fig. 5.4 Concentration profiles caused by surface segregation

and hence to an under-estimation of the bulk to surface diffusion coefficient. The initial, ideal sulphur concentration profile at a surface is shown in diagram 1. If the sample were heated to a suitable equilibration temperature, surface segregation would occur with a $t^{\frac{1}{2}}$ dependence of the sulphur arrival rate, and would produce the final state shown in diagram 2. The segregant would then be localised at the surface and there would be a sub-surface depletion zone. If the surface was not sufficiently ion bombarded before the next segregation experiment, a shallow concentration gradient would remain as shown in diagram 3. The experiment would then start with an effective bulk concentration, C_o' , lower than the true value, and would produce the final depletion profile shown in diagram 4. While the observed time dependence in the second experiment would approximate to $t^{\frac{1}{2}}$, the calculated diffusion coefficient would be too low.

That proportion of the sulphur not in solid solution would have been present as iron sulphide or iron-chromium sulphide particles. It is interesting to consider how such sulphide inclusions might affect the kinetics of the surface segregation of sulphur. In the absence of phase transformations, the solid solubility of sulphur in iron tends to increase with increase in temperature. When a sample was heated to its equilibration therefore, the sulphide particles would begin to dissolve. A freshly ion-bombarded surface represents a section through the bulk of the sample. It is likely that some of the sulphide particles would have been situated at or close to the surface in this undepleted case. Under these circumstances, the surface could be flooded with sulphur by the dissolving sulphide particles, giving rise to high time-dependences of sulphur segregation as was observed on the pure-alloy samples.

An analysis of surface segregation kinetics by Lea & Seah (see section four of Chapter Two) has predicted that where evaporation from the free surface is a significant factor, the observed segregation level should not reach saturation, but should pass through a maximum before falling to a low level. The reason for this is that the segregant's arrival rate at the surface decreases with time ($t^{\frac{1}{2}}$) while the evaporation rate is proportional to the surface concentration. In the present work, this type of falling-away in the sulphur level was only rarely observed below 850°C on the pure alloys. This may be contrasted with the report by Seah & Lea (1975) that their measurements of sulphur segregation on iron showed such strong evaporation from the surface that a meaningful quantitative analysis was not possible above 500°C. The absence of evaporation effects in the present case may have been due to the sulphide particles. In all those experiments where there was an initial $t^{\frac{1}{2}}$ dependence in the sulphur arrival rate, the rate subsequently increased before surface saturation was achieved. This is attributed to the arrival at the surface of the flux of sulphur atoms from a dissolving sulphide particle. The increased arrival rate of sulphur could buffer the surface concentration against the effects of evaporation, obscuring the fact that evaporation was still taking place. Seah & Lea had added manganese to their alloys. Manganese forms sulphides which are considerably more stable than those of iron or chromium (Elliott & Gleiser (1960)). If manganese sulphide particles do not dissolve readily, they would not have been able to buffer the surface coverage. The effect of manganese additions on sulphur segregation is discussed further in the last section of this chapter, which deals with the results from the commercial HCC alloy.

As described above, the segregation process is fueled by the free sulphur in the bulk and as a result, a sub-surface depletion zone is created in the form of a concentration gradient of gradually increasing length. If, however, the segregated layer was formed from a dissociating sulphide particle, a depletion zone would not be produced unless heating was continued long enough for there to have been a significant loss of segregant by evaporation. If the sample were subsequently given a superficial bombardment to remove the layer of segregant, the first experiment would merely have removed the surface sulphide particles, leaving an almost ideal sub-surface concentration profile. The next segregation experiment would then exhibit a $t^{\frac{1}{2}}$ dependence at first, but the sub-surface sulphide particles could still affect the result. The expected segregation behaviour in the presence of sulphide particles is shown in Fig. 5.5. Diagram 1 shows the initial concentration profile below the surface. The first stage of segregation would have a $t^{\frac{1}{2}}$ dependence and produce a growing surface concentration at the expense of the bulk level. When this concentration gradient reached a sulphide particle it would start to lower the local equilibrium sulphur concentration as shown in diagram 2. The sulphide particle would then begin to dissolve in order to maintain the local equilibrium. If the rate of dissolution was fast enough, the concentration gradient would be 'pinned' in the vicinity of the inclusion. There would then be an essentially constant source concentration at a fixed distance from the surface, and the concentration gradient would become linear, as shown in diagram 3. In this situation the observed segregation rate would develop a t^{1} dependence. The analagous situation for carbide particles in iron has been considered by Gibbs (1965) and Oldham & Stowell (1973).

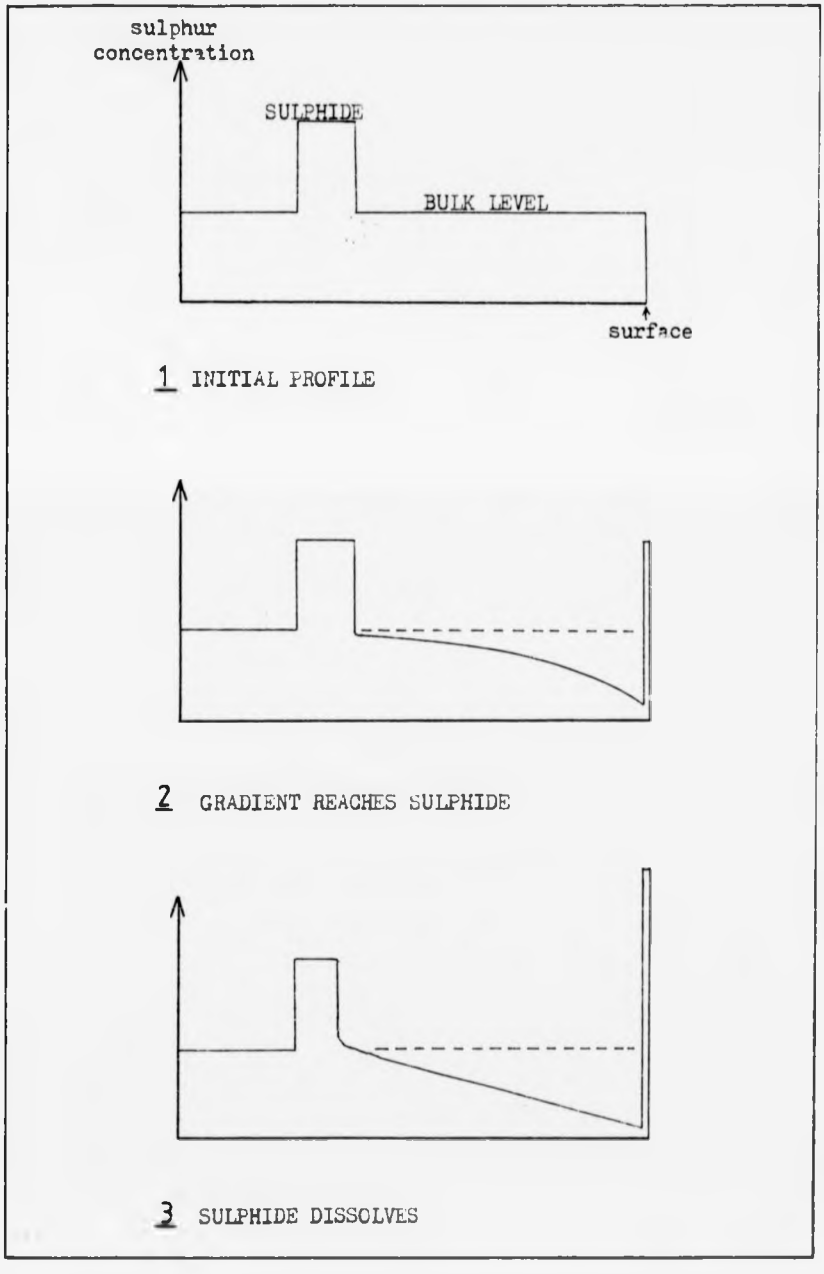

Fig. 5.5 Concentration profiles with sulphide particle

Two examples of experiments during which the time dependence of sulphur segregation changed from $t^{\frac{1}{2}}$ to t^{1} were given in Chapter Four as Figs. 4.38 and 4.52. The transition between the two rates was in one case abrupt and in the other case gradual. One factor which might affect the way in which the change occurred is the spatial distribution of sulphide particles with respect to the area of the surface analysed. Fig. 5.6 illustrates how this might occur for the situation where the sulphide particles were large and widely spaced with respect to the diameter of the analysing electron beam. If we suppose that the limit of the segregation-induced sulphur concentration gradient moves inward with time from the line A-A to the line B-B, then it would be pinned in the vicinity of the sulphide particle. At a point on the surface, X, directly opposite the inclusion, the change in segregation rate should be an abrupt one provided that the sulphide particle dissolved readily. At point Y, some distance to one side of the inclusion, the effect of the encounter with the sulphide particle would take longer to arrive at the surface because of the longer pathway for bulk diffusion. In the meantime, the surface concentration at point X would have begun to increase at the faster rate. Cross-surface diffusion is known to be several orders of magnitude faster than lattice diffusion. If sulphur diffused away from point X it could smooth the rate transition at point Y. Similar reasoning can be applied to show that a similar effect could occur in two other likely cases of particle distributions. If, because the inclusions were smaller and hence more closely spaced, there were sulphide particles beneath the surface at both X and Y, then the particle at Y could be further from the surface than that at point X. Alternatively, if all sulphide particles were located

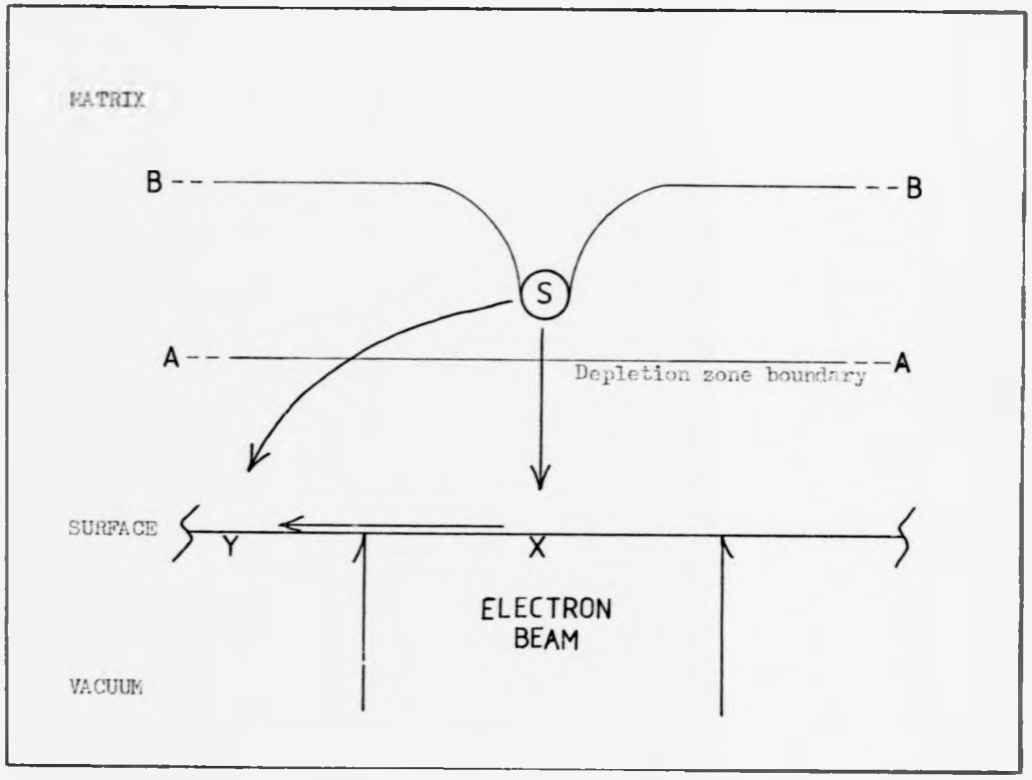

Fig. 5.6 Effect of a sulphide particle on sulphur diffusion

at grain boundaries, the sharpness of the rate transition would depend on whether the analysing electron beam was placed at or away from the intersection of a grain boundary with the surface.

If, at the end of an experiment where the concentration gradient had been pinned by sub-surface sulphide particles, the sample was only given a superficial ion bombardment, the depletion zone would be retained. Under these circumstances a linear time dependence would be expected from the start of the next experiment. This was indeed the behaviour observed on sulphur-depleted samples which had been given a superficial bombardment. A deep bombardment, to remove the depletion zone, returned the surface to its initial state and restored the incidence of time dependences greater than $t^{1.3}$. There were short-term deviations from linear behaviour at the start of some experiments but this could have been due to there having been some removal of the depletion zone by the superficial ion bombardment.

With a constant source concentration, C_o, at a fixed distance, I, from the surface, the amount of sulphur at the surface after a time, t would be given by:

$$C_s = \frac{DC_o t}{L}$$

Hence, expressing C_s and C_o in monolayers, the value of L may be calculated from the intercept of the log(coverage) versus log(time) plot at saturation coverage. Thus it is possible to find the distance between a pinning sulphide particle and the surface. Because there was originally at least one sulphide particle at the surface, this technique can be used to obtain some measure of the average spacing between particles in the bulk. Values of L were determined from all

the results which had given a linear time dependence of segregation. This gave eleven values in the surprisingly narrow range, 1.2 - 8.0 μ_m. Self-consistent values of the lattice diffusion coefficient were used in these calculations. The spread in the literature values was such that the range of gradient lengths might be scaled by a factor of three.

The actual sulphide particle distributions within the alloys were not determined. There is little information in the literature about the expected sizes and distributions of sulphide particles in manganese-free iron alloys. Even where the details of the distributions are given (see for example Wyjadlowski et al (1974)) there is no description of the heat treatments which gave rise to them. However, some general rules have been established and these will now be applied to the present case. If gamma iron with sulphur in solid solution is cooled, sulphur may be precipitated in two ways (Leymonie (1957), Kiessling & Lange (1966)). During slow cooling in the alpha range, sulphur has time to diffuse to the growing sulphide particles at favoured nucleation sites in the grain boundaries. Quenching, on the other hand, produces a supersaturated solid solution which decomposes to give intra-granular precipitation. Thus the relative extent of precipitation of the two sorts depends on the rate of cooling, and both may occur simultaneously. Brammar & Honeycombe (1964) found that a medium cooling rate of 18°C per minute from 910°C produced preferential precipitation at the alpha grain boundaries.

The distribution of sulphide particles in the experimental alloys would have depended upon the rate of cooling in the UHV sample-heating stage. Although this was some twenty times faster than that used by Brammar & Honeycombe in the temperature range

where sulphur diffusion was significant, there could still have been some precipitation at grain boundaries. It is estimated that with the cooling rate available in the present work the characteristic diffusion length of sulphur would have been of the order of three microns when cooling from 800°C or half a micron when cooling from 700°C. This represents the radius of the sphere from which the sulphur could diffuse to reach a sulphide, and corresponds to a range in L of one to six microns. This is of the same order as the values estimated by means of the arguments presented above.

If the distance between the surface and a pinning sulphide particle can indeed be taken to be a measure of the average particle spacing, the model may be extended further to predict the average particle radius. Each sulphide particle will contain that portion of the total sulphur concentration not in solid solution at the experimental temperature. Assuming stoichiometric FeS with all atoms of sulphur displacing iron atoms in the 'nickel arsenide' structure of the particle, the number of atoms in the sulphide will be twice the number of sulphur atoms. It is also assumed that the sulphide particles are all spheres of radius R, arranged such that each lies at the centre of a cube of side L. If the cubes are arranged in a close-packed formation then the ratio between the volume of the particle and the volume of the cube will be approximately equal to two times the atom fraction of precipitated sulphur in the lattice; ie.

$$2.C_{FeS} = \frac{4\pi R^3/3}{L^3}$$

If this relationship is applied to the range of values of L that was given above, the predicted range of sulphide particle radii is 0.02 - 0.15μm.

To summarise: sensible values of the sulphur lattice diffusion coefficient have been deduced from segregation experiments exhibiting a $t^{\frac{1}{2}}$ dependence of the sulphur arrival rate. It has been shown that the presence of labile sulphide particles at or near the surface can explain three main features of the observed sulphur segregation:

1) the occurrence of time dependences greater than t^1 in samples with no near-surface depletion of sulphur,
2) the apparent absence of evaporation effects below about 820°C,
3) the occurrence of linear time dependences under certain conditions in samples with near-surface sulphur depletion.

From experiments exhibiting the third of these features, some measure of the bulk sulphide particle size and distribution has been calculated.

5.1.2. Phosphorus

Phosphorus only appeared at the surface of the pure alloys when the segregation rate of sulphur had been reduced by near-surface depletion. Phosphorus was, however, the second most important segregant and on several occasions came close to reaching saturation coverage. The maximum level observed was 54% of a close-packed monolayer: slightly less than the saturation levels on iron reported by Hondros (1965) and Yen et al (1978). During phosphorus segregation, $t^{\frac{1}{2}}$ dependences of the arrival rate were observed on several occasions but there was no occurrence of higher time dependences as observed with sulphur segregation. The phosphorus content of all the alloys studied was much lower than its solid solubility limit in iron, and phosphide particles are not expected to have been present. This could account for the absence of higher time dependences than $t^{\frac{1}{2}}$ as well as the apparent importance of evaporation. The phosphorus level at the surface always passed through a maximum before falling to a

low level; exactly the behaviour predicted by Lea & Seah for a system where evaporation from the free surface is important.

From those occasions when the segregation rate showed a $t^{\frac{1}{2}}$ dependence, bulk to surface diffusion coefficients were calculated in the same way as for sulphur. They are plotted in Figs. 5.7 and 5.8 for alpha and gamma phase diffusion respectively. The error bars in these figures now reflect the uncertainties in the intercepts of the log(coverage) versus log(time) plots because all the phosphorus was in solution. There was a greater amount of scatter in the phosphorus diffusion coefficients than there had been with sulphur, partly because there were often only a very few points obtained before the phosphorus coverage reached its maximum. The literature values are plotted in the same figures, as before. The data due to Yen et al are an extrapolation from low temperature results which were obtained by means of a similar AES technique to the present work. The large spread in the gamma phase literature values could well be due to the errors inherent in extrapolation from very high temperatures.

The alpha phase results show quite good agreement with the literature, although at the lowest temperature there was probably a grain boundary contribution. There was again one result from the three-phase $\alpha+\gamma+(Fe,Cr)_3C$ region and this was calculated on the basis of both alpha and gamma phase diffusion as before. The alpha phase value was low while the gamma phase value was reasonable as had been the case with the sulphur result. There was clear evidence of evaporation of phosphorus during these experiments. As the equation used in the calculation of the diffusion coefficients was based on a 'no evaporation' case, it is possible that the values calculated

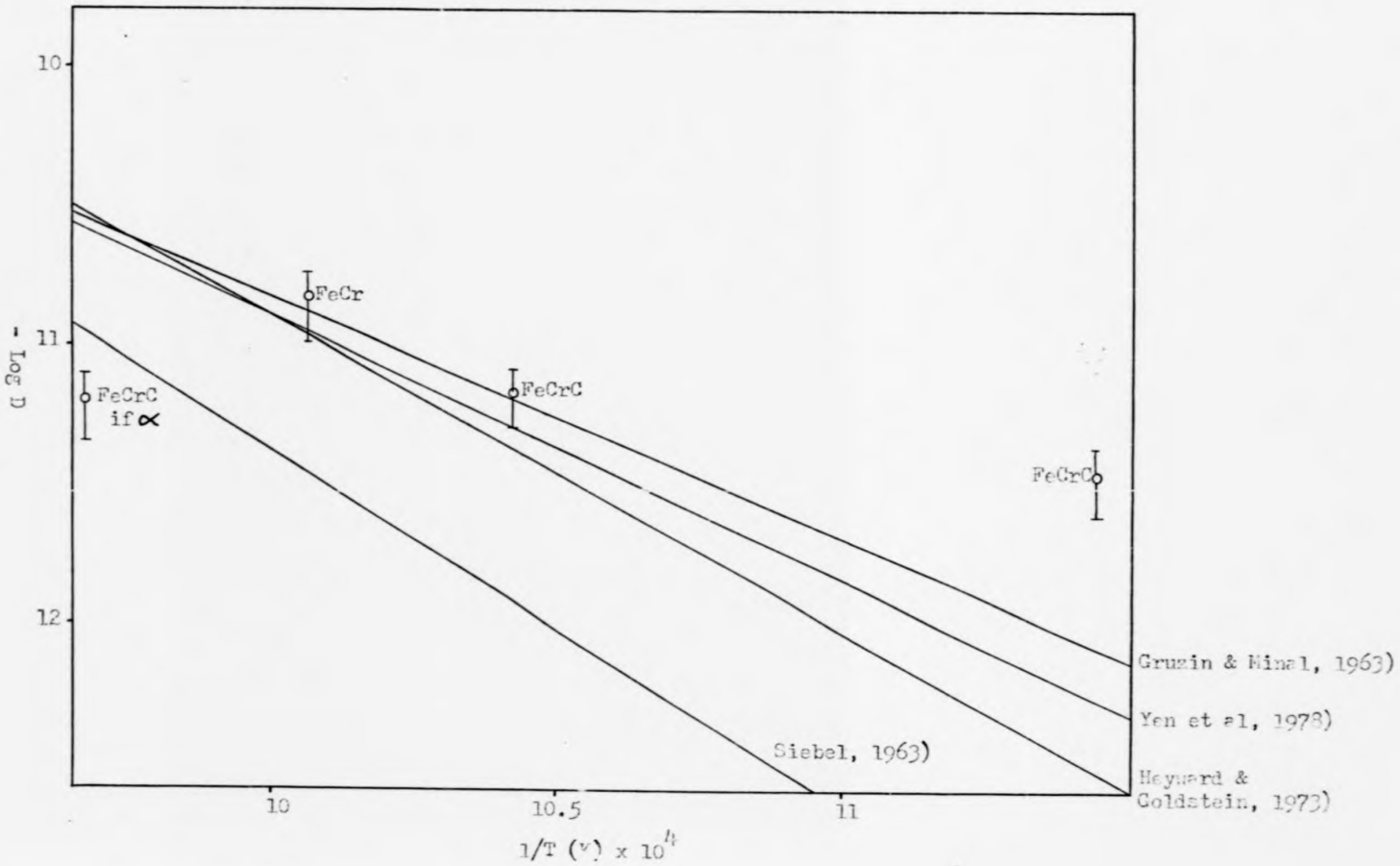

Fig. 5.7 ∝ phase phosphorus diffusion data

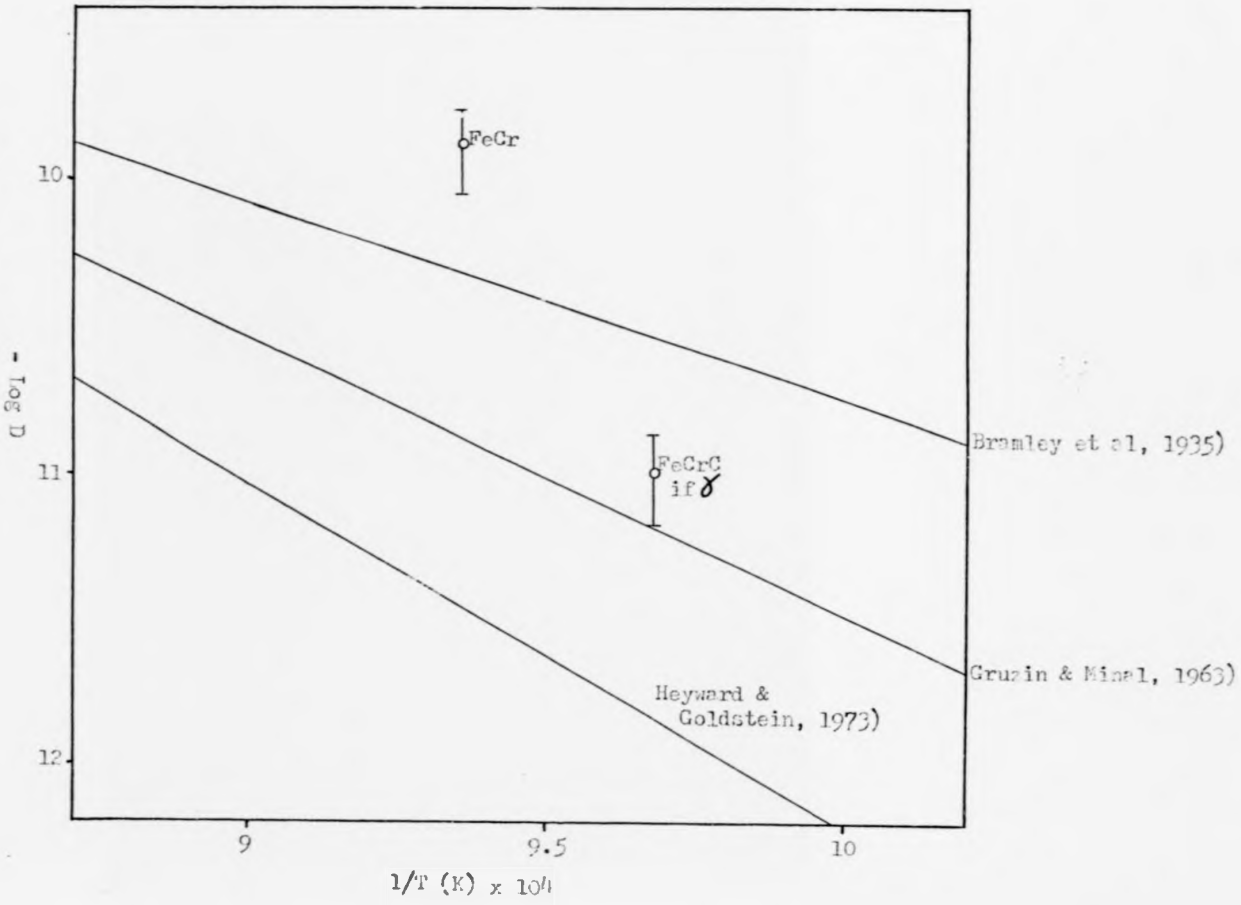

Fig. 5.8 γ phase phosphorus diffusion data

here could be an underestimation. It is also true, however, that in the experiments for which these calculations were possible the phosphorus level was generally less than half the saturation level, so that the effect of evaporation could be small. The observation that an increase in the sulphur arrival rate produced an increase in the phosphorus disappearance rate is discussed in the sub-section devoted to site competition.

It is interesting to note that for both sulphur and phosphorus there was an experiment where both the alpha and gamma phases were present in the bulk, and where a calculation based on gamma phase diffusion gave a more plausible result. There is some evidence that preferential surface nucleation of austenite may occur. It is well known that when austenite nucleates in ferrite-carbide aggregates it does so preferentially at grain boundaries. In pearlitic samples, austenite nucleates at the boundaries between pearlite colonies. According to an analysis developed by Speich & Szirmae (1969) the austenite nucleation rate at a boundary is given by:

$$I^B = 10^{24} \exp(-\Delta G_c^B / kT) \quad cm^{-3}sec^{-1}$$

where ΔG_c^B is the Gibbs free energy change associated with the formation of a critical nucleus on the boundary. The interfacial free energy available at a boundary can be used to decrease ΔG_c^B, and it is the exponential term containing this quantity which overwhelmingly determines the rate of nucleation. A second reason why interfacial nucleation is favoured is that the boundary can act as a fast diffusion path for the carbon necessary for austenite growth. In the case of alloys containing chromium, it is the diffusion of the alloying element that determines the rate of austenite growth. Both of the

above factors apply equally well to the surface as to the grain boundaries. Finally, there is a volume expansion associated with the transformation of ferrite+carbide to austenite, and this would obviously favour surface nucleation and growth. It is thought that all these factors may have combined to produce a surface layer of austenite through which the segregating elements had to diffuse.

5.1.3. Nitrogen

Surface segregation of nitrogen was only observed on the FeCr alloy, and then only under conditions of sulphur depletion or experimental temperatures below 650°C. It was a transient segregant; probably because of evaporation from the surface. Grabke et al (1977) have established that desorption from the surface is important above 500°C. No observations of the rate of segregation were possible, but its relationship with the other segregants, appearing after carbon but before the rest, was in line with reported lattice diffusion coefficients. The maximum surface concentration that was observed in the present work was about 5% of a close-packed monolayer.

5.1.4. Chromium

Segregation of chromium is expected to have taken place by substitution of iron atoms in the surface layer. The maximum chromium signal that was observed represented an approximate 40% substitution of the surface layer, and occurred during an experiment on the FeCr alloy that is described below. On the FeCrC alloy, the chromium levels were lower and chromium segregation tended to be associated with the appearance of a carbon Auger peak from the surface. Both the carbon and chromium Auger peaks disappeared at about the time that the interstitial segregants reached saturation coverage (either phosphorus-plus-sulphur or sulphur on its own). It is thought that

there was still chromium present at a low level at the surface but its Auger peaks lay in a particularly noisy part of the spectrum. Chromium readily substitutes for iron atoms in cementite because of its strong affinity for carbon (Whalen et al (1962)) and this strong interaction was probably responsible for the apparently lower activities of both elements in the FeCrC alloy than in the FeCr alloy.

During two experiments on the FeCr alloy the behaviour of chromium at the surface was particularly interesting. At 795°C (Fig. 4.45) chromium was initially present at the surface at a high level but declined as phosphorus began to segregate. The chromium level passed through a minimum at about the time that the time dependence of sulphur segregation changed from t^{1} to t^{4}. When all the phosphorus had been displaced by sulphur the chromium level recovered somewhat. In the depth-profile which was taken after this experiment (Fig. 4.47), there was an initial increase in the chromium Auger signal as the sulphur overlayer was bombarded away. This could have been due to attenuation of the chromium Auger signal in the sulphur layer. Grabke et al (1977) have reported that they were able to measure attenuation of the iron Auger peaks due to a sulphur overlayer. The behaviour of chromium during an experiment at 720°C on the same alloy was shown in Fig. 4.43. It is thought that the fall in the sulphur signal and corresponding rise in the chromium Auger signal might possibly have resulted from a surface reconstruction to form a two-dimensional chromium sulphide. This has been reported by Oudar et al (1975) to have occurred at the surface of an iron-18% chromium alloy under conditions of sulphur segregation. The two-dimensional chromium sulphide is reported by

Bénard et al (1979) to have a very high enthalpy of formation. A depth-profile was also taken after the experiment at 720°C (Fig. 4.44) and did not show the same sharp increase in the chromium level as before. This might be an indication that all the chromium was no longer beneath the sulphur layer.

5.1.5. Site competition

Surface site-competition between segregants usually involves two types of inter-species interaction. The first arises from the limited number of surface sites available to the segregants. Thus, if two species are competing for the same surface sites, their combined coverage should not be greater than the saturation coverage of either segregant on its own. The second type of interaction is an attractive or repulsive force between two species of segregant at the surface and is termed a lateral interaction. This results in the jump probability of one species out of the surface layer being dependent upon the concentration of the other species. Interactions of this second kind have commonly been observed between an alloying element and an interstitial; often an impurity. Examples may be found in the papers by Stein et al (1969), Ohtani et al (1976), Krahe & Guttmann (1973) and Clayton & Burstein (1979). An analytical treatment of this type of interactive segregation has been formulated by Guttmann (1974),(1975) based on the enthalpies of compounds formed between the segregants. If the formation of a compound is an energetically favourable process then segregation of either element can enhance the segregation of the other. Strictly speaking, the term 'site-competition' should not be applied to the case of an attractive interaction. For this reason the chromium-sulphur interaction was discussed in the previous sub-section.

Phosphorus and sulphur appeared to be in competition at the surface of the pure-alloy samples. Sulphur was the dominant segregant and phosphorus was only able to segregate when it was depleted. An interaction of the first type (ie. competition for a limited number of surface sites) was evident from the behaviour of the phosphorus-plus-sulphur curves which were plotted in some of the figures in Chapter Four. The total coverage never exceeded saturation coverage of sulphur. There were also indications that the other, less strongly segregating impurities were forced from the surface when saturation coverage of phosphorus-plus-sulphur was approached. There was always a peak in the combined curve which coincided with the maximum in the phosphorus curve. It has been argued that the fall in the phosphorus level beyond its maximum was due to evaporation. The combined-coverage curve also always fell away after the maximum in the phosphorus time-history. Hence phosphorus was departing from the surface faster than it was being replaced by sulphur. However, the fractional coverage of sulphur at the time of the extinction of the phosphorus Auger peak, averaged over all but one experiment, was 0.73 ± 0.1. This nearly constant value indicates that phosphorus was departing from the surface because of the presence of sulphur as well as because of evaporation. In some experiments (see for example Figs. 4.53, 4.54 and 4.55) it could be seen that the rate of fall of the phosphorus level increased when the arrival rate of sulphur increased. In the one experiment where, despite some degree of sulphur depletion, the sulphur segregation rate had a greater than $t^{\frac{1}{2}}$ dependence throughout, (Fig. 4.40) phosphorus was not able to leave the surface fast enough and its extinction was delayed until sulphur had reached 95% of saturation coverage. It can be seen that sulphur was the dominant

segregant of the two because at low sulphur coverages the combined level could reach saturation, whereas once 73% of the surface sites were occupied by sulphur, all the phosphorus was displaced. This behaviour appeared to be the result of a repulsive lateral interaction between phosphorus and sulphur. The behaviour of phosphorus at the surface in the absence of competition from sulphur is described in the third section of this chapter.

Another apparent case of site competition at the surface was the interaction between carbon and sulphur on the pure-carbon alloys. The carbon was present as a graphite precipitate and there was the possibility that the graphite layer could grow on top of the sulphur layer as well as displacing it from the surface. Before this interaction can be described it will be necessary to discuss graphite precipitation and the attenuation of Auger signals in an overlayer in more detail.

5.2. Surface precipitation

On the basis of evidence which is presented below, it was concluded that carbon was present at the surface of the plain-carbon alloys as a three-dimensional precipitate of graphite. It was not possible to determine unambiguously the chemical state of carbon at the surface of the chromium-containing alloys. General features of the observed precipitation are discussed below. Several Auger calibrations for monolayer graphite upon iron are then derived, and these are compared with an Auger calibration deduced from the present work. Finally, using this calibration, the probable graphite-layer growth processes are discussed.

5.2.1. General aspects of graphite precipitation

Carbon could have been present at the surface as either a graphite precipitate or as a dispersed segregant. Published work by Grabke et al (1975),(1977) has suggested that carbon is present on the (100) surface of iron in accordance with the iron-graphite equilibrium phase diagram. They were able to use low energy electron diffraction to distinguish between dispersed carbon and graphite. In the present work it was necessary to infer the chemical state of carbon from several pieces of indirect evidence. The closest thing to direct evidence that was available was the shape of the carbon Auger peak, which is known to contain information about its chemical state. Fig. 5.9 shows carbon Auger peaks from both segregated carbon and precipitated graphite on iron due to Grabke et al (1975). Also shown is a carbon Auger peak from the surface of a plain-carbon sample in the present work. The similarity between this peak and that from graphite is evidence that graphite was present in that particular case, but it was only possible to make this comparison when the carbon

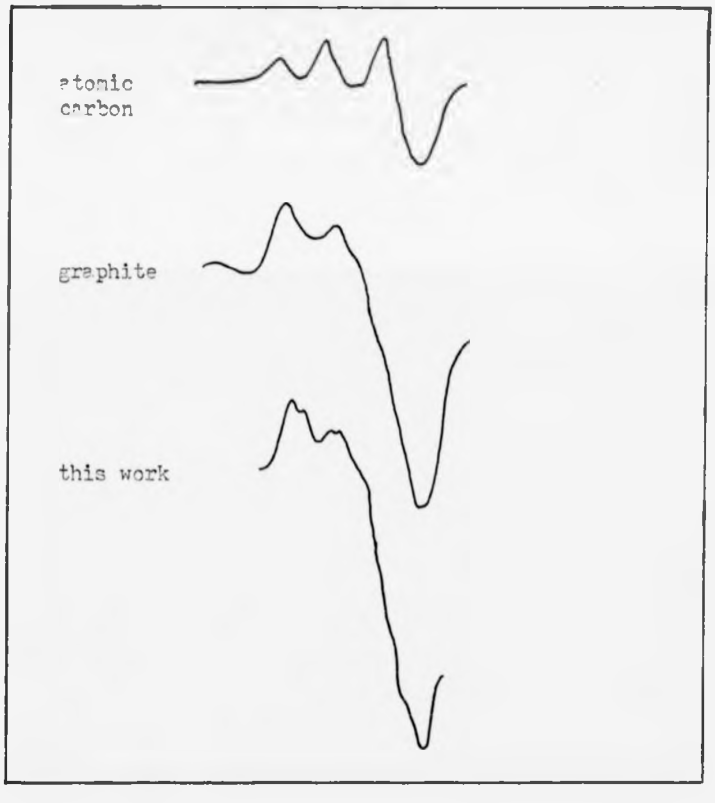

Fig. 5.9 Auger peaks from carbon in various chemical states

peak was large enough to show such fine detail. On the chromium-containing alloys, the carbon Auger peak was always too small to be able to tell its chemical state.

Another observation which gave some information about the chemical state of surface carbon was the large attenuation of the Auger signal from the iron substrate that its presence produced. Shelton et al (1974) found large attenuations of their nickel substrate Auger peaks when graphite precipitated at the surface. When carbon was present as a dispersed segregant, on both Shelton's and Grabke's samples there was no attenuation of the substrate Auger peaks. The evidence for attenuation of the iron Auger peaks on the chromium-containing alloys in the present work was variable. When there was a small carbon Auger peak from the surface, there was sometimes a small reduction in the iron peaks and sometimes no detectable difference. On samples of the plain-carbon alloys, the substrate attenuation varied from area to area of the surface. This is thought to have been due to variations in the thickness of the graphite layer. The samples were polycrystalline, and the nucleation and growth of graphite is known to be strongly dependent upon surface orientation (Speich (1961)). This variable graphite thickness introduced a good deal of scatter into depth-profiles of graphite-covered surfaces because the sample had to be turned to face the ion gun between Auger analyses. Having turned the sample away from the analyser, it was not possible to locate exactly the same area of the surface when it was turned back. Implanted argon atoms from these ion bombardments were trapped at the surface when they diffused out of the bulk during subsequent graphitisation experiments. It is suggested that outgassing was prevented because the argon atoms were too large

to pass through the graphite mesh. A segregated layer of carbon should not have provided any barrier to outgassing.

From the above evidence it was concluded that graphite was precipitating at the surface of the plain-carbon alloys. As far as could be determined, its precipitation was in accordance with the iron-graphite phase diagram; its dissolution, however, did not occur at the predicted temperature. For example, in a hypo-eutectoid iron-carbon alloy, bulk graphite is expected to go into solution at temperatures above 738°C. On the Fe.65C alloy, however, surface graphite appeared to be stable at 800°C (provided that there was no competition from sulphur segregation), although the carbon signal was reduced from its level in the $\alpha+Fe_3C$ phase region. Shelton found that the energy change per atom upon growing a monolayer of graphite on a (111) surface of nickel, from carbon in solution, was about 0.05eV more favourable than precipitating graphite in the bulk (neglecting any strain that this might cause). This was apparently the result of good lattice-matching between the graphite basal plane and the close-packed nickel surface. The similarly good matching with a close-packed plane of austenite has been shown in Fig. 2.7. In addition, graphite precipitation from carbon in solution results in a volume expansion, which can be better accomodated at the surface than in the bulk. Both of these factors could stabilise surface graphite at higher temperatures than would be expected from the bulk equilibrium phase diagram. The implication of Shelton's finding is that not only should surface graphite be stable at higher temperatures, but that given a favourable surface orientation, an increase in the thickness of the graphite layer should be less energetically favourable than an increase in the area of the surface covered by the first layer.

In the present work, graphite precipitation was apparently occurring in competition with sulphur segregation. The kinetics of internal graphitisation are known to be retarded by sulphur. Pope & Grieveson (1977) have suggested that sulphur acts by segregating to potential graphite nucleation sites, depressing the local carbon concentration and so reducing the frequency of nucleation. Surface graphitisation of nickel was studied by Mojica & Levenson (1976) who proposed that it involved two distinct processes: bulk-to-surface carbon diffusion, which provided a 'base-level' concentration of segregated carbon, and cross surface diffusion of this carbon to fuel the growth of graphite at the favourable surface nucleation sites. If surface graphitisation of iron occurred by means of the same two processes, sulphur segregation could interfere in two ways. It could displace carbon from the favourable nucleation sites, and it could suppress the base-level carbon concentration at the surface. Sulphur has been shown to suppress segregation of carbon to the surface of iron (Grabke et al (1975)). Chromium appeared to be effective in removing surface graphitisation of the FeCr and FeCrC alloys. It probably acted by stabilising cementite and so reducing the carbon supply. Spheroidisation of the bulk cementite should also have this effect. The experiments shown in Figs. 4.15 and 4.34 showed this to have been true in the present case, as graphite was slow to precipitate on spheroidised samples, even in the absence of sulphur segregation. The growing layer of graphite might have had to displace segregated sulphur or it might have been able to grow over the top of it. Before its actual behaviour can be interpreted, it will be necessary to calculate the attenuation of Auger electrons in an overlayer of graphite.

5.2.2. Auger calibrations for monolayer graphite on iron

No direct measurement of the carbon to iron peak-height ratio corresponding to monolayer graphite upon iron has been reported in the literature. There are, however, three ways in which certain published data may be used to deduce estimates of this calibration. One method of arriving at an approximate calibration is to take Grabke et al's (1977) Auger calibration for carbon segregation on an iron (100) surface and scale it up to account for the increased carbon atom density in a graphite monolayer. Sulphur saturation produced a c(2x2) structure (12.5% of a close-packed monolayer) and gave an Auger peak-height ratio; C(272eV)/Fe(651eV) = 0.54. It is assumed that this was obtained with a retarding-field analyser (RFA) because LEED measurements were also made. A CMA will measure a different peak-height ratio from the same surface structure because it produces Auger spectra with a different energy dependence. While an RFA produces N(E) spectra, a CMA produces E.N(E) spectra, and hence gives larger high-energy peaks. The expected value of Grabke's calibration will thus become: 0.54x272/651 = 0.22. The number of carbon atoms per unit area in a graphite monolayer should be more or less independent of the iron surface orientation, and so should not vary from area to area on a polycrystalline surface. A calculation based upon a carbon-carbon bond length in graphite of 1.42Å gives the density of carbon atoms as 78% of a close-packed monolayer. The expected C(272eV)/Fe(651eV) peak-height ratio from a monolayer of graphite is thus: 0.22x78/12.5 = 1.37 . For convenience, this will be converted to a ratio with the 47eV iron Auger peak using the Phi Handbook of Standard Auger Spectra. This contains Auger spectra which were obtained from standard samples using a CMA operated under

standard conditions. For this conversion, the heights of the Fe 47eV and 651eV peaks are compared and the ratio with carbon corrected accordingly. This gives a result of 0.77 for the C(272eV)/Fe(47eV) peak-height ratio.

The second method also makes use of the Phi Handbook. This contains standard spectra from both graphite and iron. To a first approximation, therefore, the carbon peak from the graphite standard can be combined with the 47eV iron peak from the iron standard to produce a ratio of 0.31. We have already seen, however, that a graphite layer will cause strong attenuations of the Auger signal from an iron substrate. This must be taken into account in both of the calibration values described so far. In addition, the carbon Auger signal from a block of graphite will be an over-estimation because it will contain contributions from more than just the first monolayer. It would be useful to know the attenuation function of electrons in a graphite monolayer in order to account for both of these factors.

The attenuation of the substrate Auger signal is the result of inelastic scattering of the Auger electrons as they pass through the overlayer. Having suffered an energy loss, the electrons no longer contribute to the Auger peak because they have been shifted away from its position in the energy spectrum. Data for inelastic mean free paths (imfp's) of electrons in graphite are not well established, and the path length in the overlayer is itself a function of both the detector configuration and the angular emission from the surface. Fortunately, Shelton et al (1974), who studied graphite precipitation on nickel, have investigated this complex problem, and their results may be adapted to the present case.

Shelton took the general attenuation function for an arbitrary detector configuration and solved it for his particular experimental arrangement, which was an RFA operating on axis. The function is of the form:

$$A(\theta, x/\lambda) = A_o \int \mathcal{E}(\Omega) \exp\left\{ (-x/\lambda) \sec(\Omega . \underline{n}) \right\} d\Omega$$

where θ is the angle between the surface normal and the analyser axis, λ is the electron imfp in an overlayer of thickness x, Ω is the direction of emission, $\mathcal{E}(\Omega)$ describes the angular emission from the source, $\underline{n}$ is the unit vector normal to the surface and A_o is chosen such that $A(0,0) = 1$. Shelton assumed cosine emission from the source. In order to obtain the relationship between the energy of an Auger electron and its imfp in graphite it was necessary to construct a composite curve using both experimental results from Steinhardt et al (1972) and Jacobi & Holtzl (1971), and a theoretical curve due to Lundqvist (1969). Using this approach, Shelton was able to predict the attenuation of his nickel substrate Auger peaks as a function of graphite layer thickness.

The detector configuration used in the present work was different to that used by Shelton, being a CMA operating on axis. The attenuation has also been solved for this case, however, by Seah (1972) and Norman & Woodruff (1978). Their results were combined with the electron imfp curve used by Shelton, and the expected attenuations of some relevant Auger peaks were predicted for the present case. The results are presented in graphical form in Fig. 5.10. A monolayer of graphite is expected to cause attenuations of 40% for the iron 47eV peak, 50% for the carbon 272eV peak and 63% for the sulphur 150eV peak.

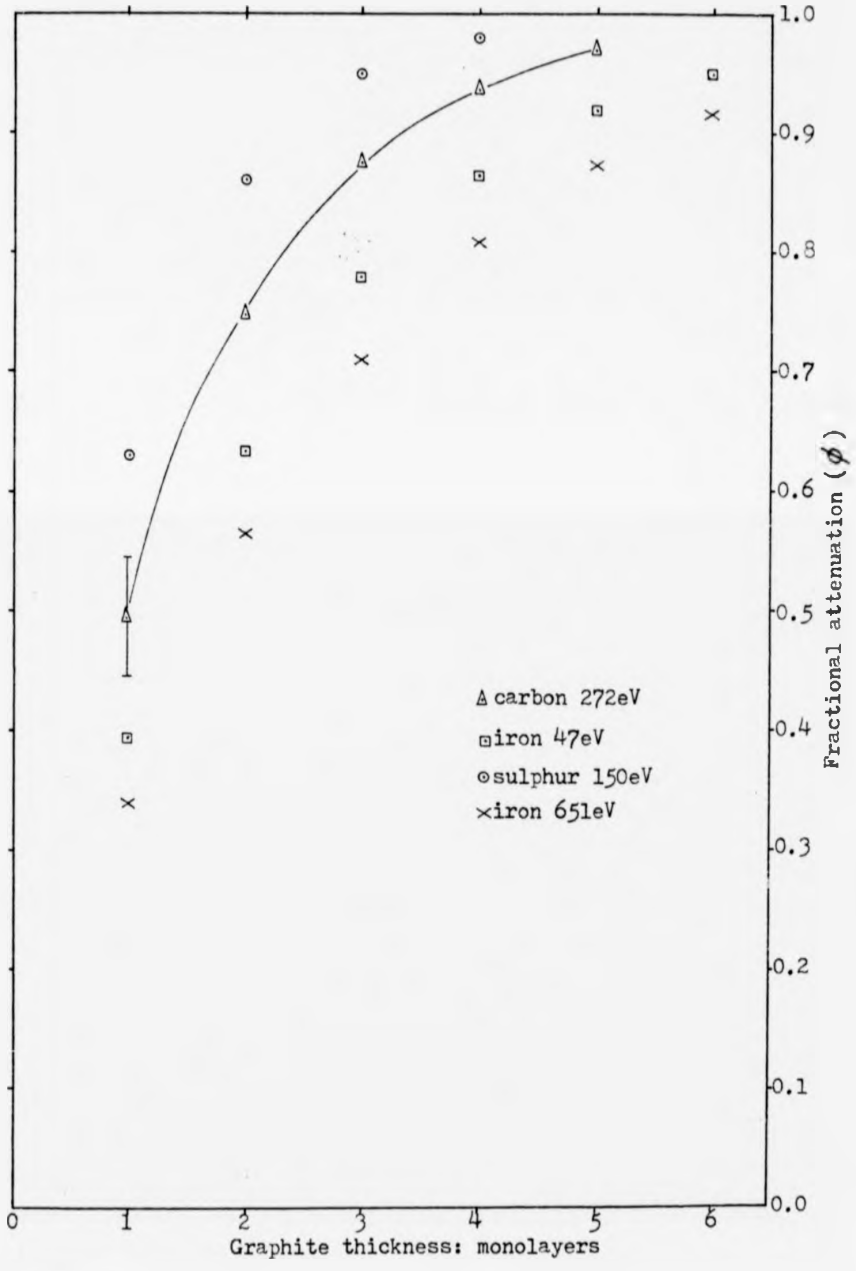

Fig. 5.10 Attenuation of Auger electrons in graphite

On the basis of these approximate attenuations, it is now possible to apply the necessary corrections to the two Auger calibrations that were calculated above. The scaling-up of Grabke's c(2x2) value neglected the change in attenuation of the iron Auger peaks upon replacing segregated carbon with graphite. If this is allowed for, a new value of 1.28 is produced. The calibration that was calculated from the Phi Handbook requires two corrections. If a monolayer of graphite attenuates the carbon Auger signal by 50%, it can be seen that half of the carbon signal from solid graphite will have arisen in the outermost monolayer. Correcting for this, and for the 40% attenuation of the iron 47eV Auger peak, a new calibration value of 0.26 results. These two calibrations give greatly different results, but fortunately a third value is available to act as a check. The Auger calibration for monolayer graphite upon nickel that was obtained by Shelton may be converted to a calibration for graphite upon iron. The Phi Handbook is used to compare the heights of the relevant iron and nickel Auger peaks from iron and nickel standards. A further correction must then be made, to take into account the different imfp's of iron and nickel Auger electrons in graphite. The final value obtained predicts a C(272eV)/Fe(47eV) peak-height ratio of 0.22 for monolayer graphite upon iron, in good agreement with the value of 0.26 that was calculated using the Phi Handbook.

Using the Phi Handbook value of the Auger calibration it was found possible to interpret the results of the isothermal surface transformation experiments in terms of specific graphite growth mechanisms on a sulphur-covered surface. It emerged, however, that the best fit of the predictions to the experimental results was obtained if the calibration value was altered slightly to 0.32.

We have, therefore, four values of the Auger calibration for monolayer graphite upon iron: 1.28 (scaled-up c(2x2)), 0.22 (Shelton/Phi), 0.26 (Phi) and 0.32 (the present work). The first of these is clearly different to the rest. It is thought that this high value could be a function of the analysis system used by Grabke et al because their value of the Auger calibration for monolayer sulphur upon iron was also found to be a factor of about five greater than the values obtained from other sources.

5.2.3. Graphite layer growth

The results of the isothermal transformation experiments were found to contain a good deal of information about the growth characteristics of the surface layer of graphite. The first attempt to interpret them was based upon the two-process graphite growth mechanism due to Mojica & Levenson which was described above. Gijzeman et al (1978) undertook a mathematical analysis of Mojica & Levensons' data based upon a treatment of nucleation and two-dimensional growth by Avrami (1939). They found that the graphite growth could be described by an equation of the form:

$$(h_c^t - h_c^o) / (h_c^\infty - h_c^o) = 1 - \exp(-\beta t^2/2)$$

where h_c^o is the carbon Auger peak height from the base-level carbon segregation, h_c^∞ that from a monolayer of graphite and h_c^t that from some mixture of the two at time t. β is a constant related to the carbon arrival rate. The mechanism can be verified by plotting $\ln(1 - \text{LHS})$ against t^2, when a straight line should be obtained. In the present work, this equation could not be satisfactorily fitted to any of the results. This was taken to be an indication that sulphur segregation, which had not occurred during Mojica &

Levensons' experiments, had forced a change of mechanism by suppressing the segregation of carbon. While no alternative mechanism for the growth of graphite is proposed in the present work, it was found possible to determine some of the processes by means of which a sulphur-covered surface became a graphite dominated surface.

Before considering the results in detail, a model of the possible growth modes will be used to determine how each would manifest itself on log(coverage) versus log(time) plots of the carbon and sulphur time-histories. Argile & Rhead used this approach to good effect in their attempts to interpret the growth mechanisms of vacuum-deposited films, and their nomenclature will be used here. Four basic assumptions are made:

1) initial 100% surface coverage by sulphur (called state I),

2) a carbon arrival rate with a constant time dependence,

3) no sulphur segregation to the surface of the graphite layer,

4) no desegregation of sulphur in those areas free of graphite.

The sulphur level was always allowed to reach saturation before the sample was cooled to the transformation temperature. The time dependence of the carbon arrival rate could change during the course of an experiment because of the presence of carbide particles in the bulk. The arguments for this are similar to those advanced to explain the effects of sulphide particles on the rate of sulphur segregation. In fact, there was little evidence for changes in the carbon time dependences, but this will be discussed later in this sub-section. Included in the assumption of no sulphur desegregation in graphite-free areas is the assumption that there was no significant sulphur evaporation during the transformations. The possible growth modes will now be described on the basis of these assumptions.

In order to illustrate the modes and their combinations, graphite growth is considered to occur in two equal stages: from zero coverage to half a monolayer, and from half a monolayer to full coverage. The initial state (I) is a sulphur-covered surface. Fig. 5.11 presents a schematic of the six possible outcomes of the two-stage process. In the first stage, graphite might displace sulphur from the surface (process S) or grow over the top of it (process C). In the second stage, either of these two processes might occur again. In addition, however, there is now the possibility that the second half of the graphite layer might grow on top of the first (process D). The six final states will be denoted by a two letter code corresponding to the processes which produced them. Two of these states, SC and CS, can be seen to be essentially the same but the paths which lead to them were different. The corresponding carbon and sulphur time-histories can now be considered.

Log(coverage) versus log(time) plots are used because a constant time dependence appears as a straight line, simplifying the interpretation of the result. A plot of the expected carbon signal during the formation of the six final states is shown in Fig. 5.12. A time dependence of $t^{\frac{1}{2}}$ was used in calculating this figure. For the two modes which involved an increase in the graphite layer thickness, the attenuation coefficient of carbon 272eV Auger electrons in a monolayer of graphite (ϕ_c) was taken from Fig. 5.10 to be 0.5. Up to the end of the first stage, the processes are indistinguishable. During the second stage, the onset of process D causes a divergeance from the straight line because of self-attenuation of the carbon signal. The line followed during processes SD and CD is sensitive to the value of ϕ_c. Values of 0.4 and 0.6 were used to calculate the

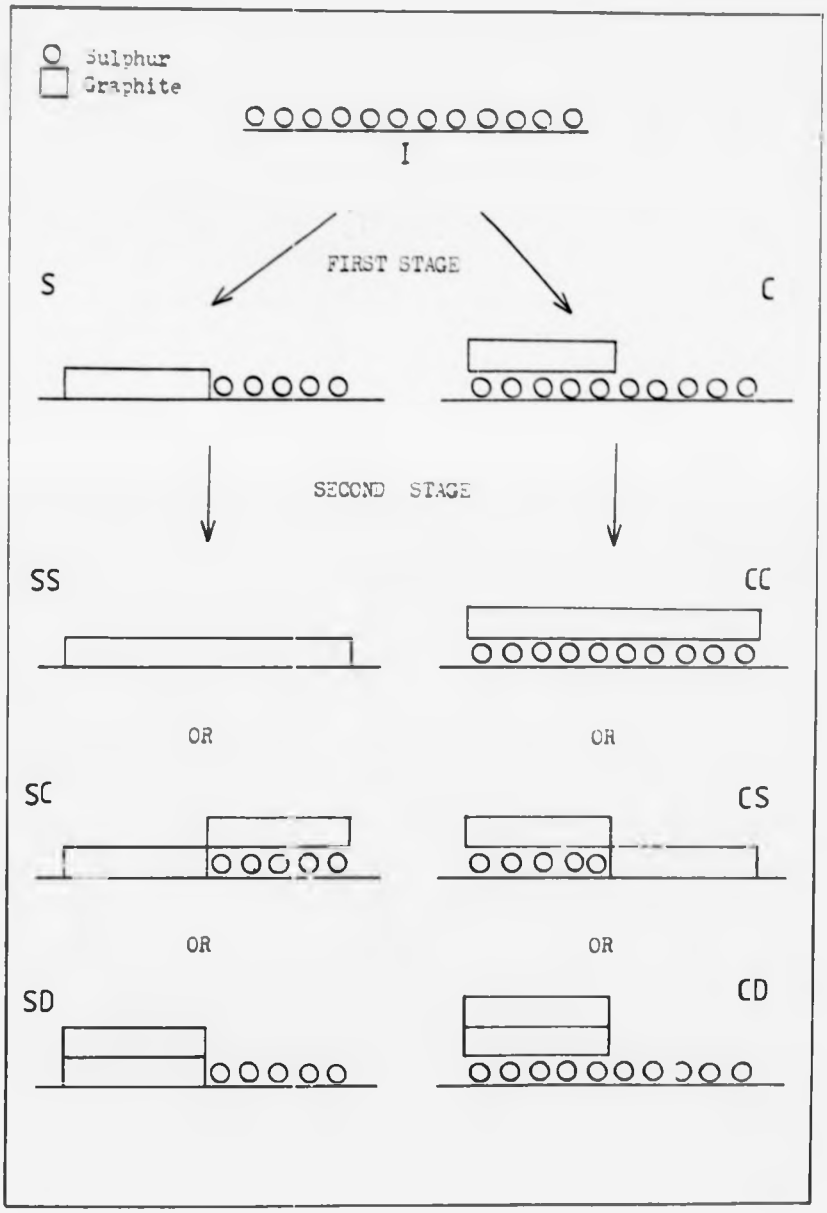

Fig. 5.11 Two-stage graphite growth on a sulphur-covered surface

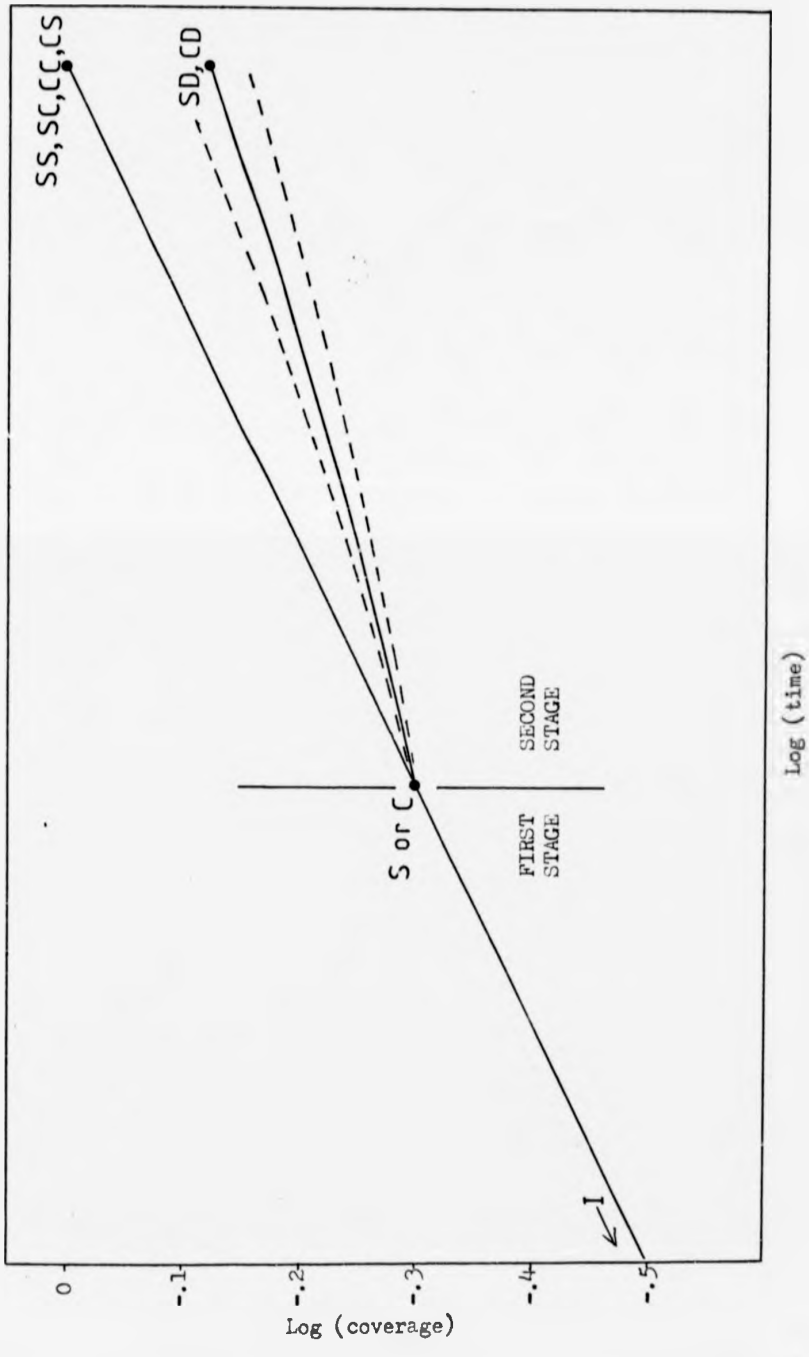

Fig. 5.12 Carbon time-history resulting from processes in Fig. 5.11

broken lines above and below the line corresponding to a value of 0.5. In principle, observations of the carbon time-history during this process of overgrowth could lead to quite an accurate measurement of the self-attenuation coefficient. In practice, care must be taken when interpreting the results because more than one process could be occurring at the same time in different areas of the surface. Restricting the size of the area analysed (in this case to a 20μm diameter spot) can help to reduce this possibility.

When considering the effect of these processes on the sulphur time-history, it is more convenient to plot log(1 - coverage) rather than log(coverage) because this 'inverse-sulphur' function can be more easily related to the carbon function when plotted on the same graph. For example, for process S the inverse-sulphur function and the carbon function produce straight lines which would be coincident if plotted on the same graph. The behaviour of the inverse-sulphur function during the formation of the six final states is shown in Fig 5.13. Each growth-mode now produces a distinct line. During the first stage, process C results in a straight line parallel to that from process S but a distance below it which depends on the attenuation coefficient of sulphur 150eV Auger electrons in a monolayer of graphite (ϕ_s). In calculating Fig. 5.13, ϕ_s was set equal to 0.63; the value predicted in Fig. 5.10. Values of 0.73 and 0.53 respectively were used to calculate the broken lines above and below the line I - C. If, as the graphite layer grows, all the sulphur is covered and not partially displaced a plot of this type provides a quite sensitive means of calculating ϕ_s. The second stage lines were calculated in the same way as for carbon. Having produced this model, the actual results can now be compared with its predictions.

Fig. 5.13 Sulphur time-histories from processes in Fig. 5.11

The results are presented in order of increasing temperature, irrespective of alloy. This was also the order of increasing complexity of interpretation. Fig. 5.14 presents a result at 665°C on the Fe.87C alloy. The straight line drawn through the graphite points has a slope of 0.5 indicating a $t^{\frac{1}{2}}$ dependence in the carbon arrival rate. The parallel broken line marks the expected inverse-sulphur time-history for process CC (ie. no sulphur displaced). It was calculated with ϕ_s set equal to 0.63. The close correspondence between the inverse-sulphur points and this line is evidence that in this experiment the graphite layer grew over the top of the sulphur layer. The first and last points on each line have been marked with error bars. These show the effect that a ±5% change in the Auger peak-to-peak heights would produce. The graphite points are fairly insensitive to changes of this order. The inverse-sulphur points, however, are very sensitive to measurement errors at the start of an experiment but become much more reliable as time passes.

On the Fe.87C alloy, the maximum rate of surface transformation was observed to occur at 665°C. Fig. 5.15 shows a result at this temperature, from which it can be seen that the carbon arrival rate had a t^1 dependence. This type of linear dependence only occurred at the temperature of maximum transformation rate and its significance is discussed later in this sub-section. At other temperatures, the carbon arrival rate always had a $t^{\frac{1}{2}}$ dependence. In this experiment, all of the sulphur layer once again appeared to remain at the surface as the graphite layer grew over the top of it. At time A the first monolayer of graphite was complete. The carbon and inverse-sulphur results then began to follow the paths expected for growth of a second monolayer of graphite. The solid curves are the theoretical

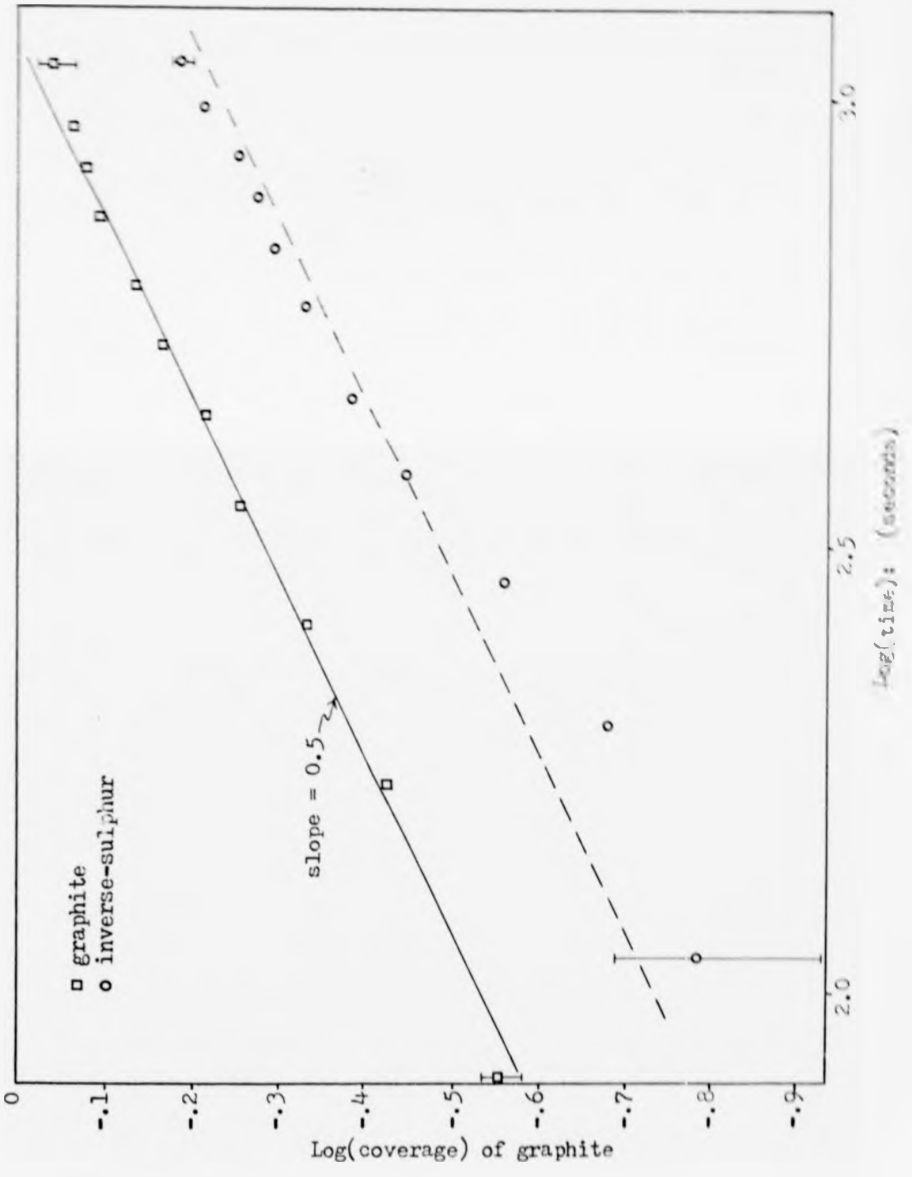

Fig. 5.14 Fe.87C: surface transformation at 655°C

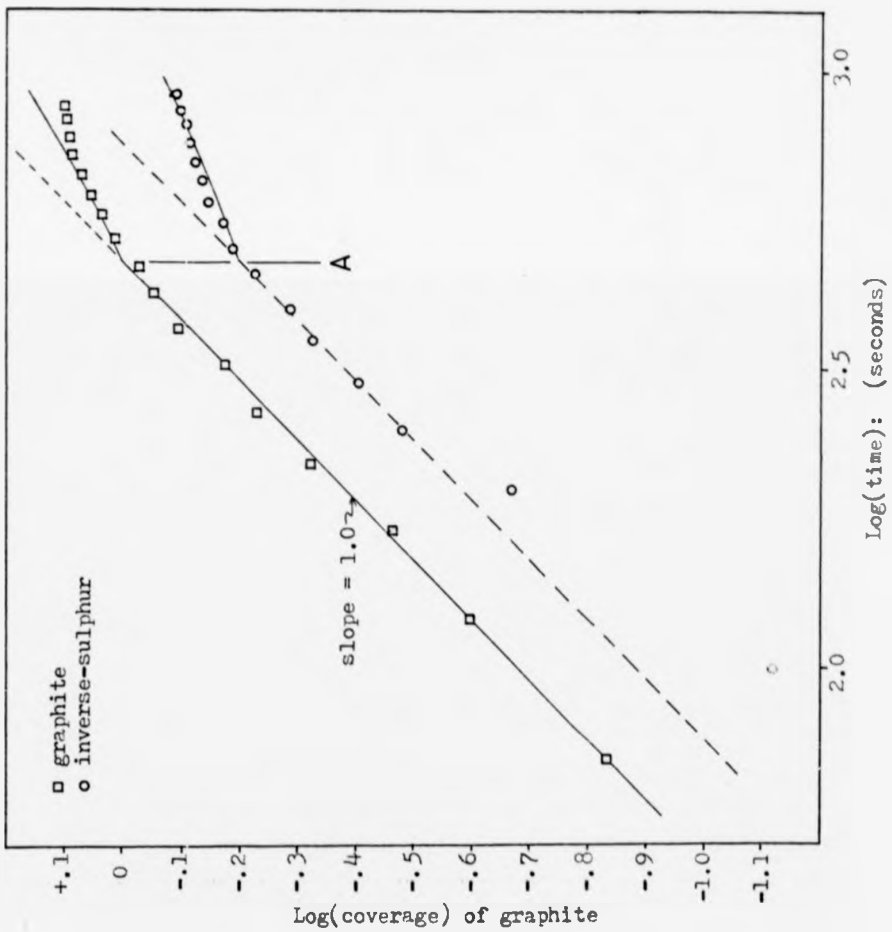

Fig. 5.15 Fe.87C: surface transformation at 665°C

lines drawn assuming values of 0.5 for ϕ_c and 0.63 for ϕ_s. They were in reasonable agreement with the experimental results.

At temperatures of 670°C and above there was always some evidence that sulphur had desegregated to some extent once it had been covered by graphite. A result at 670°C on the Fe.65C alloy is shown in Fig 5.16. The carbon arrival rate had a $t^{\frac{1}{2}}$ dependence and the graphite monolayer appeared to grow evenly. The inverse-sulphur result, however, was rather complex and will be considered in four stages. Up to time A, graphite was assumed to have grown over the top of the sulphur layer. Between times A and B, all new graphite growth was assumed to have displaced sulphur, and the solid curve drawn through the inverse-sulphur points was calculated on the basis of process CS. Between times B and C the small amount of overridden sulphur appeared to diffuse away from the surface. This effectively restored the surface to the state expected if process S had operated from the start of the experiment. Under these conditions, the carbon and inverse-sulphur points should lie on the same straight line. This experiment provided an upper limit to the carbon/iron Auger calibration because, assuming no sulphur segregation to the surface of the graphite layer, the inverse-sulphur points should never lie above those of graphite. There was some indication that some sulphur was again being overridden by the end of the experiment.

The driving force for surface graphitisation is expected to be the low interfacial energies possible as a result of lattice matching between the graphite basal plane and the iron surface. Whilst the austenite (111) plane is an excellent match to the graphite basal plane, none of the ferrite low-index planes are as good. At best they can be fitted to it along one axis. Along the perpendicular

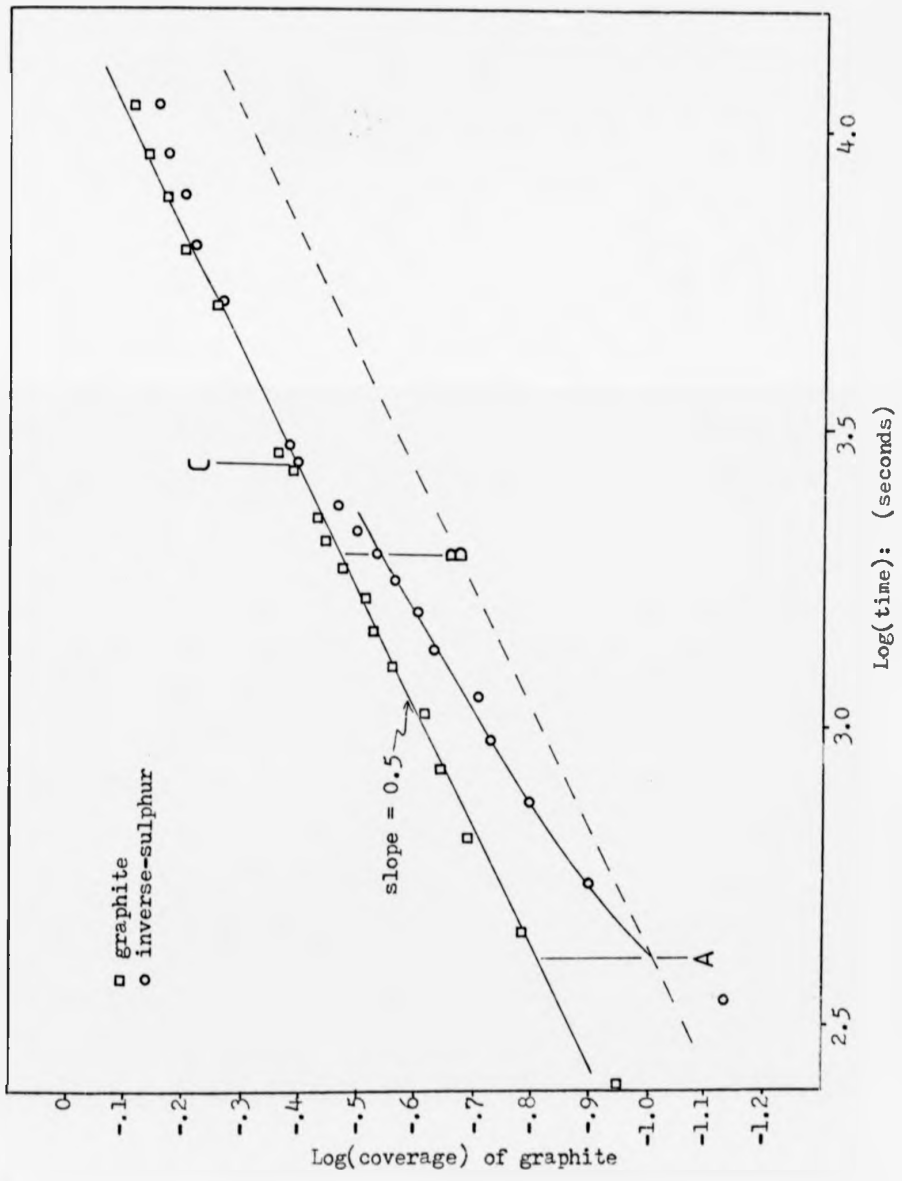

Fig. 5.16 Fe.65C: surface transformation at 670°C

axis, the two lattices will only come into registration at intervals. In some areas of the surface, a monolayer of graphite could precipitate without disturbing the layer of segregated sulphur. In other areas the sulphur was displaced. Presumably, the outcome at any particular point on the surface would have been that particular combination of segregation and/or precipitation that resulted in the lowest interfacial energy. The desegregation of sulphur once it had been covered by graphite could be due to two factors. At the start of graphite growth, the rate of linear expansion of the graphite islands would have been at its fastest, and some sulphur could have been overridden simply because it could not diffuse into the bulk fast enough. Desegregation of sulphur later in an experiment could have been due to some surface rearrangement; for example, if the surface were able to facet to a more favourable orientation.

Another example of desegregation of sulphur, once it had been covered by graphite, is shown in Fig. 5.17. This was another result at 670°C on the Fe.65C alloy. The graphite points were a nice fit to the theoretical line of process CD ($\phi_c = 0.5$) with growth of the second graphite monolayer beginning at time A. If this had been the only process occurring, the inverse-sulphur points would be expected to follow the broken curve beyond time A. The continuing fall in the sulphur Auger signal is thought to have been due to its desegregation from beneath the graphite layer. At time A, some 61% of the surface was covered by graphite. If all the sulphur was removed from beneath the graphite layer, the surface state would then be equivalent to that resulting from process SD. It can be seen from Fig. 5.13 that the inverse-sulphur level would then have remained constant at a value equal to the graphite level at time A.

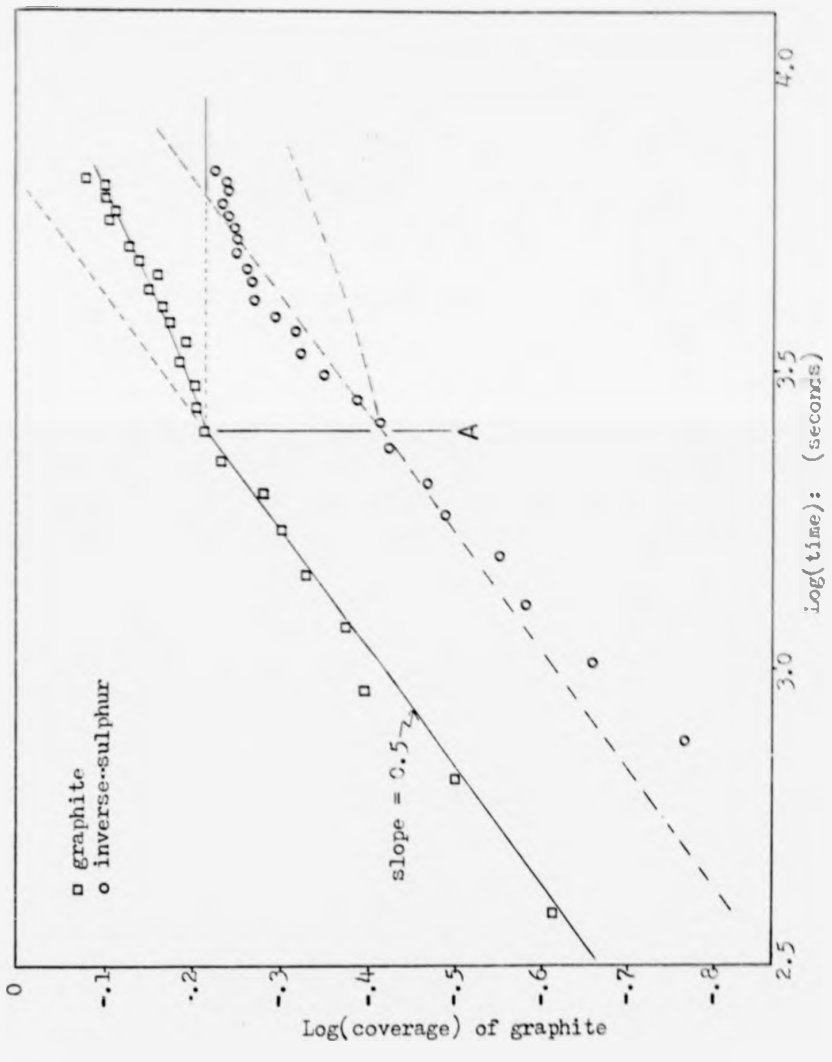

Fig. 5.17 Fe.65C: surface transformation at 670°C

This line has been drawn in on Fig. 5.17 to show how the inverse-sulphur points were levelling out towards this value.

At 685°C on the Fe.65C alloy, Fig. 5.18, there was uniform expansion of the graphite monolayer and complete coverage of the sulphur layer until time A was reached. At this point, the graphite layer began to increase in thickness. Both the graphite and inverse-sulphur points followed the prediction for process CD (solid curves) until time B. Beyond this point, however, the results cannot be explained in terms of any one of the simple processes on its own. The broken curves are the paths that the results would follow if expansion of the first graphite layer had resumed at time B. The actual points lie between the two predictions, and it is possible that both processes were occurring at the same time in the area of the surface that was being examined.

The final result that will be considered in detail is shown in Fig. 5.19 and is from an experiment at 690°C on the Fe.87C alloy. The carbon arrival rate had an apparent $t^{\frac{1}{2}}$ dependence and the first graphite monolayer grew uniformly until time A. The solid curve between times A and B was the prediction from process CD. Between times B and C, however, the graphite points regained the original straight line by means of a rapid increase with a slope of 1.8. If it is assumed that the carbon time dependence was constant during this experiment, the observed result can be explained in terms of a process which was not considered in the original model. It is proposed that at time B the expansion of the first graphite monolayer was resumed, but now supplied both by fresh carbon arriving at the surface and by the dissociation of the second graphite layer. The inverse-sulphur result supports this hypothesis. There had been some

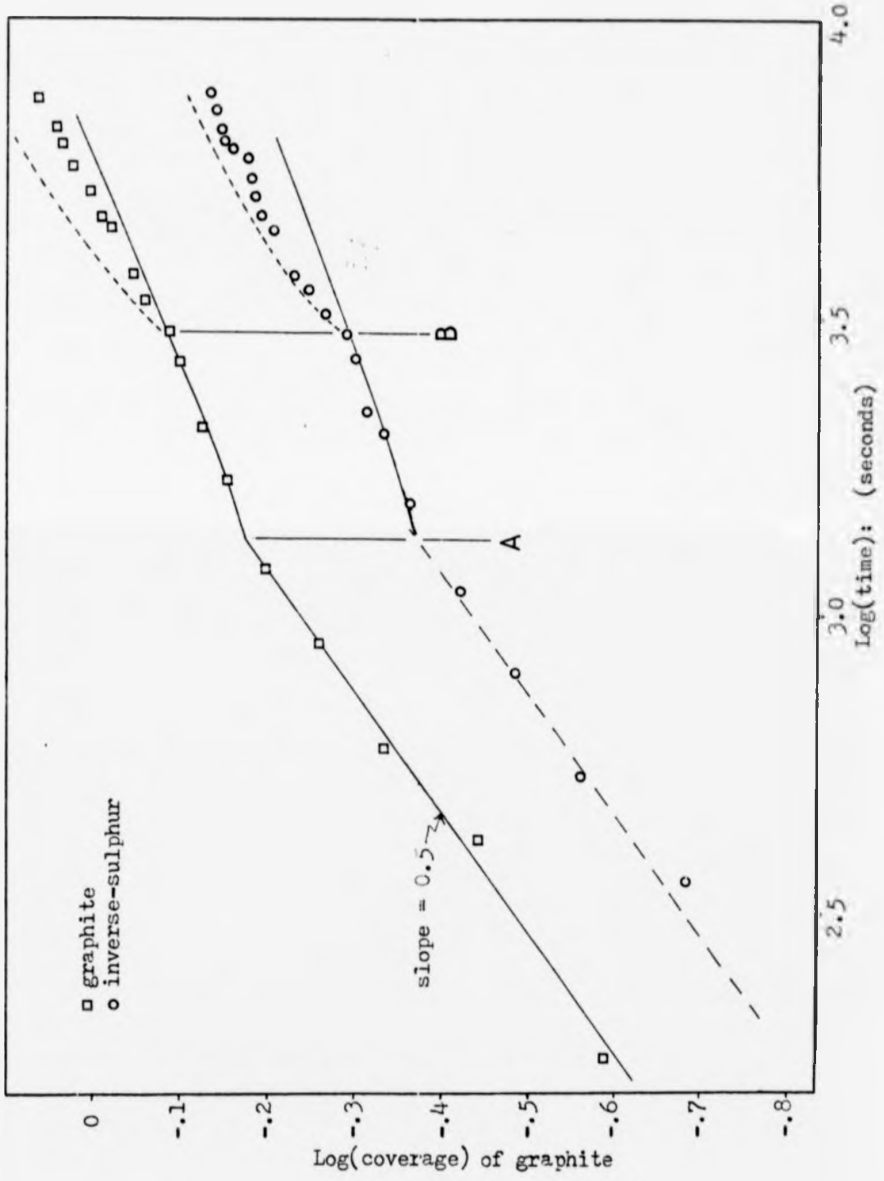

Fig. 5.13 Fe.65C: surface transformation at 685°C

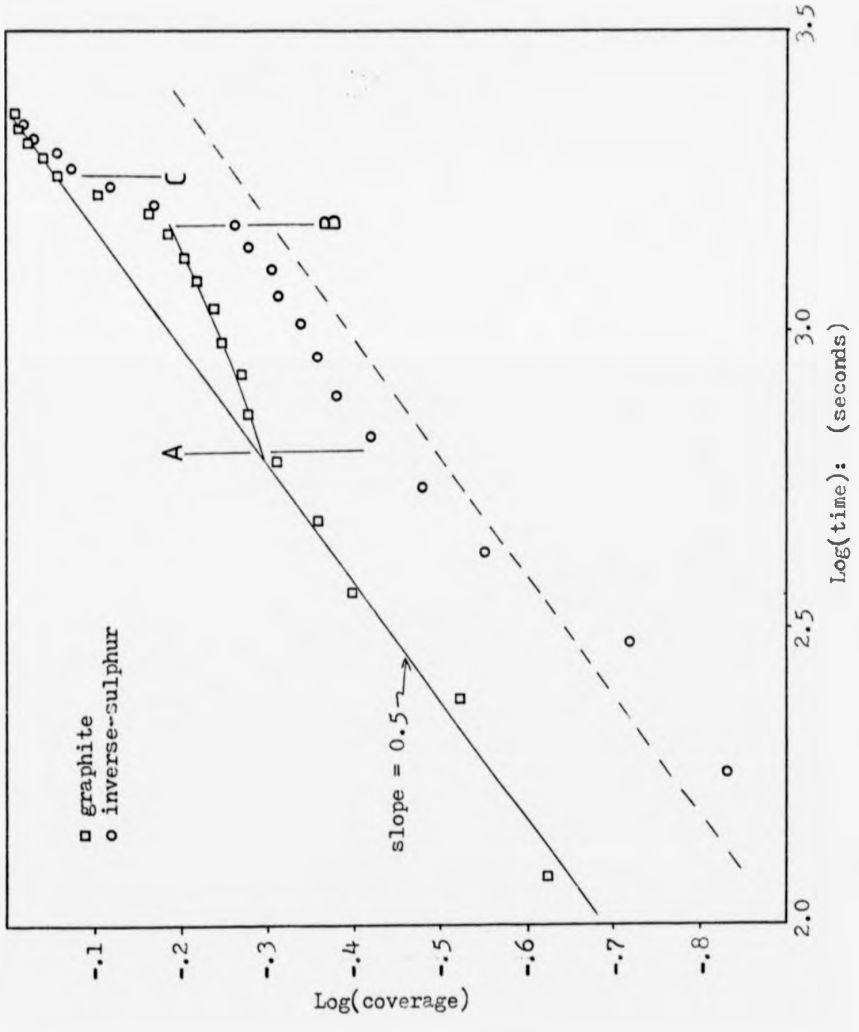

Fig. 5.19 Fe.87C: surface transformation at 690°C

desegregation of sulphur during the first two stages, but between times B and C virtually all the remaining sulphur was displaced from the surface, showing that the graphite layer was indeed expanding.

Olney & Smith (1959) observed that a sharp increase in the growth rate of graphite on an iron surface was accompanied by surface facetting in the region of growth. Although facetting to a suitable orientation leads to an increase in surface area, it can also promote the expansion of the graphite layer, leading to a net lowering of the surface energy. It is possible that all the more favourable areas of the surface of the Fe.87C sample had been covered by graphite by time A so that the second monolayer began to form on top of the first. If facetting had occurred at time B, this could explain the sudden renewed expansion of the first monolayer. It was argued above that epitaxial growth on a suitable orientation can lead to a lower-energy state than can an increase in graphite thickness. On this basis it could have been energetically favourable for the second monolayer to dissociate in order to fuel the growth of the first.

During the isothermal transformation experiments, only two time dependences of the carbon arrival rate were observed: $t^{\frac{1}{2}}$ and t^{1}. A $t^{\frac{1}{2}}$ dependence indicates that the process is diffusion limited and the rate of arrival at the surface decreases with time as the sub-surface carbon concentration gradient becomes shallower. In the first section of this chapter it was shown that labile sulphide particles in the bulk could interact with the sub-surface sulphur concentration gradient to produce a linear time dependence of surface segregation. It may be similarly argued that cementite platelets could act in the same way to produce a linear carbon arrival rate.

In this respect, some relevant work has been reported. Burke (1959) and Gibbs (1965) have analysed the kinetics of graphite-nodule formation in the bulk of an iron sample. They concluded that in principle any of the following processes could be rate limiting:

1) diffusion of carbon, iron or an alloying element,

2) dissolution of cementite,

3) crystallisation of graphite.

If the first of these is rate controlling then a $t^{\frac{1}{2}}$ dependence results. For graphite precipitation at a surface, however, only carbon diffusion is important because there is no need for iron or other atoms to diffuse away from the growing graphite crystal. Thus, the diffusion-limited precipitation process is conceptually similar to surface segregation of carbon except that the surface sink is a separate phase rather than an enriched part of a single-phase region.

Both Burke and Gibbs predicted linear graphite growth laws for the dissolution-controlled process. This will, however, only apply once the carbon concentration gradient has reached the carbide particle. Up to that time, the diffusion limitation will apply and there will be a $t^{\frac{1}{2}}$ dependence. Higgins & Jeminson (1965) found that in a high purity 0.78% carbon steel, carbide particles some distance from the graphite nodule began to dissolve before those carbides immediately adjacent to the nodule had disappeared. This indicates that the dissolution rate of cementite is insufficient to pin the concentration gradient in the vicinity of the carbide particle. The gradient may still be linear between the carbide particle and the graphite nodule, however, if the shortfall in dissolution rate is small. In this event, the diffusion gradient beyond the carbide may feed sufficient carbon into the vicinity of the dissolving

particle to maintain an essentially constant concentration there, although this concentration would be lower than the equilibrium value.

If crystallisation of graphite is the rate-controlling process, the graphite growth law should again be linear, because the rate at which carbon atoms were supplied to the surface would no longer be important. In the bulk, graphite crystallisation may be distinguished from carbide dissolution as the rate-controlling process because it is rate-limiting from the start of an experiment, while carbide dissolution would only produce a linear time dependence after an initial period with a $t^{\frac{1}{2}}$ dependence. In the present work, two consecutive experiments at 665°C on the Fe.87C alloy exhibited a t^{1} dependence, and a linear plot of these results is shown in Fig. 5.20. It is possible to fit these results with lines passing through the origin. This would appear to indicate that graphite crystallisation was the rate-limiting process, but this has never been observed to be the case during bulk graphitisation. Sulphur segregation experiments which exhibited a linear time dependence from the start were thought to have been conducted on samples where the sub-surface concentration gradient had already been pinned by an inclusion. In the present case, the sample had only received a superficial ion bombardment before the first of the two experiments. Although the previous experiment had only exhibited a $t^{\frac{1}{2}}$ dependence, it is thought likely that pinning by a carbide particle was responsible for the linear time dependence at 665°C. The fact that the transformation rate of a graphite-covered surface was fastest around this temperature may be explained as follows. As the transformation temperature is increased, the carbon diffusion rate increases and permits a faster transformation

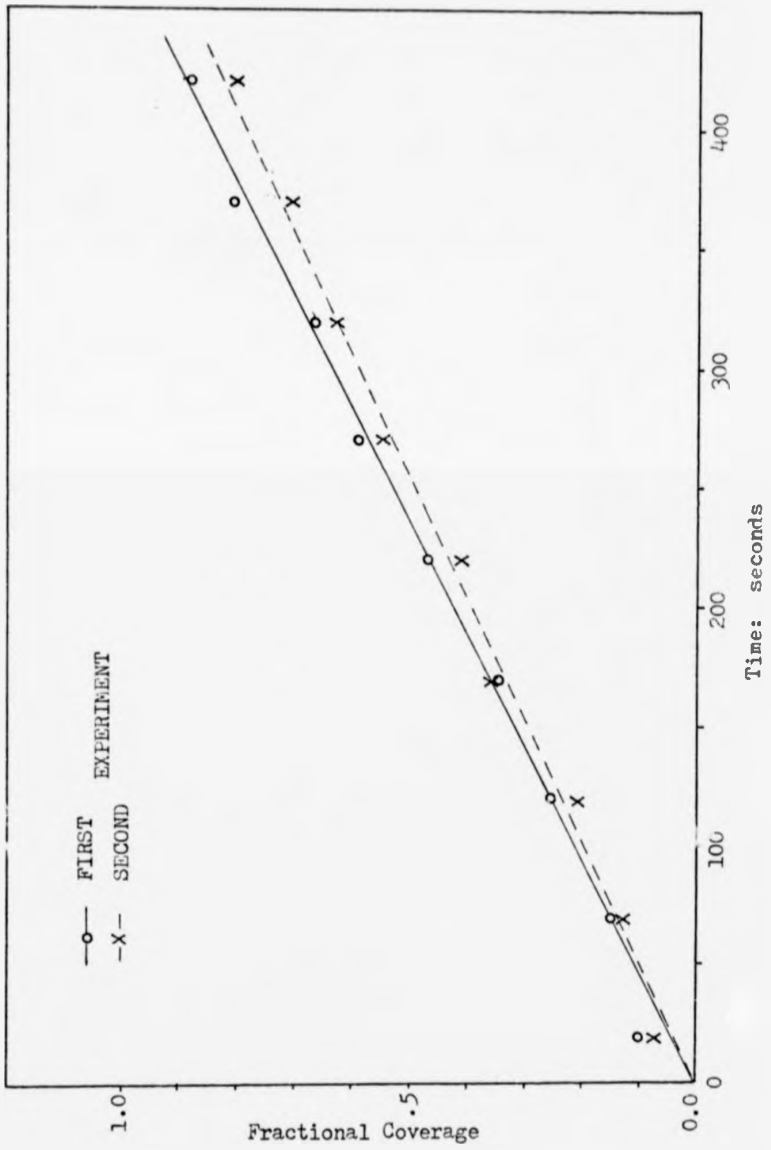

Fig. 5.20 Fe.37C: linear graphite growth at 665°C

rate. Acting in the opposite sense to this is the rate of nucleation, which decreases with increase in temperature (and hence degree of undercooling). The combination of these two opposing trends would be expected to produce a maximum in the transformation rate at some intermediate temperature. This type of behaviour occurs with the transformation of austenite to ferrite+cementite, as was described in section two of Chapter Two.

To summarise: an Auger calibration for monolayer graphite upon iron has been developed from the present work and compared with some other values adapted from published work. This calibration, when applied to the results of the isothermal surface transformation experiments, permitted an analysis to be made of the various types of graphite growth process which had occurred. The kinetics of graphite growth have been discussed in terms of the interaction of bulk carbide particles with the sub-surface carbon concentration gradient.

5.3. Surface behaviour of the HCC alloy

The results from the HCC alloy were different in character to those from the pure alloys. The surface segregation was rather erratic and non-reproducible. It was also particularly subject to the effects of evaporation and depletion. Surface enhancements of sulphur, phosphorus, carbon, nitrogen and chromium were observed, and these are now considered in turn.

5.3.1. Sulphur

The behaviour of sulphur at the surface of the HCC samples was similar to its behaviour on sulphur-depleted samples of the FeCr and FeCrC alloys in that it was slow to appear and was therefore preceeded by other segregating impurities. On the HCC alloy, however, sulphur never achieved saturation coverage, but passed through a maximum before falling away to a low level. This type of behaviour is symptomatic of evaporation from the free surface. There was no evidence of regular time dependences in the segregation rate.

The sulphur content of the HCC alloy was considerably higher than that of the pure alloys, and its comparatively weaker segregation in HCC is attributed to the presence of manganese in the alloy. Seah & Lea (1975) found that by adding manganese to their iron-tin alloys they could largely remove surface segregation of sulphur. When sulphur did segregate, it only reached a low level and required an induction period before it first appeared at the surface. Seah & Lea suggested that sulphur had only segregated at all because manganese had evaporated from the surface, increasing the sulphur activity in the sub-surface zone. Manganese is a very strongly sulphide-forming element, and they had added sufficient not only to precipitate all the sulphur present in their alloys but also to maintain a high

enough concentration in solid solution to suppress dissociation of the manganese sulphide.

In the present work, there was not always an induction period before sulphur segregated, and the level of segregation could be as high as half saturation coverage. The induction period arises from the time delays caused by the following series of events:

1) manganese evaporates from the surface, producing a sub-surface concentration gradient,
2) the concentration gradient lengthens until it encounters a bulk sulphide particle and lowers the local manganese concentration below its equilibrium value,
3) the sulphide particle starts to dissolve in order to maintain the local equilibrium,
4) sulphur diffuses to the surface, where it appears as a segregant.

The sulphur concentration gradient would be very shallow and hence the rate of segregation very slow. For example, with an effective bulk concentration of sulphur around 1ppm instead of a manganese-free value of 10ppm, the time taken to reach saturation would be one hundred times as long. In order to obtain the segregation rates observed in the present work, some other process must have been operating. It is considered likely that, in the same way as with deep-bombarded samples of the pure alloys, there would have been manganese sulphide particles at the surface. Direct dissolution of such particles could then account for the faster and stronger segregation of sulphur observed in some cases. The effects of sulphur evaporation which were observed on samples of the HCC alloy could also have been a result of the very low segregation rates possible in the presence of manganese.

In pure iron, sulphur segregates strongly to the grain boundaries in the alpha range, but hardly at all to austenite grain boundaries (Ramasubramanian & Stein (1973)). Edwards et al (1976) did find some evidence of sulphur segregation to austenite grain boundaries in an EN30A commercial steel, but only at a low level. The manganese content of HCC steel should be sufficient to prevent sulphur segregation to ferrite grain boundaries (Brammar & Honeycombe (1964)). It is calculated from Sawle (1974) that some 20 wtppm of sulphur could be in solution at the temperature of the hot-piercing operation, but Seah & Hondros (1973) have found that the tendency of sulphur to segregate in iron falls with increasing temperature. In the present work, sulphur segregation at temperatures in the gamma range was probably due to surface effects, which would not occur at the grain boundaries. It is not thought likely that sulphur would be the primary cause of poor hot-workability by segregating to austenite grain boundaries in HCC steel.

5.3.2. Phosphorus

The segregation of phosphorus in the HCC alloy followed the same general pattern as in sulphur-depleted samples of the FeCr and FeCrC alloys. Although there was no longer any possibility that sulphur segregation might have displaced it from the surface, it was still a transient segregant. This is therefore firmly attributed to phosphorus evaporation from the free surface. Phosphorus segregation sometimes approached saturation coverage, and it was certainly the most important segregant on HCC samples. If phosphorus segregated to the grain boundaries of HCC steel as strongly as it segregated to the surface, it could be responsible for the observed poor hot-workability.

In pure iron, phosphorus segregation to grain boundaries is reported to follow a similar pattern to sulphur. Ramasubramanian & Stein (1973) found that it segregated strongly in the alpha range but not in austenite. In a nickel-chromium steel, however, Banerji et al (1978) observed phosphorus segregation at prior-austenite grain boundaries after oil quenching from 1160°C. Mulford et al (1976) have reported that chromium appeared to enhance phosphorus segregation, and Banerji found that the addition of manganese to a high-purity steel seemed to have the same effect. Kaneko et al (1965) investigated the effect of alloying elements on the solubility of phosphorus in iron. They found that most alloying elements did indeed reduce its solubility in iron. The solid solubility of an impurity in a metallic solvent has been found to be inversely proportional to its tendency to segregate (Hondros & Seah (1972)). Some alloying elements, however, whilst reducing the impurity's solid solubility, also form such stable compounds with it that none is available to segregate. Manganese appears to combine with sulphur in this way, but no additions are made to HCC to combine with the phosphorus. Certain alloying elements have been found to act as scavengers for phosphorus; notably molybdenum and titanium (Graham & Yen (1978)). Additions of these elements to HCC steel might be found to be beneficial to its hot-workability.

5.3.3. Carbon

It was not possible to confirm whether carbon was present at the surface of HCC as a segregant or a graphite precipitate, because its Auger peak was always too small to show any convincing chemical information. As carbon was a transient surface impurity on HCC samples, it is possible that evaporation was a significant

factor. The evaporation rate of graphite is expected to be less than that of iron (Honig & Kramer (1969)). This might be an indication that carbon was present as a dispersed segregant, and its surface coverages were calculated on this basis. Carbon segregation to grain boundaries has been found to be de-embrittling in iron, and Seah (1976) has related this property to its small atomic size. This allows it to segregate to grain boundaries without distortion of the iron-iron spacings there.

5.3.4. Nitrogen

Nitrogen segregated to the surface of the HCC alloy with comparatively low coverages. Grabke et al (1977) found that evaporation became important at temperatures above 500°C. This might have been a factor in its transient appearance at such low levels in the much higher temperature experiments reported here. Grain boundary segregation of nitrogen has frequently been found to occur in nickel-chromium steels (see for example Edwards et al (1976), Banerji et al (1978)). Rowe (1979) reported its segregation to austenite grain boundaries in iron-3% silicon. It is possible that nitrogen segregation plays a part in the poor hot-workability of HCC steel. Banerji et al suggested the addition of aluminium to suppress nitrogen segregation.

5.3.5. Chromium

Chromium segregation passed through an early peak before declining to a low level, which was also its usual behaviour on the pure alloys. Chromium is thought to promote phosphorus segregation in alpha iron (Marcus et al (1972)). The almost complete absence of phosphorus segregation in the chromium-free pure alloys cannot be solely attributed to the absence of chromium because of the strong interference by graphite precipitation.

REFERENCES for Chapter Five

Ainslie N.G. & Seybolt A.U., J.I.S.I. 194(1960)341

Argile C. & Rhead G.E., Surface Science 53(1975)659

Avrami M., J. Chem. Phys. 7(1939)1103

Banerji S.K., McMahon C.J. & Feng H.C., Met. Trans. 9A(1978)237

Bénard J., Oudar J., Barbouth N., Margot E. & Berthier Y., Surf. Sci. 88(1979)L35

Berrer R., Diffusiya v Tvergykh Telakh, 1948

Bramley A., Hayward F.W., Cooper A.T. & Watts J.T. Trans. Farad. Soc. 31(1935)707

Brammar I.S. & Honeycombe R.W.K., J.I.S.I. 202(1964)335

Burke J., Acta Met. 7(1959)268

Clayton J.Q. & Burstein G.T., Metal Science, Sept(1979)530

Edwards B.C., Bishop H.E., Riviere J.C. & Eyre B.L., Acta Met. 24(1976)957

Elliott J.F. & Gleiser M., Thermochemistry of Steelmaking, 1(1960)245

Gibbs G.B., Trans. Met. Soc. A.I.M.E. 233(1965)1969

Gijzeman O.L.T., Schouten F.C. & Bootsma G.A., Surf. Sci. 71(1978)174

Grabke H.J., Tauber G. & Viefhaus H., Scripta Met. 9(1975)1 81

Grabke H.J., Paulitschke W., Tauber G. & Viefhaus H., Surf. Sci. 63(1977)377

Graham W.R. & Yen A.C., Met. Trans. 9A(1978)1461

Gruzin P.L. & Minal V.V., Fiz. Met. Metall. 16(1963)551

Guttmann M., Thèse, Université d'Orsai, 1974

Guttmann M., Surface Science 53(1975)213

Hager J.P. & Elliot J.F., Trans. Met. Soc. A.I.M.E. 239(1967)513

Heyward T.R. & Goldstein J.I., Met. Trans. 4A(1973)2335

Higgins G.T. & Jeminson G.V. J.I.S.I. 203(1965)146

Hondros E.D., Proc. Roy. Soc. A286(1965)479

Hondros E.D. & Seah M.P., Scripta Met. 6(1972)1007

Honig R.E. & Kramer D.A., RCA Review 30(1969)285

Jacobi K. & Holtzl J., Surface Science 26(1971)54

Kaneko H., Nishizawa T., Tamaki K. & Tanifuji A.,
J. Jap. Inst. Met. 29(1965)166

Kiessling R. & Lange N., Non-metallic Inclusions in Steel: Part II,
London 1966

Kononyuk I.F., Fiz. Met. Metall. 19(1965)311

Krahe P.R. & Guttmann M., Scripta Met. 7(1973)387

Leymonie C., Comptes Rendus 245(1957)931

Lundqvist B.I., Phys. Stat. Solidi 32(1969)273

Marcus H.L., ASTM S.T.P. Nº 499, 1972

Mojica J.F. & Levenson L.L., Surface Science 59(1976)447

Morris J.P. & Buehl R.C., Trans. A.I.M.E. 188(1950)317

Mulford R.A., McMahon C.J., Pope D.P. & Feng H.C.,
Met. Trans. 7A(1976)1183

Norman D. & Woodruff D.P., Surface Science 75(1978)179

Ohtani H., Feng H.C. & McMahon C.J., Met. Trans. 7A(1976)1123

Oldham D.H. & Stowell M.J., T.I. Research Report Nº 334, Jan 1972

Olney M.J. & Smith G.C., J.I.S.I. 193(1959)107

Oudar J., Barbouth N. & Bénard J., Mem. Sci. Rev. Met. 72(1975)649

Pope M. & Grieveson P., Metal Science, Apr(1977)137

Ramasubramanian P.V. & Stein D.F., Met. Trans. 4A(1973)1735

Rosenqvist T. & Dunicz B.L., Trans. A.I.M.E. 194(1952)604

Rowe R.G., Met. Trans. 10A(1979)997

Sawle R., Thesis, University of Sheffield, 1974

Seah M.P., Surface Science 32(1972)703

Seah M.P., Proc. Roy. Soc. A349(1976)535

Seah M.P. & Lea C., Phil. Mag. 31(1975)627

Seah M.P. & Hondros E.D., Proc. Roy. Soc. A335(1973)191

Seibel M.G., Mem. Sci. Rev. Met. 61(1964)431

Seitz W. & Berrer R., Diffusiya v Metallakh, 1958

Shelton J.C., Patil H.R. & Blakely J.M., Surf. Sci. 43(1974)493

Siebel G., Comptes Rendus 256(1963)4661

Speich G.R. & Szirmae A., Trans. Met. Soc. A.I.M.E. 245(1969)1063

Stein D.F., Joshi A. & Laforce R.P., Trans. A.S.M. 62(1969)776

Steinhardt R.G., Hudis J. & Perlman M.L., Phys. Rev. B 5(1972)1016

Swisher J.H., Trans. A.I.M.E. 239(1967)110

Turkdogan E.T., Ignatowicz S. & Pearson J., J.I.S.I. 180(1955)349

von Wang S.J. & Grabke H.J., Z. für Metall. 61(1970)597

Whalen T.J., Kaufman S.M. & Humenik M., Trans. A.S.M. 55(1962)778

Wyjadlowski T., Poyet P., Boos J.Y. & Goux C.,
Mem. Sci. Rev. Met. 71(1974)711

Yen A.C., Graham W.R. & Belton G., Met. Trans. 9A(1978)31

Zemskii S.V., Gruzdeva V.M. & Lvov V.S., Izv. V. V. Z. Chern. Met.
13(1970)106

CHAPTER SIX CONCLUSIONS AND FUTURE WORK

6.1. The Fe.65C and Fe.87C alloys

Graphite precipitated according to the iron-graphite equilibrium phase diagram. Once it had precipitated, however, it was stable above the predicted dissolution temperature in some areas of the surface. This was in agreement with the reported behaviour of graphite at the surface of nickel.

Sulphur was the dominant surface segregant and commonly achieved saturation coverage. The strong competition between sulphur segregation and graphite precipitation prevented the segregation of other impurities, except for one transient appearance by phosphorus when sulphur was depleted.

Implanted argon atoms from the ion bombardments were observed to be trapped at the surface in the presence of a graphite layer.

From isothermal graphite precipitation experiments it was possible to deduce an Auger calibration for monolayer graphite upon iron: C(272eV)/Fe(47eV) = 0.32 ±0.02. This was in reasonable agreement with calibration values obtained by means of indirect calculations

The expected attenuation coefficients of carbon and sulphur Auger electrons in a monolayer of graphite were calculated from the attenuation function for the present detector configuration and published values of the electron imfp's in graphite. The values obtained, $\phi_c = 0.5$ and $\phi_s = 0.63$, were supported by the results of the isothermal surface precipitation experiments.

Using this calibration, it was possible to interpret the carbon and sulphur time-histories during graphite precipitation at a sulphur-covered surface in terms of the following graphite growth processes:

1) uniform growth of a graphite monolayer over the top of a segregated layer of sulphur,
2) subsequent diffusion away of the covered sulphur in some areas of the surface,
3) displacement of the segregated sulphur layer from the surface by the expanding graphite islands,
4) growth of a second monolayer of graphite on top of the first,
5) dissociation of the second graphite monolayer in order to provide a supply of carbon for further expansion of the first monolayer.

The growth rate of the graphite layer exhibited a $t^{\frac{1}{2}}$ dependence, indicating that the process was diffusion limited. The precipitation rate was at its maximum at around 665°C, at which temperature there was an apparent change from diffusion-limitation to dissociation-limitation.

6.2. The FeCr and FeCrC alloys

The 1.5wt% chromium content of these alloys was sufficient to largely prevent surface precipitation of graphite.

Sulphur was the dominant segregant in all the phase regions studied and usually achieved saturation coverage, even when depleted near the surface. Its segregation kinetics were analysed and found to involve three classes of time-dependence: $t^{\frac{1}{2}}$, t^{1} and $t^{1.3 - 5}$.

Bulk-to-surface diffusion coefficients were calculated from those results which displayed a $t^{\frac{1}{2}}$ dependence. They were found to be in reasonable agreement with published values of the lattice diffusion coefficient.

The apparent absence of sulphur evaporation at temperatures

below about 850°C, together with the t^1 and higher dependences were shown to be due to the influence of labile sulphide particles in the bulk or at the surface.

It was found possible to estimate the average sizes and spacings of the sulphide particles from those results exhibiting t^1 dependences. The values obtained were plausible in the light of the heat treatments that the samples had received.

When sulphur was depleted, phosphorus segregation became an important feature, although it never reached saturation coverage. Its segregation rate only exhibited $t^{\frac{1}{2}}$ dependences, but it is not expected that phosphide particles were present in the bulk. Bulk-to-surface diffusion coefficients were calculated from these results and were in reasonable agreement with published values of the lattice diffusion coefficient.

Surface segregation of nitrogen and chromium were also observed, but only at a low level. There were sometimes small carbon Auger peaks, but it was not possible to establish whether they were due to segregated carbon or precipitated graphite.

6.3. The HCC commercial alloy

The presence of manganese in this alloy largely removed surface segregation of sulphur. It did not reach saturation coverage and appeared to suffer evaporation effects. The sulphur segregation that did occur was thought to be due to the dissociation of surface sulphide particles and to manganese evaporation.

With sulphur segregation controlled by manganese, surface segregation of phosphorus became the most important feature of surface behaviour. It came close to achieving saturation coverage in some experiments.

Surface enhancements of nitrogen, chromium and carbon were also observed. The chemical state of carbon could not be determined.

It was concluded that phosphorus and nitrogen segregation to grain boundaries could be a cause of the poor hot-workability exhibited by some HCC steel.

6.4. Suggestions for future work

The presence of labile sulphide particles in manganese-free alloys has important implications for kinetic studies of surface or grain boundary segregation. It would be interesting to undertake a combined AES and metallurgical study in order to verify whether the sizes and spacings of sulphide particles in iron can indeed be estimated from surface segregation experiments. It would also be interesting to study phosphorus segregation in an alloy containing labile phosphide particles to see whether higher time dependences than $t^{\frac{1}{2}}$ did then appear. It should be possible to develop Rowlands & Woodruff's general theory of surface segregation to model interactions between segregants. By this means it might be possible to determine the influence of sulphur on the rate of phosphorus desegregation or evaporation.

The growth of graphite layers upon segregant-covered iron surfaces could be utilised to measure the energy dependence of electron inelastic mean free paths in graphite. By means of the type of analysis employed by Shelton et al in their study of graphite upon nickel, observations of graphite growth on segregant-free surfaces of iron could yield data concerning the binding energies of graphite as a function of surface orientation. Determination of the graphite growth mechanism at a sulphur-covered surface could have important

implications for the study of bulk graphitisation in iron alloys.

It has been determined that, with sulphur immobilised by the addition of manganese, surface segregation of phosphorus and nitrogen becomes more important in the HCC alloy. There is, however, only indirect evidence that segregation of these impurities could occur at austenite grain boundaries and so affect the hot-workability. Because of the problems involved with the quenching of samples from high temperatures prior to fracture and in-vacuo analysis, it might be simpler initially to add a phosphorus-scavenging element to HCC steel and measure its effect on the at-temperature ductility.

APPENDIX A Glossary of Metallurgical Terms

AUSTENITE - gamma iron containing other elements in solid solution and stable only above the transformation range. Austenite can contain up to about 2 wt% carbon in solution. Its structure is face-centred cubic.

AUSTENITISING - the process of producing austenite in a ferrous alloy by heating within or above the transformation range. The general term includes both complete and partial transformation.

BLOOM - a bar of iron or steel, of cylindrical or square cross-section, formed from an ingot by forging or rolling.

CEMENTITE - iron carbide with an ideal composition of 6.7 wt% carbon balance iron, although in alloy steels there may be substitution of some of the iron by carbide-forming alloying elements.

COGGING - the process whereby ingots are rolled or forged into blooms.

EUTECTOID - a solution of any material with a composition such that it cools without change to its temperature of final composition.

FERRITE - a solid solution of alpha iron whose crystal structure is bcc. Ferrite is only capable of dissolving very small amounts of carbon.

FORGING - the process of hammering, pressing or rolling used to work metal to some predetermined shape.

HOT-PIERCING - a piercing operation in which the hole is formed in heated metal.

HOT-WORKING - the process of shaping metal that has been made plastic by heating.

HYPER-EUTECTOID - an alloy containing more of some element than the eutectoid composition.

HYPO-EUTECTOID - an alloy containing less of some element than the eutectoid composition.

INCLUSIONS - particles of dirt, slag or other impurities present in metals; either by entrapment during solidification or formed by reactions within the metal.

INGOT - a special kind of casting made for subsequent rolling or forging.

MANDREL - a smooth cylindrical or conical-shaped core or die around which metal may be forged or drawn; an internal die.

PEARLITE - the lamellar aggregate of ferrite and carbide in steel that results from the direct transformation of austenite at the lower critical point of cooling.

PIERCING - producing a hole in metal by forcing a pointed tool through it. In the present case this refers to the production of seamless tubes by forcing a pointed mandrel through the bloom while special rolls revolve about the bar externally.

SOAKING - the prolonged heating of a metal at a predetermined temperature for sufficient time to allow complete and uniform absorption of heat throughout the mass.

SPHEROIDISATION - any proceedure of heating and cooling which produces a round or globular form of carbide.

TIME-TEMPERATURE-TRANSFORMATION (TTT) CURVES - isothermal transformation curves which show the time that austenite takes to transform isothermally at various temperatures.

APPENDIX B Auger Calibrations

The first stage of an Auger calibration must be the definition of a monolayer. It was decided that the number of segregant atoms in a close-packed layer would be a suitably unambiguous reference. In practice, however, this level of coverage would rarely be achieved because the saturation coverage is limited by the number of available surface sites. For example, sulphur has a saturation c(2x2) structure on bcc iron (100) planes, corresponding to a sulphur:iron atom ratio of 1:2. The atomic density of the iron plane is 1.22×10^{15} atoms cm^{-2}. Hence the sulphur density is 6.1×10^{14} atoms cm^{-2}. If we take the covalent radius of sulphur as 1.04Å, the area occupied by a sulphur atom in a close-packed layer will be $2.08 \times 2.08 \times \sin(60^{\circ}) = 3.75 Å^2$. The sulphur density in a close-packed layer is therefore the reciprocal of this and is 2.67×10^{15} atoms cm^{-2}. Hence a c(2x2) structure is 23% of a close-packed layer.

On a polycrystalline sample, the number of available surface sites will vary with the position on the surface that is sampled, and so will be different for every experiment. Fortunately, sulphur reached saturation coverage during most experiments. If it is assumed that the other interstitial segregants are limited to the same number of sites, then the sulphur Auger signal can be used as a standard for these elements. In the following sections, Auger calibrations are developed for close-packed monolayers on iron of each segregant in turn.

1. Sulphur

Perdereau (1971) has produced an Auger calibration for sulphur on nickel. He deposited radioactive sulphur on the surface and used the measured radioactivity to calibrate the sulphur Auger signal.

At a density of 5.65×10^{14} atoms cm^{-2}, the S(150eV)/Ni(62eV) peak height ratio was 0.2 when measured with an RFA. To correct this to the equivalent measurement with a CMA the different energy dependences must be taken into consideration. That of a CMA is the N(E) distribution multiplied by E, the energy of the Auger peak concerned. Hence the S(150eV)/Ni(62eV) ratio has to be multiplied by 150/62 to correct for the difference between an RFA and a CMA. Using the Phi Handbook of Standard Auger Spectra, this new ratio can be converted from a nickel substrate to an iron substrate by comparing the heights of the relevant Auger peaks from the iron and nickel standards. The final value of the Perdereau calibration is then S(150eV)/Fe(47eV) = 0.2 x 150/62 x 88/122.5 = 0.35. However, 5.65×10^{14} atoms cm^{-2} is only 21% of a close-packed monolayer. If the Perdereau calibration is scaled up accordingly, the S/Fe ratio for a close-packed monolayer becomes 1.66.

2. Phosphorus

Phosphorus has a covalent radius of 1.10Å. Hence the density of a close-packed monolayer is 2.39×10^{15} atoms cm^{-2}. Hondros (1965) found that the saturation coverage on bcc iron at 1723K was 1.4×10^{15} atoms cm^{-2}, which is 59% of a close-packed monolayer. Yen et al (1978) found that the saturation level of phosphorus on bcc iron in the alpha range was independent of temperature and gave a P(120eV)/Fe(703eV) peak height ratio of 0.8 using a CMA. This may be transferred to the ratio with the iron 47eV Auger peak by means of the Phi Handbook. Assuming that the saturation coverages observed by Hondros and by Yen et al were the same, the P(120eV)/Fe(47eV) peak height ratio for a close-packed monolayer is 0.86.

3. Carbon

Carbon has a covalent radius of 0.77Å. Hence, for a close-packed monolayer the density will be 4.9×10^{15} atoms cm^{-2}. Grabke et al (1977) found that a c(2x2) carbon structure on a bcc iron (100) plane gave a C(272eV)/Fe(651eV) peak height ratio of 0.54 using an RFA. Hence the density of carbon atoms was 6.1×10^{14} atoms cm^{-2}, which is 12.5% of a close-packed monolayer. This must be corrected to a CMA by multiplying by 272/651, and may be altered to the ratio with the 47eV iron peak using the Phi Handbook. This gives a C(272eV)/Fe(47eV) peak height ratio for a close-packed monolayer of 1.02. The derivation of an Auger calibration for a monolayer of graphite upon iron was described in section two of Chapter Five.

4. Nitrogen

Nitrogen has a covalent radius of 0.74Å. Hence, for a close-packed monolayer the density will be 5.27×10^{15} atoms cm^{-2}. There are no published Auger calibrations for nitrogen, so an approximate value was deduced from the Phi Handbook. The nitrogen standard was TaN, which is an interstitial compound (Wells (1962)). The number of nitrogen atoms in each layer will therefore be 1.3×10^{15} cm^{-2}, which is 25% of a close-packed layer. Hence, if all the nitrogen Auger signal from the standard arose from the first layer, the N(381eV)/Fe(47eV) peak height ratio for a close-packed monolayer will be 2.04.

5. Chromium

Chromium has a radius of 1.29Å. Hence, for a close-packed monolayer the density will be 1.73×10^{15} atoms cm^{-2}. The Phi Handbook was used to deduce an approximate calibration. An average of the two

chromium Auger peaks was used, in order to improve the signal-to-noise ratio in the Auger spectra. It is assumed that chromium atoms will segregate by substituting for iron atoms in the surface layer. The chromium density would therefore be dependent upon the original iron atom density. The approximate chromium(average)/Fe(47eV) peak height ratio for a close-packed monolayer is 0.73.

References

Grabke H.J., Paulitshke W., Tauber G. & Viefhaus H., Surf. Sci. 63(1977)377

Hondros E.D., Proc. Roy. Soc. A286(1965)479

Perdereau M., Surface Science 24(1971)239

Wells A.F., Structural Inorganic Chemistry, 1962, Clarendon Press

Yen A.C., Graham W.R. & Belton G., Met. Trans. 9A(1978)31